

In vivo measurement of excitatory synaptic transmission between identified neurons in layer 2/3 mouse barrel cortex

THÈSE N° 6299 (2014)

PRÉSENTÉE LE 24 OCTOBRE 2014
À LA FACULTÉ DES SCIENCES DE LA VIE
LABORATOIRE DE TRAITEMENT SENSORIEL
PROGRAMME DOCTORAL EN NEUROSCIENCES

ÉCOLE POLYTECHNIQUE FÉDÉRALE DE LAUSANNE

POUR L'OBTENTION DU GRADE DE DOCTEUR ÈS SCIENCES

PAR

Aurélie PALA

acceptée sur proposition du jury:

Prof. W. Gerstner, président du jury
Prof. C. Petersen, directeur de thèse
Prof. M. Hausser, rapporteur
Dr A. Holtmaat, rapporteur
Prof. R. Schneggenburger, rapporteur



ÉCOLE POLYTECHNIQUE
FÉDÉRALE DE LAUSANNE

Suisse
2014

ABSTRACT

The neocortex is the most distinctive feature of the mammalian brain and it is considered to be the substrate of high-order cognitive functions. The nature and the arrangement of the diverse neuronal elements constituting its multiple areas have received longstanding attention. Progressively such anatomical and functional investigations are undertaken in the context of an intact living being. It offers the possibility of examining the role of particular areas, networks or even individual neurons during various behavioral states. Synaptic connectivity and synaptic transmission have been traditionally investigated in reduced preparations. Typically, electrophysiological and optical techniques have been used to control and record the propagation of electrical activity between two or more neurons in acute brain slices *in vitro*. The purpose of this thesis is the investigation of synaptic connectivity and synaptic transmission within the intact neocortex of the living mouse. Here I took advantage of the recent development of optogenetics, in combination with electrophysiology and two-photon microscopy to systematically and directly record synaptic transmission between a single excitatory neuron and two main types of GABAergic neurons in layer 2/3 of the mouse barrel cortex *in vivo*. Overall, I discovered stronger excitatory connections onto GABAergic neurons than onto excitatory neurons, irrespective of the absolute or relative locations of the pre- and postsynaptic neurons somas. I further revealed that parvalbumin-expressing (PV) and somatostatin-expressing (Sst) GABAergic neurons received excitatory inputs that were similar in magnitude, but were more reliable and faster in PV neurons than in Sst neurons. Exploring postsynaptic responses to multiple presynaptic action potentials elicited at high frequency, I found a strong short-term facilitation accompanied by significant input summation in Sst neurons, but little short-term dynamics with no summation in PV neurons. Lastly, I compared the amplitude of single action potential-evoked postsynaptic responses as a function of neocortical activity level and found that it was unchanged in both neuron types. Overall, the results of this thesis provide new insights into the functioning of microcircuits *in vivo* while confirming many findings from reduced preparations. In the future, it will be interesting to extend these initial *in vivo* measurements to other neuron and synapse types, particularly in awake animals engaged in different behavioral states.

Keywords: Neocortex, Barrel cortex, Excitatory synaptic transmission, GABAergic neurons, Parvalbumin-expressing neurons, Somatostatin-expressing neurons, Slow oscillations, UP and DOWN states, Single-cell optogenetics, Whole-cell patch-clamp *in vivo*

RÉSUMÉ

Au niveau évolutif, le néocortex est la partie la plus récente du cerveau des mammifères. C'est aussi une de ses caractéristiques propres, car il est généralement considéré comme la partie du cerveau servant de substrat aux fonctions cognitives. La compréhension de la nature et de l'arrangement des divers éléments neuronaux qui constituent ses différentes zones a depuis longtemps été le sujet d'une attention particulière. Progressivement, de telles investigations anatomiques et fonctionnelles sont entreprises dans le contexte de l'être vivant intact ouvrant la possibilité d'examiner le rôle de certaines zones, de certains réseaux neuronaux et même de neurones individuels lors de divers états comportementaux. Cette thèse est une première étape dans cette direction, car elle s'intéresse à la connectivité synaptique et à la transmission synaptique, telles que présentes dans le néocortex de la souris vivante. Traditionnellement, ces dernières ont été plutôt étudiées dans des préparations réduites. Des méthodes électrophysiologiques et optiques ont typiquement été utilisées pour contrôler et enregistrer la propagation de l'activité électrique entre deux neurones ou plus dans des coupes de cerveau *in vitro*. Ici, j'ai tiré parti de l'émergence de l'optogénétique, en combinaison avec l'électrophysiologie et la microscopie à deux photons afin d'enregistrer directement et systématiquement la transmission synaptique entre un neurone excitateur et en majorité deux types de neurones GABAergiques dans la couche 2/3 du barrel cortex de la souris *in vivo*. J'ai remarqué une connectivité excitatrice plus grande entre neurones excitateurs et neurones GABAergiques qu'entre neurones excitateurs uniquement, et ceci indépendamment des positions des corps cellulaires des neurones pré- et postsynaptiques. En comparant les neurones GABAergiques exprimant la parvalbumine (PV) avec ceux exprimant la somatostatine (Sst), j'ai constaté que la taille de l'input excitateur qu'ils reçoivent est similaire, mais que celui-ci est plus fiable et plus rapide dans les neurones PV que dans les neurones Sst. En explorant la réponse postsynaptique à de multiples potentiels d'action présynaptiques, j'ai observé une facilitation à court-terme des inputs accompagnée d'une sommation significative dans les neurones Sst et peu de dynamique à court-terme, ainsi qu'une absence de sommation dans les neurones PV. Finalement, j'ai comparé l'amplitude de réponses postsynaptiques lors de différents niveaux d'activité néocorticale et n'ai trouvé aucune modulation claire de la taille de l'input par le niveau d'activité. Globalement, les résultats de cette thèse apportent de nouveaux éléments quant au fonctionnement des circuits neuronaux *in vivo* tout en confirmant les observations précédemment faites *in vitro*. Il sera intéressant d'étendre ces premières mesures *in vivo* à d'autres types de neurones et d'autres types de synapses, ainsi qu'à un animal éveillé, potentiellement engagé dans des comportements distincts.

Mots-clés: Néocortex, Barrel cortex, Transmission synaptique excitatrice, Neurones GABAergiques, Parvalbumin, Somatostatin, Oscillations lentes, Optogénétique, Whole-cell patch-clamp *in vivo*

ACKNOWLEDGEMENTS

I would first like to thank my thesis supervisor, Prof. Carl Petersen. By welcoming me in his research group five years ago, he gave me a unique opportunity to not only learn about the brain and neurosciences in general, but also to experience and develop as a scientist. His genuine enthusiasm about science and endless curiosity along with his constant support and positivism gave me motivation through the ups and the downs of my PhD journey.

As a member of his laboratory I crossed paths with many great individuals and scientists. I would like to thank first Céline Matéo and Yves Kremer, for their guidance, support and reassurance during my first months in the lab and for having cared since the beginning. I would like then to thank Varun Sreenivasan and Alexandros Kyriakatos, with whom I shared most of this journey, for many helpful and animated conversations about the brain and beyond. I would especially like to thank Takayuki Yamashita, Luc Gentet, Emmanuel Eggermann and Sylvain Crochet, for their availability, insight and help with practical and theoretical aspects of electrophysiology. Finally, I would like to thank Michael Avermann and Tanya Sippy, who were both inspiring sources of perseverance and enthusiasm at the beginning and end of my PhD respectively, and all other members of the LSENS lab, for their help, advice and support.

I would like to thank my three PhD Thesis examiners, Prof. Michael Häusser, Prof. Anthony Holtmaat and Prof. Ralph Schneggenburger, for their excellent and detailed feedback, as well as Prof. Wulfram Gerstner, president of the PhD Thesis jury committee.

I would like then to thank all of my friends, for their understanding, patience, interest and support. In particular I would like to thank Nadia, for her continuous encouragement and interest as well as for being a refreshing source of creativity and originality.

I would like to thank my family and especially my parents, Martine and Renato, for supporting my choices, and for their constant care for my well-being and happiness.

Finally, Bilal, my warmest and most grateful “thank you” goes to you, for sharing my joys and frustrations during this whole journey and for always believing in me.

The cortex is a very difficult matter, a tissue of endless complication, where any kind of simplistic approach is bound to fail.

Santiago Ramón y Cajal

CONTENTS

Chapter 1: Introduction.....	1
1.1 Chemical synaptic transmission.....	3
1.1.1 Synaptic organization of the neocortex.....	4
1.1.2 Presynaptic mechanisms of neurotransmitter release	6
1.1.3 Short-term synaptic plasticity	8
1.1.4 PSP modulation in dendrites.....	10
1.2 Somatosensory cortex.....	11
1.2.1 Peripheral inputs: from whiskers to neocortex	11
1.2.2 Intracolumnar microcircuits.....	12
1.2.3 L2/3 circuits and cell types	14
1.3 Patterns of cerebral activity	19
1.3.1 Slow oscillations.....	19
1.4 Rationale and aims of the PhD thesis	21
Chapter 2: Materials and methods	23
2.1 Animal implantation	23
2.2 Intrinsic signal optical imaging (ISI)	23
2.3 Craniotomy and durotomy	25
2.4 In vivo single-cell electroporation	25
2.5 In vivo electrophysiological recordings.....	27
2.5.1 Targeted juxtacellular recordings	27
2.5.2 Targeted whole-cell patch-clamp recordings.....	27
2.5.3 Local field potential recordings	28
2.6 Optogenetic stimulation.....	28
2.7 Tissue fixation and histology	29
2.8 Morphology reconstruction.....	29
2.9 Data analysis.....	30
2.9.1 Optogenetic control of ChR2-expressing neuron action potential firing.....	30
2.9.2 Electrophysiological properties of postsynaptic neurons.....	31
2.9.3 Connection identification.....	31
2.9.4 Properties of synaptic transmission	32
2.9.5 Short-term synaptic plasticity	33
2.9.6 State modulation of synaptic transmission.....	33

2.9.7 Intersomatic distances and neuron depth measurement	33
2.9.8 Statistical analysis.....	34
2.10 Parvalbumin and somatostatin immunohistochemistry	34
2.10.1 Single immunohistochemistry	34
2.10.2 Double immunohistochemistry	35
Chapter 3: Results.....	37
3.1 Optogenetic control of single excitatory neuron AP firing in vivo.....	39
3.1.1 ChR2 variant selection.....	39
3.1.2 Properties of in vivo light-evoked action potential firing	41
3.2 Postsynaptic cell types	44
3.2.1 Molecular specificity of tdTomato-expressing GABAergic neurons	44
3.2.2 Electrophysiological properties	47
3.3 Properties of unitary excitatory synaptic transmission in vivo	48
3.3.1 Connectivity rate, connection amplitude, reliability and kinetics.....	48
3.3.2 Distance dependence of connectivity.....	52
3.3.3 Other influences on connectivity and connection amplitude	53
3.4 Short-term synaptic dynamics	55
3.5 Modulation of synaptic transmission by network state.....	57
3.6 Morphology of recorded neuron pairs	59
3.7 Tables.....	61
Chapter 4: Discussion	63
4.1 Single-cell optogenetics for measuring synaptic transmission in vivo	63
4.2 In vivo connectivity analysis	65
4.3 In vivo vs in vitro measurement of synaptic transmission.....	66
4.4 PV and Sst inhibitory neurons in vivo	69
4.5 Modulation of uEPSP amplitude by UP and DOWN states	71
References.....	73
Curriculum Vitae	97

CHAPTER 1: INTRODUCTION

The neocortex is one of the distinctive and most recent features of the mammalian brain (Herculano-Houzel, 2009; Rakic, 2009). It is commonly considered as the substrate of “high-order” cognitive processes, such as learning, memory, reasoning, decision making, but also sensory perception and motor control. Currently, one of the major challenges of neurosciences is to understand the role of the anatomical and functional structures of the neocortex in the various combinations of these processes, namely behaviors. Though the neocortex can be partitioned into cytoarchitecturally distinct areas with attributed functions, horizontal anatomical layers, and functional vertical columns, its most elementary structure consists of individual neurons of various identities structurally and functionally connected to each other by synapses. In contrary to the relative stability of its cellular composition throughout life, as neurogenesis and age-related cell death are rare in the mature neocortex (Morrison and Hof, 1997; Gould, 2007), structural and functional neocortical synaptic organization is highly variable. Modulation of synaptic strength occurs on a range of time scales spanning milliseconds to hours, while synapses turnover happens over days. Both are mediated by genetic, molecular and cellular mechanisms ultimately governed by the level of ongoing activity of the pre- and postsynaptic neuronal partners, which is directly influenced by the level of activity of the neocortical circuit they belong to and whose macroscopic correlate can be found in the various levels of behavioral and arousal states.

Chemical synapses provide the principal way of rapid communication amongst neurons, through the transformation of an incoming electrical signal into a chemical one via a sequence of precisely ordered events. It starts with the conduction of the action potential down the axon, and its conversion into a chemical signal via the release of neurotransmitters at the synapse. This chemical signal is subsequently transformed back to an electrical signal in the form of a postsynaptic potential, and is integrated with thousands of other synaptic inputs during its propagation towards the site of action potential initiation in the postsynaptic neuron. Full understanding of this process necessitates a level of resolution that is difficult to achieve within the intact neocortex. For this reason, most of the work on synaptic connectivity and synaptic transmission has been conducted in reduced preparations, such as acute brain slices and neuronal cultures.

This thesis provides a study of synaptic transmission and synaptic connectivity within the intact brain *in vivo*. By taking advantage of stimulation and recording techniques with single cell resolution, I directly and systematically measured synaptic transmission during various regimes of pre- and postsynaptic neuronal activity typical of the anesthetized neocortical state. In the future perspective of linking anatomical and functional connectivity of a given neocortical area with its implication in macroscopic behaviors, we chose the barrel cortex of the mouse as a model system, where functional and anatomical somatotopy overlap at the level of the barrel column. Moreover, we

decided to investigate excitatory synaptic transmission within supragranular layer 2/3 (L2/3), due to its role in the dynamic integration of the sensory information from multiple vibrissae as well as in its propagation to other neocortical areas.

The first section of this introduction will address the basic principles of neocortical synaptic organization, with a focus on glutamatergic synapses and receptors. The molecular events underlying chemical synaptic transmission will be reviewed, as well as the mechanisms involved in the variation of its reliability on a short time scale (short-term plasticity). Finally the role of dendrites in shaping synaptic inputs will be briefly discussed. The second section of this introduction will cover the synaptic organization of the rodent vibrissal somatosensory pathway, starting from the vibrissae located on the snout of the animal to the neocortical barrel columns. The intra- and intercolumnar excitatory and inhibitory connectivity underlying the neocortical flow of tactile sensory information will be summarized with an emphasis on L2/3. Finally, L2/3 excitatory and inhibitory neuron types will be reviewed, together with the properties of the synapses linking them. The third section of this introduction will cover the rhythmic patterns of activity observed in the intact brain, with a focus on the cortical slow (< 1 Hz) oscillations, which are the dominant pattern of spontaneous activity during anesthesia in the rodent neocortex. Finally, the last section of this introduction will present the current state of in vivo synaptic transmission research, leading to the main rationale and aims of the thesis.

1.1 CHEMICAL SYNAPTIC TRANSMISSION

The initial observations by Ramón y Cajal that neurons were distinct and independent entities, physically discontinuous from each other, set the ground for attempts at understanding their way of interacting. It was in 1897 that Charles Scott Sherrington used the word “synapse” for the first time. From the Greek “syn” meaning together and “haptain” meaning to clasp, he defined a synapse as the zone of close contact between two neurons (Eccles, 1987). Then, in the midst of the measurements of electrical signal propagation, Otto Loewi and Henry Hallett Dale postulated that its propagation was of chemical nature at the synapse (Fishman, 1972; Zimmer, 2006), which was later confirmed by John Carew Eccles (Brock et al., 1952). In the coming years, Bernard Katz, taking advantage of the development of microelectrodes for performing intracellular recordings, discovered key mechanisms of functioning of the presynaptic part of the synapse. While recording electrical signals in the frog sartorius muscle, he noticed spontaneously occurring depolarizations of small amplitude (Figure 1.1A), but of similar waveform, as those evoked by presynaptic stimulation of the afferent motor neuron (Figure 1.1B). These miniature end-plate potentials (mini-EPPs) had a Gaussian amplitude distribution (Fatt and Katz, 1952). In comparing their amplitude distribution with the amplitude distribution of evoked end-plate potentials (EPP) he noted that the latter was constituted of multiple step-like peaks of decreasing amplitude, with each peak being roughly located at an integer multiple of the peak of the mini-EPPs amplitude distribution (Figure 1.1C). He concluded that EPPs were occurring in response to the presynaptic release of multiple fixed amounts of neurotransmitter, or quanta, which upon presynaptic stimulation could be released simultaneously (Del Castillo and Katz, 1954).

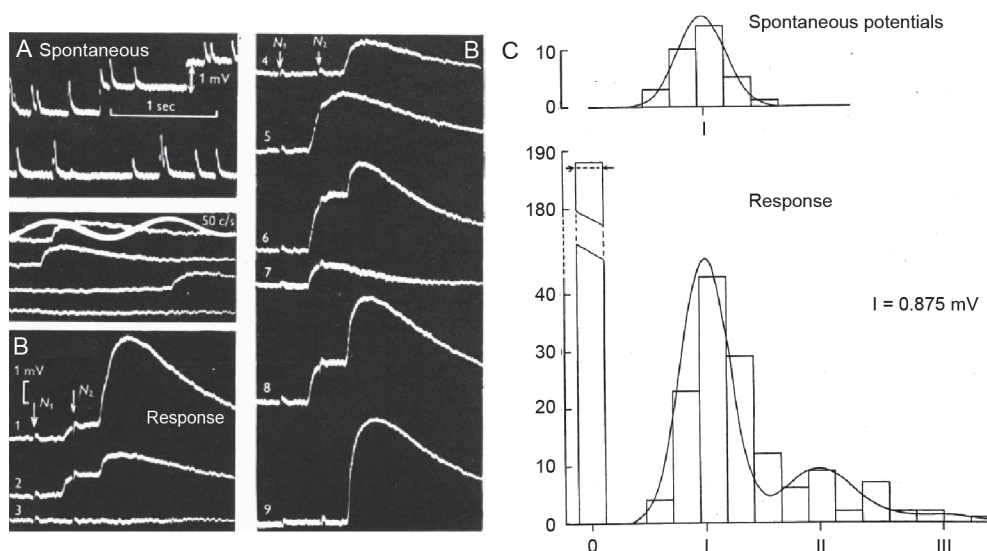


Figure 1.1 Intracellular recording from a single muscular junction. (A) Spontaneous miniature end-plate potentials (mini-EPPs). (B) Example responses to paired nerve impulses (N1, N2). (C) Histograms showing the amplitude distribution of mini-EPPs (*above*) and of evoked end-plate responses (*below*). (Modified from Del Castillo and Katz, 1954)

He also attributed the physical correlates of such quanta to circular nanostructures present in the presynaptic terminals, the vesicles, to which neurotransmitters were thought to be associated (Del Castillo and Katz, 1956). Finally, he and others detailed the previously known role of calcium in chemical synaptic transmission, by establishing that EPP amplitude was proportional to the fourth power of the extracellular calcium concentration, suggesting that possibly four calcium ions at a time were involved in the vesicular release inside the nerve terminal (Dodge and Rahamimoff, 1967; Katz and Miledi, 1967, 1970). In parallel with these discoveries concerning the presynaptic part of the synapse, John Langley and Paul Ehrlich, through numerous studies across many years came to the conclusion of the existence of chemoreceptors, possibly sensing transmitter action at defined locations on the postsynaptic muscle cell or neuron (see Bennett, 2001). Finally, the excitatory and inhibitory effects of amino acids on neurons were demonstrated in the spinal cord (Curtis and Watkins, 1960) and eventually identified in the brain as well (Hayashi, 1952; Purpura et al., 1957; Hayashi, 1959; Curtis and Watkins, 1961), where glutamic acid and γ -aminobutyric acid were found to be the major excitatory and inhibitory neurotransmitters respectively.

1.1.1 SYNAPTIC ORGANIZATION OF THE NEOCORTEX

Together with electrical coupling, either indirect via local ionic interactions between closely located cellular membranes (ephaptic interactions) (Jefferys, 1995) or direct through gap junctions (Fukuda, 2007), chemical synapses are the main way of fast communication between neurons. Within the central nervous system, a chemical synapse is defined as a discrete point of contact between the plasma membrane of two neurons of 0.5-2 μm diameter, spaced by about 20 nm (Ribault et al., 2011). As plasma membranes can sometimes be in similarly close contact at extra-synaptic locations, the ultimate criterion to conclude to the existence of a chemical synapse is the ultrastructural confirmation of the presence of synaptic vesicles in the presynaptic compartment together with pre- and/or postsynaptic membrane densities. In this way, chemical synapses have been found to belong to two types, as a function of the shape of their presynaptic vesicles and the symmetry of their pre- and postsynaptic membrane density. Type I synapses have typically round-shaped vesicles with an asymmetric membrane density and are commonly thought to have an excitatory action. Type II synapses have rather flattened vesicles with symmetric membrane density and are thought to be inhibitory (Gray, 1959). The density of neocortical chemical synapses has been estimated from $10.94 \cdot 10^8$ syn/ mm^3 (human temporal cortex) to $29.31 \cdot 10^8$ syn/ mm^3 (mouse barrel cortex) with a proportion of excitatory synapses of 80-90% versus 10-20% for inhibitory synapses, irrespective of the species considered (DeFelipe et al., 2002).

In the neocortex, neurons are connected to each other by more than one synapse. As a general principle, excitatory neurons make less synaptic contacts with their postsynaptic partners than inhibitory neurons. In the rodent somatosensory cortex for instance, an individual excitatory neuron contacts other excitatory or inhibitory neurons with, on average, 2-8 synapses per partner (Deuchars et

al., 1994; Deuchars and Thomson, 1995; Markram et al., 1997; Feldmeyer et al., 1999; Wang et al., 2002; Silver et al., 2003; Markram et al., 2004; Feldmeyer et al., 2006). Inhibitory neurons, on the other hand, innervate excitatory and inhibitory neurons with an average of 10-21 synaptic contacts per partners (Gupta et al., 2000; Wang et al., 2002; Markram et al., 2004). Another distinction between excitatory and inhibitory synapses is the postsynaptic compartment they target, i.e. soma, dendrites (spines or shaft) and axon (Douglas, 2004; Markram et al., 2004). Excitatory synapses are mainly located on the dendritic spines of excitatory neurons, as well as on their dendritic shaft, though in a lesser proportion (Beaulieu and Colonnier, 1985). The axon initial segment and the soma of excitatory neurons are usually void of excitatory synapses. In inhibitory neurons, which for most of them are aspiny, excitatory synapses are located mainly on the proximal portion of the dendritic tree, as well as directly on the soma and to a lesser extent on the distal dendrites. Inhibitory synapses are located on every cellular compartment of the excitatory neurons, including the axonal initial segment and a small fraction of dendritic spines, as a consequence of the high heterogeneity and specificity in axonal projection targets of neocortical inhibitory neurons. Inhibitory neurons receive inhibitory contacts mainly on their proximal dendrites and soma.

1.1.1.1 Glutamate and its receptors

Glutamate is the principal excitatory neurotransmitter of the brain. Its postsynaptic excitatory action is produced on a fast and a slow time scale, through the binding of the neurotransmitter molecules to two main families of receptors, ionotropic and metabotropic receptors respectively.

Ionotropic glutamate receptors are ligand-gated ion channels, which can be further subdivided into three groups, namely AMPA, kainate and NMDA receptors. All three types of receptors are tetramers, whose four subunits, which form the wall of the ion channel, are encoded by a small group of evolutionary related genes. GluR1-4 genes encode the subunits constituting the AMPA receptor protein, while GluK1-5 genes encode the subunits of the kainate receptor proteins and NR1, NR2A-D and NR3A-B genes those of the NMDA receptors. Most AMPA and kainate receptors are heteromers, made of two subunits encoded by one type of GluR or GluK gene respectively and two other subunits encoded by another type. NMDA receptors are heteromers as well, made of two subunits encoded by the NR1 gene and two other subunits encoded by either NR2 genes or a combination of NR2 and NR3 genes (Traynelis et al., 2010). The different possible combinations of receptor subunits therefore give rise to a variety of electrophysiological postsynaptic properties, due to diverse ionic permeabilities and biophysical properties. However, most AMPA and kainate ion channels are permeable to Na⁺ and K⁺, and sometimes also to Ca²⁺ (see below). They thus have a depolarizing reversal potential, close to 0 mV. The rising and decaying phases of the AMPA channel conductance is fast (~ 1 ms), while kainate channel conductance has an equally fast rising phase with a slower decaying phase (~100 ms) (Hollmann and Heinemann, 1994; Traynelis et al., 2010). NMDA channels are different than AMPA and kainate at many levels. First, their conductance is dominated

mainly by Ca^{2+} ions, though the channel is also permeable to Na^+ and K^+ ions. Second, at the usual resting membrane potential of most neurons, NMDA channels are gated by extracellular Mg^{2+} ions and it is only upon local depolarization that the Mg^{2+} block they will be released, allowing the flux of others cations through the channel. Compared to the rising and decaying phases of the AMPA conductance, the NMDA conductance is also slower (Ascher and Nowak, 1986; Traynelis et al., 2010).

Metabotropic glutamate receptors are G-protein coupled, seven-transmembrane domains dimer receptors. They can be subdivided in three groups, based on their gene sequence homology and the type of G-protein they are coupled to. Group I includes mGluRs 1 and 5, group II includes mGluRs 2 and 3 and group III includes mGluRs 4, 6, 7, and 8. Only group I receptors are located postsynaptically, where they are mainly coupled to G_q/G_{11} protein (Meldrum, 2000). Their activation leads to the eventual mobilization of intracellular calcium stores and to the activation of protein kinase C, through the production of IP3 and diacylglycerol resulting in an overall slow excitatory effect, mediated by a decrease in K^+ conductance (for details, see Niswender and Conn, 2010).

In the neocortex, the exact location at the synapse (or extrasynaptically) of the different types of receptors as well as their subunit composition and their level of expression are relatively unknown, though they are likely to be area and cell-type specific (Blatow et al., 2005). Of interesting note, it has been shown that in contrast to glutamatergic synapses located on excitatory neurons, glutamatergic synapses located on inhibitory neurons express a type of AMPA receptor that does not contain the GluR2 subunit, therefore rendering it permeable to Ca^{2+} in addition to Na^+ and K^+ (Hestrin, 1993; Jonas et al., 1994). Furthermore, these excitatory synapses show little contribution of the NMDA current to the postsynaptic membrane potential depolarization (Thomson et al., 1996), though NMDA receptor mRNA is found in the cytoplasm of inhibitory neurons (Blatow et al., 2005).

1.1.2 PRESYNAPTIC MECHANISMS OF NEUROTRANSMITTER RELEASE

Within the presynaptic terminal fast neurotransmitter release occurs at a distinct location facing the synaptic cleft, called the active zone (Landis et al., 1988). In images obtained by electron microscopy, the active zone appears as a dark (electron-dense) area, which is made of cytoskeletal elements and numerous proteins (amongst which, those from the Munc13, RIM and ERC families) forming a macromolecular complex (for review, see Ashery et al., 2014) that interacts with the proteins located on the vesicles (Dresbach et al., 2001). Synaptic vesicles are tiny organelles (~ 30 nm diameter, see Ribault et al., 2011) made of phospholipids with associated proteins that can be found at different stages of a cycle supporting the repeated release of neurotransmitters via a sequence of trafficking, exocytosis, recycling and filling events (Sudhof, 2004). One can identify vesicles that are docked to the plasma membrane at the active zone and that have been primed for fusion, which form the so-called readily releasable pool (RRP). In addition, vesicles can be found in a reserve pool, which together with the RRP form the recycling pool, encompassing all potential releasable vesicles upon

various types of presynaptic membrane depolarization. Finally a third group exists, the “resting” pool, which contains most of the presynaptic vesicles, but that is only rarely recruited for exocytosis (Sudhof, 2000; Rizzoli and Betz, 2005). The exact molecular mechanisms underlying the transitions between the different stages of the cycle as well as their regulation are quite complex and involve a large number of proteins (see Ashery et al., 2014). One can however distinguish the synapsins, which are involved in the organization and mobilization of the vesicles, the SNAREs, complexins and SM proteins (Sec1 and Munc18), which are involved in the docking, priming and fusion of the vesicles at the plasma membrane (Figure 1.2) and the clathrins and dynamins, which are implicated in the endocytosis of the vesicles following neurotransmitter release. Upon depolarization of the presynaptic terminal plasma membrane by an incoming action potential, the opening of voltage-gated Ca^{2+} channels, mainly of the P/Q- and N-types, leads to an influx of Ca^{2+} ions that results in a transient increase in local intracellular Ca^{2+} concentration. This brief change in local Ca^{2+} concentration will be detected by various Ca^{2+} -sensor proteins, amongst which, the synaptotagmin-1 protein that will then bind to the SNARE-complexin-SM protein complex and initiate fusion of the primed vesicles of the RRP with the plasma membrane (Figure 1.2). Recycling and re-filling of the fused vesicles will then take place according to various endocytic mechanisms (kiss-and-run, clathrin-mediated, bulk endocytosis, amongst others), in order to keep the number of vesicles in the pools as well as the amount of plasma membrane at the synaptic terminal constant (Sudhof, 2004). In addition to this fast, synchronous Ca^{2+} -dependent release of neurotransmitters, another type of neurotransmitter release happens on a slower time scale (asynchronous release), which is likely mediated by other members of the synaptotagmin protein family and whose function is still to be clarified (Goda and Stevens, 1994; Atluri and Regehr, 1998; Lu and Trussell, 2000; Bacaj et al., 2013).

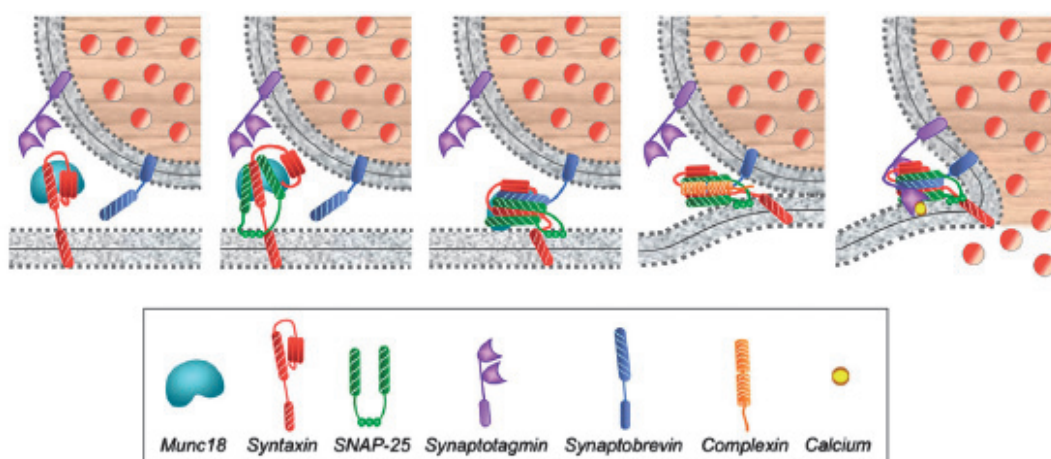


Figure 1.2 Molecular mechanism of vesicle docking, priming and fusion. (From Ashery et al., 2014)

In the neocortex, where multiple synaptic contacts exist between neurons (see Section 1.1.1), only one vesicle is released at a given synapse in response to a single presynaptic action potential (Silver et al., 2003). However, in the hippocampus, where the excitatory connection between two neurons is often mediated by a single synapse, multi-vesicular release seems to occur (Oertner et al., 2002; Biro et al., 2006; Christie and Jahr, 2006) in addition to single-vesicle release (Gulyas et al., 1993; Lawrence et al., 2004; Biro et al., 2005).

Having detailed the sequence of molecular events controlling the release of neurotransmitters in the synaptic cleft, it is important to keep in mind that not every action potential will successfully trigger neurotransmitter exocytosis; thus neurotransmitter release occurs with a certain probability. The fact that chemical synaptic transmission is probabilistic comes from the fact that some of its underlying molecular events involve a small (and varying) number of molecules (voltage-gated Ca^{2+} channels, Ca^{2+} ions, vesicular proteins), whose behavior upon action potential-mediated plasma membrane depolarization (channel opening, ions diffusion, conformational change) is stochastic (Ribault et al., 2011). In the neocortex, different release probabilities (P_r) have been estimated for different type of synapses (see Branco and Staras, 2009), with in addition, synapses stemming from the same axon having a possibly different P_r (Markram et al., 1998; Reyes et al. 1998, P_r estimated by paired-pulse ratio). This seems to indicate a possible influence of the postsynaptic cell type on the P_r of the presynaptic terminal.

Finally, in order to have a more complete understanding of the variable nature of chemical synaptic transmission, one should also take into account processes happening after the exocytosis of neurotransmitters, such as their random diffusion in the synaptic cleft, which might generate fluctuations in neurotransmitter concentration at the postsynaptic site or the stochasticity of postsynaptic ion-channel opening upon binding of ligand as well as their desensitization (Jones and Westbrook, 1996), which can both modulate the kinetics and amplitude of the postsynaptic potential.

1.1.3 SHORT-TERM SYNAPTIC PLASTICITY

As a function of the level of activity in the pre- or postsynaptic neuron, or of the interplay of both, synaptic transmission can be modulated on various time-scales, resulting in a change in its strength that is reflected in the amplitude of the postsynaptic potentials. Here we will focus on changes happening in the range of tens of milliseconds to seconds (Fioravante and Regehr, 2011), and that are linked to the level of activity of the presynaptic neuron. Upon arrival at the presynaptic terminal of multiple action potentials with a short time interval, the elicited postsynaptic potential amplitude will be dictated by an interaction between different forms of synaptic plasticity, including facilitation and depression (Dittman et al., 2000).

Facilitation, which relates to an increase of the amplitude of successive postsynaptic potentials upon multiple presynaptic action potentials, is supported by different molecular mechanisms having a solely presynaptic origin and resulting in an overall increase of the P_r (Fisher et al., 1997). One

possible mechanism leading to an increased P_r is the “residual calcium hypothesis” (Katz and Miledi, 1968). It implies the persistence of Ca^{2+} ions in the presynaptic terminal upon activation of the synapse, which will affect subsequent neurotransmitter releases. Evidence favoring its validity comes from several investigations (reviewed in Zucker and Regehr, 2002). Intracellular Ca^{2+} concentration was found to be correlated with the magnitude of the facilitation, and reducing or increasing it through various ways (exogenous Ca^{2+} buffers, blockage of voltage-gated Ca^{2+} channels, change in the extracellular Ca^{2+} concentration, photolysis of caged Ca^{2+} chelators) lead to a reduction, respectively an augmentation of the observed facilitation. In addition, the effect of the residual Ca^{2+} is likely to be mediated via a different calcium sensor than synaptotagmin, which is the one involved in the synchronous release of neurotransmitters (see Section 1.1.2) (Atluri and Regehr, 1996; Tang et al., 2000). Other mechanisms by which facilitation can take place and that are mediated by an increase in the presynaptic Ca^{2+} concentration, include the saturation of endogenous calcium buffers upon repetitive action potential-triggered Ca^{2+} influx (Blatow et al., 2003; Matveev et al., 2004), the upregulation of voltage-gated Ca^{2+} channels (Catterall and Few, 2008) or the increase in Ca^{2+} influx due to action potential broadening (Geiger and Jonas, 2000).

As opposed to facilitation, depression relates to a decrease of the amplitude of successive postsynaptic potentials upon multiple closely timed presynaptic action potentials. Depression is mediated by a combination of pre- and postsynaptic mechanisms. At the presynaptic level, the most widespread mechanism is the depletion of the RRP (Zucker and Regehr, 2002). If an action potential releases a large fraction of the RRP, subsequent stimuli occurring before the replenishment of the RRP will trigger the release of fewer vesicles. Independently of the state of the RPP, vesicle fusion itself can prevent further exocytosis at the same location, due to the time taken to clear the vesicular proteins from the plasma membrane (Neher and Sakaba, 2008). Regulation of Ca^{2+} channels by Ca^{2+} -sensing proteins leading to a decreased intracellular Ca^{2+} concentration has also been shown to contribute to depression (Catterall and Few, 2008). In addition, molecules such as GABA (Ramoia and Sur, 1996; Gil et al., 1997), acetylcholine (Gil et al., 1997) and dopamine (Rowlands and Roberts, 1980) released in the extracellular space can activate metabotropic (Wu and Saggau, 1997) or ionotropic receptors (MacDermott et al., 1999) located on the presynaptic terminal, eventually decreasing neurotransmitter release. The neuromodulatory substances can be released from the presynaptic neuron itself (homosynaptic modulation) (Lambert and Wilson, 1994) or from a neighboring synapse (heterosynaptic modulation) (Dittman and Regehr, 1997), as well as from the postsynaptic neuron (retrograde modulation) (Wilson and Nicoll, 2001). At the postsynaptic level, the main phenomenon involved in depression is the desensitization of the postsynaptic receptors (Jones and Westbrook, 1996).

1.1.4 PSP MODULATION IN DENDRITES

Dendrites are the cellular compartment that receives most of the excitatory synaptic inputs. From the postsynaptic terminals located on dendritic spines or on dendritic shafts, synaptic potentials must travel down different dendritic branches to reach the soma and axon initial segment. Moreover, a given neuron receives thousands of excitatory (and inhibitory) inputs (DeFelipe et al., 2002), whose interactions within the dendritic tree will ultimately dictate action potential generation. Apart from the architecture of the dendritic tree, passive and active properties of dendrites are crucial for determining the propagation and interactions of synaptic inputs.

Initially, dendrites were considered to be passive, meaning that the electrical parameters governing the propagation of voltage are invariant. Such an assumption allowed to apply the cable theory used to describe the passive flow of current in cable structures to neurons (Rall, 1959, 1967). In its simplest form, cable theory for dendrites implies that the whole dendritic tree is considered as a single cable. The spatial and temporal attenuation of voltage along the dendrites upon transient and localized current increase can be described by a partial differential equation, whose constants ultimately relate to the specific membrane resistivity (R_m), the specific membrane capacitance (C_m), and the intracellular resistivity (R_i) of the neuron. In addition, a fourth constant, λ , is used to describe the electrotonic properties of dendrites. λ is the space constant of the dendrite and it is proportional to the square root of the R_m/R_i ratio as well as to the dendrite diameter (d). It represents the distance from the site of current injection at which the voltage amplitude has decreased to 37% ($1/e$) of its initial value (Spruston et al., 1994). The cable theory therefore predicts that postsynaptic potentials (PSPs) traveling from dendritic sites to the soma are attenuated as a function of R_m , R_i and d , which was confirmed by simultaneous dendritic and somatic recordings performed in L5 pyramidal neurons (Stuart and Spruston, 1998) and Purkinje neurons (Roth and Hausser, 2001). Simultaneously, PSPs are broadened due to their filtering through C_m . Cable theory also predicts the interactions between multiple PSPs as a function of their electrotonic proximity within the dendritic tree. PSPs being electrotonically isolated tend to sum linearly, whereas closely located PSPs produce an attenuated response, possibly due to a decrease in local dendritic resistance (Segev and Rinzel, 1995). Such a phenomenon was confirmed in the neocortex (Tamas et al., 2002).

Dendrites, however, are not passive entities, as a variety of voltage-gated conductances are distributed throughout their branches (reviewed in Reyes, 2001; Migliore and Shepherd, 2002). Their activation can enhance PSP amplitude, but can also attenuate it. Transient and persistent Na^+ currents are found in neocortical pyramidal neuron dendrites (Stuart and Sakmann, 1994), as well as delayed-rectifying and transient K^+ currents (Kornegreen and Sakmann, 2000) and Ca^{2+} -dependent K^+ currents (Kang et al., 1996). In addition, data from recordings performed in hippocampal pyramidal neurons suggest the existence of dendritic high-voltage activated and low-voltage activated Ca^{2+} currents (Magee and Johnston, 1995). Finally, I_h current is also present in neocortical dendrites (Williams and Stuart, 2000). Enhancement of PSP amplitude, as a mechanism to counteract their attenuation due to

the passive dendritic properties, occurs mainly via local dendritic spikes upon activation of Na⁺ or Ca²⁺ or even NMDA receptor mediated currents as well as through larger and more widespread Ca²⁺ spikes, which are particularly prominent in L5 pyramidal neurons (Larkum et al., 1999; reviewed in London and Häusser, 2005).

1.2 SOMATOSENSORY CORTEX

The earliest description of the cytoarchitecture of the rodent somatosensory cortex noted the ‘peculiar’ organization of one of its sub-regions (see Woolsey and Van der Loos, 1970). Nissl-stained neocortical layer 4 tangential sections of this sub-region revealed many individual circular regions with high cellular density at its side (wall) and low cellular density at its center (hollow) separated by regions of even lower cell density (septa). When viewed in the coronal plane, these particular motifs looked like wooden barrels, hence the choice of nomenclature by Thomas Woolsey and Hendrik Van der Loos in the 1970s (Woolsey and Van der Loos, 1970; Welker and Woolsey, 1974). In the more posterior and medial part of the so-called barrel field, namely the Posteromedial Barrel Subfield (PMBSF), were found barrels of clear size and shape, whose organization was consistent across hemispheres and animals. An initial evoked-potential study attributed the location of the barrel field to the head-face area of the rodent (Woolsey, 1967) and a subsequent microelectrodes study with finer spatial resolution refined the location of the PMBSF to the mystacial vibrissae, with a one-to-one correspondence between individual vibrissae and barrels (Welker, 1971). Further functional mapping of the PMBSF - or barrel cortex - based on electrophysiological and optical measurements (reviewed in Petersen, 2007) together with additional anatomical identification methods, such as cytochrome (Land and Simons, 1985) or succinic dehydrogenase staining (Killackey and Belford, 1979), have allowed the establishment of a clear anatomical and functional somatotopy between individual barrels and vibrissae. Interestingly functional arrangement was found to be existent not only in layer 4, but also in the more superficial (Masino et al., 1993; Brecht et al., 2003; Ferezou et al., 2006) and deep layers of the barrel cortex (Manns et al., 2004; de Kock et al., 2007), giving rise to the notion of a barrel column, as an equivalent to the functional cortical column initially described in cat somatosensory and visual cortices (Mountcastle, 1957; Hubel and Wiesel, 1962, 1963). However, the barrel column is unique (although perhaps analogous to ocular dominance columns in cat and monkey) in the sense that its functional specificity emerges from its topographical arrangement of peripheral inputs as well as from its intracolumnar circuitry.

1.2.1 PERIPHERAL INPUTS: FROM WHISKERS TO NEOCORTEX

Rodents are nocturnal animals relying mostly on their sense of olfaction and touch to actively gather information about their close environment. By protracting and retracting their vibrissae at a frequency of about 8-10 Hz (Berg and Kleinfeld, 2003), in what is defined as “whisking”, rodents can collect tactile information about location, shape and texture of objects (Hutson and Masterton, 1986; Carvell

and Simons, 1990; Krupa et al., 2001; O'Connor et al., 2010) as well as about conspecifics (Bobrov et al., 2014). Upon passive or active vibrissae deflection, tactile information is transferred to the trigeminal nuclei of the brain stem by trigeminal ganglion neurons innervating the vibrissa follicles, with a given trigeminal ganglion neuron targeting a single follicle (Zucker and Welker, 1969). Three of the four trigeminal nuclei (principalis (Vp), interpolaris (SpVi) and caudalis (SpVc)) possess a complete representation of the vibrissal array, as revealed by the presence of structures equivalent to the cortical barrels: the barrelettes. The axons of individual trigeminal ganglion neurons that target a given follicle project to the four trigeminal nuclei (including oralis (spVo)), though they converge in a one-to-one (follicle-to-barrelette) fashion in principalis and the caudal division of interpolaris only (SpVic). In a simplified view (see Fox, 2008; Feldmeyer, 2012; Deschênes and Urbain, 2009), principalis and the rostral part of interpolaris are the two main trigeminal nuclei that project to the contralateral dorsomedial part of the ventroposterior medial (VPm) and posterior medial (POm) nuclei of the somatosensory thalamus respectively, defining the so-called lemniscal and paralemniscal pathways of tactile information. At the level of the VPm, barreloids are the somatotopic representation of the vibrissae and contain single-vibrissa receptive field relay neurons. Although no particular anatomical arrangement is present in POm, there seems to be nonetheless a rough functional map of the vibrissae, made of neurons having multi-vibrissae receptive fields (Diamond et al., 1992). Cortical projections from the relay neurons in VPm terminate principally in layer 4, in their corresponding barrels' hollows, as well as at the interface of layer 5B and 6 and in deep layer 3, though with a lesser density (Killackey and Leshin, 1975; Lu and Lin, 1993; Pierret et al., 2000; Meyer et al., 2010a). POm axons end mainly in the septal region of layer 4, with some terminals also innervating layer 1 and 5A in an area located above both the barrels and septa (Lu and Lin, 1993; Pierret et al., 2000; Meyer et al., 2010a). Functional mapping (Bureau et al., 2006) has further confirmed the segregation of these two anatomical streams, with as possible implication a separate encoding of spatiotemporal touch-related information and vibrissa motion kinetics by the lemniscal and paralemniscal pathways respectively (Alloway, 2008).

1.2.2 INTRACOLUMNAR MICROCIRCUITS

Single- and multi-vibrissae tactile information enters the barrel column at multiple locations, giving rise to multiple potentially converging streams of propagation of excitation within the column. Here we will focus on anatomical and functional evidences describing the flow of excitation within a given barrel column, starting at its stronger entrance point in layer 4 (L4), in line with the proposed canonical organization of sensory cortical columns (Douglas and Martin, 2004). In L4, VPm thalamocortical axons project mainly onto glutamatergic spiny stellate neurons and star pyramids (Brecht and Sakmann, 2002; Staiger et al., 2004; Bruno and Sakmann, 2006). Spiny stellate neurons target principally pyramidal neurons in L2/3 (Petersen and Sakmann, 2001; Feldmeyer et al., 2002; Shepherd et al., 2005), but also have dense axon collaterals within L4 (Feldmeyer et al., 1999;

Petersen and Sakmann, 2000; Lefort et al., 2009). They directly innervate infragranular layer 5A, 5B and the more superficial portion of L6 as well (Feldmeyer et al., 2005; Schubert et al., 2006; Lefort et al., 2009). Excitatory information is processed locally within L2/3 (Feldmeyer et al., 2006; Lefort et al., 2009; Avermann et al., 2012) and further spreads to infragranular layer 5A, where it reaches slender-tufted pyramidal neurons, and to layer 5B, where it reaches thick-tufted pyramidal neurons (Reyes and Sakmann, 1999; Lefort et al., 2009). Layer 5A and short L5 pyramidal neurons send projections back to L2/3 (Larsen and Callaway, 2006; Oberlaender et al., 2011). L5A also unidirectionally connect to layer 5B (Lefort et al., 2009) and both layer 5A and 5B neurons have substantial projections within their home layers.

Transmission of sensory information horizontally across barrel columns occurs to a small extent at the level of L4, where spiny neurons send axonal branches into neighboring barrels (Egger et al., 2008) while star pyramids exhibit long-range projections over several barrels (Lubke et al., 2000; Brecht and Sakmann, 2002; Egger et al., 2008). However, integration of sensory information from multiple whiskers is most preponderant in L2/3, L5 and L6. Pyramidal neurons in L2/3 send long axon collaterals within layer 2/3 and also within layer 5 (Larsen and Callaway, 2006; Bruno et al., 2009) which can depolarize several surrounding barrel columns (Petersen et al., 2003a; Adesnik and Scanziani, 2010). Slender-tufted pyramidal neurons in L5A send ascending axon collaterals to L2/3 of neighboring columns in addition to targeting their home column (Larsen and Callaway, 2006; Oberlaender et al., 2011) and layer 6A pyramidal neurons send infragranular projections across multiple columns within layer 5 and 6 (Zhang and Deschenes, 1997).

Sensory excitatory information exits the barrel field at the level of layer L2/3, where pyramidal neurons send long-distance axonal projections to ipsilateral secondary somatosensory cortex (S2), primary motor cortex (M1) as well as to contralateral primary somatosensory cortex (S1) via the corpus callosum (Petreanu et al., 2007; Aronoff et al., 2010; Chen et al., 2013; Yamashita et al., 2013). L5 is nevertheless the principal output layer of the barrel cortex, while L6 mediates mainly cortico-thalamic interactions. Intracortically, slender-tufted pyramidal neurons of sublamina of L5A project to ipsilateral S2 and M1 (Mao et al., 2011) as well as to contralateral S1 (Larsen et al., 2007), in a similar fashion as short L5 pyramidal neurons do (Le Be et al., 2007). In addition they project subcortically to the striatum (Mercier et al., 1990; Wright et al., 1999). L5B neurons project subcortically to the superior colliculus (Larsen et al., 2007), the pons (Mercier et al., 1990), the striatum (Wright et al., 1999), the trigeminal nucleus (Welker et al., 1988; Bourassa et al., 1995) as well as to the POM nucleus of the thalamus (Veinante et al., 2000; Larsen et al., 2007; Groh et al., 2008) and the zona incerta (Bartho et al., 2007). L6A neurons chiefly target the VPm and POM nuclei of the thalamus as well as the nucleus reticularis (Bourassa et al., 1995). L6B neurons are less well characterized but they have nonetheless been shown to target the POM nucleus of the thalamus (Killackey and Sherman, 2003).

In comparison to the breadth of understanding of the excitatory circuitry underlying the spread and processing of tactile information within a barrel column and across the barrel field, the existence and the fine organization of a comparable parallel network made of inhibitory neurons, as well as the interactions between the two circuits is still relatively unknown. However some basic organizational principles have started to emerge, including the specific laminar distribution of inhibitory inputs on excitatory neurons (Sun et al., 2006; Kapfer et al., 2007; Brill and Huguenard, 2009; Katzel et al., 2011), that may have significant functional contributions (Thomson et al., 2002; Kapfer et al., 2007; Helmstaedter et al., 2009a, b, c; Katzel et al., 2011).

1.2.3 L2/3 CIRCUITS AND CELL TYPES

A typical barrel column in the mouse somatosensory cortex has a diameter of 300 μm and extends through the 1-1.2 mm depth of the neocortical sheet. It contains about 6500 neurons, of which 11% are inhibitory (Lefort et al., 2009). By comparison, a typical column in the rat barrel cortex has a diameter of 400 μm and contains about 19000 neurons, of which 11.5% are inhibitory (Meyer et al., 2010b; Meyer et al., 2011). Recently it was shown that the number of neurons per rat barrel column can vary up to two fold between different columns (Meyer et al., 2013), which might explain previous quantifications reporting a smaller number of neurons per column (Ren et al., 1992; Beaulieu, 1993). As L2 and L3 have no distinguishable cytoarchitectonic organization in the rodent somatosensory cortex, they are commonly considered as a combined entity that is referred to as L2/3. Within L2/3, excitatory synapses strongly outnumber inhibitory ones, with 89% of synapses being excitatory and 11% being inhibitory (DeFelipe et al., 2002). Although much less numerous, the role of inhibitory synapses in shaping the temporal and spatial representations of the sensory signal from its arrival from the thalamus to its exit towards other neocortical areas is fundamental.

L2/3 neurons receive synaptic inputs from diverse intra and extra-columnar origin as well as from distant cortical areas. Individual L2/3 excitatory neurons are locally interconnected (Reyes and Sakmann, 1999; Holmgren et al., 2003; Feldmeyer et al., 2006; Lefort et al., 2009; Hooks et al., 2011) and receive significant excitatory input from L4 (Feldmeyer et al., 2002; Shepherd and Svoboda, 2005; Bureau et al., 2006; Lefort et al., 2009) and from layer 5A (Shepherd and Svoboda, 2005; Bureau et al., 2006; Lefort et al., 2009). Their sole source of transcolumar excitation is from L2/3 and L5A of neighbouring columns (Bureau et al., 2006; Adesnik and Scanziani, 2010). Similarly their main inhibitory input originates locally (Kapfer et al., 2007; Katzel et al., 2011), though significant contribution also comes from L4 and to a smaller extent from L1 (Chu et al., 2003; Katzel et al., 2011). Individual L2/3 inhibitory neurons, which are highly diverse, display a cell-type specific pattern of excitatory inputs, with principal contributions from L2/3, L4 and L5 (Helmstaedter et al., 2008; Xu and Callaway, 2009). In a similar fashion, their stronger source of inhibition originates from within layer 2/3, whereas inhibition from L4, L5 and L1 varied between cell types (Xu and Callaway, 2009; Jiang et al., 2013). In addition to these inputs originating within the barrel cortex, L2/3 neurons

also receive long-range projections from M1 (Petreanu et al., 2009), contralateral barrel cortex (Petreanu et al., 2007) and to a lesser extent from the thalamus (Petreanu et al., 2009). L2/3 neurons are therefore well suited to process sensory information arising from the lemniscal and paralemniscal pathways as well as to integrate it over multiple ipsilateral and contralateral columns. In addition, L2/3 is also one of the entry points within S1 of the vibrissae motor-related information arising from M1.

1.2.3.1 Excitatory neurons

In contrast to L4, which contains a mixture of three types of morphologically distinct excitatory neurons – spiny stellate neurons, star pyramids and pyramidal neurons – L2/3 contains only pyramidal neurons. Deeper L2/3 excitatory neurons display the typical pyramidal neuron morphology, with a triangular-shaped soma and a vertically oriented principal dendrite, void of proximal branches, i.e. an apical dendrite (DeFelipe and Farinas, 1992). More superficial L2/3 excitatory neurons have a very short apical dendrite, often non-vertical and branching proximally, which gives them a more star-like shape (Lubke et al., 2003; Feldmeyer et al., 2006). L2/3 neurons send axon collaterals within L2/3 as well as to L5, which can course across several neighboring barrels. More superficial neurons also send axon within L1, which can as well propagate outside of the home barrel column (Gottlieb and Keller, 1997; Feldmeyer et al., 2006). In addition to axonal projections restricted to S1, some L2/3 excitatory neurons send long-range axons to S2 or M1 (Yamashita et al., 2013). L2/3 excitatory neurons are mainly of the regular spiking (RS) subtype (Contreras, 2004). In response to long depolarizing current injections, they show obvious initial spike-frequency adaptation in vitro (Chagnac-Amitai and Connors, 1989; Connors and Gutnick, 1990; Agmon and Connors, 1992) and in vivo (Higley and Contreras, 2003). L2/3 excitatory neurons' receptive fields (RF), as defined by all the vibrissae whose deflection triggers a change in the membrane potential of the neuron, exhibit narrow suprathreshold RFs but broad subthreshold RFs, and which are broader than those observed in L4 spiny neurons (Armstrong-James et al., 1992; Moore and Nelson, 1998; Brecht and Sakmann, 2002; Brecht et al., 2003; de Kock et al., 2007). During wakefulness, L2/3 excitatory neurons show two general types of fluctuations of their subthreshold membrane potential, which are correlated with the presence or absence of whisking activity. In the absence of whisking activity, their membrane potential displays slow oscillations (see Section 1.3.1), which are converted into a more desynchronized activity together with a more depolarized and varying membrane potential upon whisking. Interestingly the low rate (< 2 Hz) of spontaneous action potential firing is unaffected by the change in whisking behavior (Crochet and Petersen, 2006; Poulet and Petersen, 2008).

1.2.3.2 Inhibitory neurons

L2/3 contains a large diversity of inhibitory neurons types that have become an intense area of recent investigation (Petilla Interneuron Nomenclature et al., 2008; DeFelipe et al., 2013). Conventionally, neocortical inhibitory neurons are identified through their morphology (dendritic structure and postsynaptic compartment targeted by the axon), their gene expression pattern (for instance: ion

channels, receptors, calcium-buffer proteins, neuropeptides), as well as through their electrophysiological properties (for instance: passive membrane properties, action potential shape, firing pattern in response to current injection) (Cauli et al., 1997; Markram et al., 2004; Burkhalter, 2008; Gentet, 2012). Based on their molecular marker expression, nearly 100% of L2/3 barrel cortex inhibitory neurons can be assigned to one of three non-overlapping classes (Figure 1.3) (Lee et al., 2010; Rudy et al., 2011).

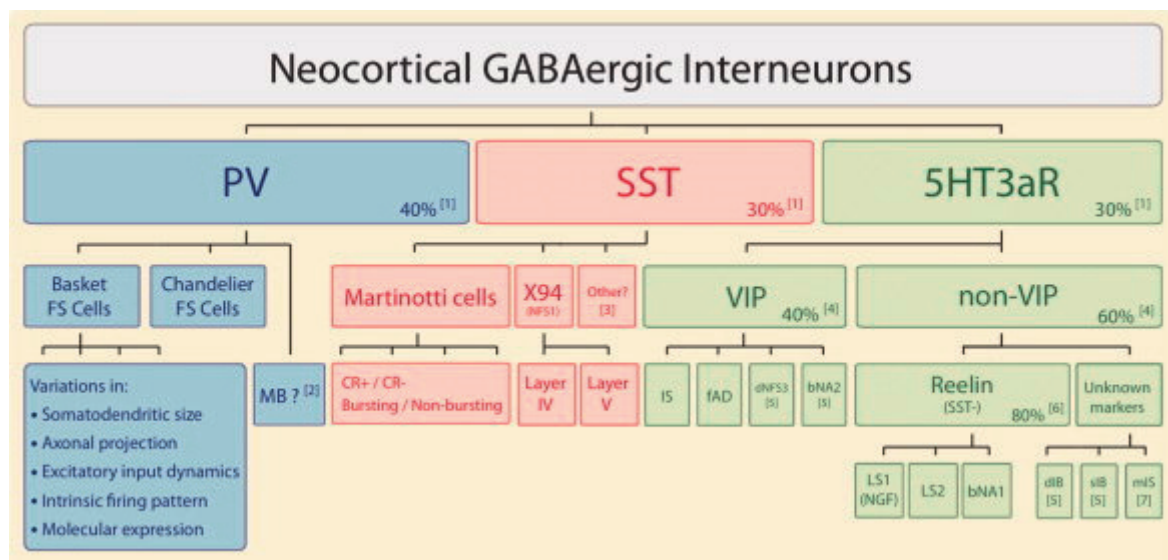


Figure 1.3 Classification of neocortical inhibitory neurons. (From Rudy et al., 2011)

The first class accounts for 30% of the total L2/3 GABAergic population and contains parvalbumin-expressing (PV) inhibitory neurons, which can further be subdivided into two main groups, according to their characteristic axonal morphologies: basket cells (Wang et al., 2002) and chandelier cells (Somogyi et al., 1982). Basket cells are named according to their particular basket-like innervation of the somas of their postsynaptic targets, while chandelier cells derive their name from their distinctive axonal terminations, which resemble the candlesticks of a chandelier and which target the axon initial segment of their postsynaptic targets. Basket cells and chandelier cells are thus the key mediators of perisomatic and axo-axonic inhibition, respectively. It is worth noting that depending upon the membrane potential of the postsynaptic neuron, chandelier cells may have an excitatory effect on excitatory neurons (Szabadics et al., 2006; Woodruff et al., 2011). Electrophysiologically, PV-expressing inhibitory neurons, irrespective of whether they are basket or chandelier cells, exhibit a typical fast-spiking (FS) behavior. Their action potential has a very short duration, due to fast repolarization and short afterhyperpolarization. In addition, upon current injection they can sustain very high frequency of firing without accommodation (McCormick et al., 1985).

The second class of L2/3 barrel cortex inhibitory neurons, which amounts to 20% of the total L2/3 inhibitory neuron population, contains somatostatin-expressing (Sst) inhibitory neurons. Sst

neurons are a diverse population at many levels. Morphologically, certain Sst neurons send an ascending axon to L1 with extensive horizontal axonal branching within L1, where they can target distal dendrites of excitatory neurons (reminiscent of Martinotti cells found in L5), while others have a more localized axonal arbor restricted to L2/3 (Ma et al., 2006; McGarry et al., 2010). In addition, certain neurons have a multipolar dendritic arbor, while others display clear bipolar dendritic organization (Halabisky et al., 2006). Finally, some Sst neurons bear sparse spines on their dendrites (Oliva et al., 2000). Molecularly, Sst neurons can be subdivided according to their expression of the calretinin protein (Xu et al., 2006). Electrophysiologically, in response to positive current injection, Sst neurons display a regular spiking behavior with various levels of accommodation (Halabisky et al., 2006). A subset of them also shows typical I_h current-mediated sag and low-threshold (LTS) spiking behavior, at the beginning and termination of negative current injection respectively (Xu et al., 2006). They consistently exhibit high input resistance and rather depolarized resting membrane potential in vitro (Fanselow et al., 2008) and in vivo (Gentet et al., 2012).

The third and largest class of inhibitory neurons accounting for 50% of the GABAergic neurons of L2/3 encompasses an even larger variety of molecular, electrophysiological and morphological cell types. However, their grouping into a class distinct from PV and Sst neurons is due to the common expression of the ionotropic serotonin receptor 5HT3a (5HT3aR), which also correlates with their developmental origin (mainly from the caudal ganglionic eminence, by opposition to the medial ganglionic eminence for PV and Sst neurons (Butt et al., 2005; Miyoshi et al., 2010)). Amongst this heterogeneous population, one can distinguish bipolar/bifurcated, irregular spiking or fast-adapting, VIP-expressing neurons with an axon descending in deeper layers (Porter et al., 1998; Bayraktar et al., 2000), as well as late-spiking neurogliaform cells, targeting the somas and proximal dendrites of postsynaptic excitatory neurons (Tamas et al., 2003; Lee et al., 2010).

The receptive field of L2/3 barrel cortex inhibitory neurons has not been extensively characterized, though chandelier cells are known to have a larger subthreshold receptive field than basket cells and excitatory neurons (Zhu et al., 2004). In addition, inhibitory neurons of L4 display a larger receptive field than excitatory neurons (Bruno and Simons, 2002), which could also be the case in L2/3. During wakefulness, similarly to excitatory neurons, L2/3 PV neurons exhibit slow oscillations of their membrane potential during quiet, non-whisking, periods, whose amplitude is greatly reduced during whisking periods. However, PV neurons do not show any change in the value of their membrane potential between whisking and non-whisking episodes, though the rate of spontaneous action potentials decreases upon whisking compared to quietness (Gentet et al., 2010). The activity of L2/3 Sst neurons under wakefulness is quite distinct from PV and excitatory neurons, as it does not display marked slow oscillations during periods of behavioral quiescence. In addition, upon whisking, Sst neurons display an hyperpolarization of their membrane potential, accompanied by a decrease in action potential firing rate (Gentet et al., 2012).

1.2.3.3 Excitatory connectivity

Within L2/3 barrel cortex, connectivity is usually lower amongst excitatory neurons than between excitatory neurons and inhibitory neurons (Reyes et al., 1998; Reyes and Sakmann, 1999; Atzori et al., 2001; Thomson et al., 2002; Holmgren et al., 2003; Koester and Johnston, 2005; Feldmeyer et al., 2006; Lefort et al., 2009; Avermann et al., 2012).

The uEPSP amplitude distribution in L2/3 excitatory neurons is dominated by small inputs (0.5-1 mV) with the rare occurrence of larger inputs (~ 3 mV) (Reyes and Sakmann, 1999; Feldmeyer et al., 2006; Lefort et al., 2009). Synaptic connections between excitatory neurons are reliable and exhibit predominantly short-term depression in response to high-frequency inputs (Gil et al., 1997; Atzori et al., 2001; Holmgren et al., 2003; Feldmeyer et al., 2006). However, such short-term synaptic dynamics seems to be age-related, as recordings performed in mature brain slices have shown reduced depression, or even facilitation (Reyes and Sakmann, 1999). Synaptic contacts between pairs of excitatory neurons are rare (2-4 contacts) and mainly located on the basal dendrites (Feldmeyer et al., 2006).

Excitatory synapses targeting inhibitory neurons exhibit cell-type specificity. Notably, excitatory synapses targeting multipolar PV fast-spiking neurons are reliable and show strong short-term depression in response to high-frequency inputs (Figure 1.4C) (Reyes et al., 1998; Holmgren et al., 2003; Kapfer et al., 2007; Avermann et al., 2012). Excitatory synapses targeting bitufted Sst neurons are less reliable and display short-term facilitation (Figure 1.4B) (Reyes et al., 1998; Rozov et al., 2001a; Kapfer et al., 2007; Fanselow et al., 2008). These observations are further supported by the fact that synapses targeting Sst neurons have a lower neurotransmitter release probability than synapses targeting PV neurons (Koester and Johnston, 2005). Finally, excitatory synapses located on VIP neurons show frequency-dependent short-term depression (Rozov et al., 2001b).

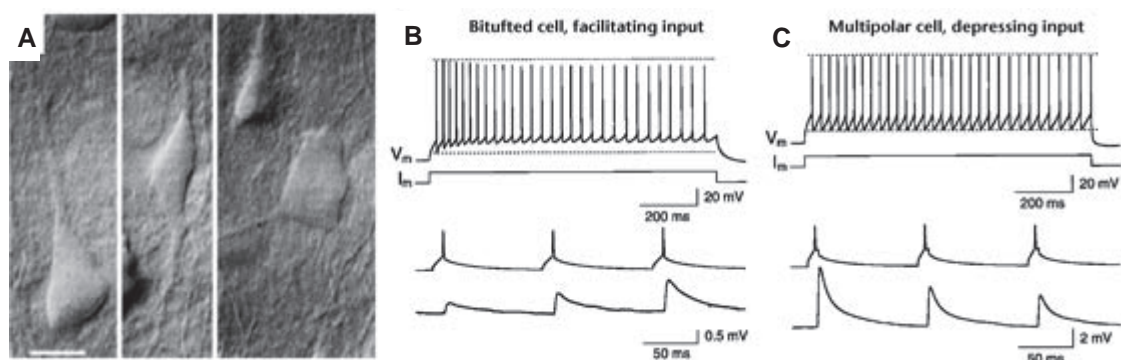


Figure 1.4 Short-term dynamics of L2/3 excitatory synapses targeting inhibitory neurons. (A) Infrared differential interference contrast video images of an excitatory neuron (*left*), inhibitory bitufted neuron (*middle*) and inhibitory multipolar neuron (*right*). (B and C) Presynaptic action potentials and associated uEPSPs evoked in bitufted and multipolar neurons during repetitive stimulation of the presynaptic excitatory neuron (*bottom*). (From Reyes et al., 1998)

1.3 PATTERNS OF CEREBRAL ACTIVITY

The first evidence that the brain was generating electrical activity came from galvanometric current measurements of rabbits and monkeys brains made by Richard Caton in 1875 (Caton, 1875). Later on, Hans Berger, applying the same recording technique to humans, realized that the cerebral activity he measured was oscillating, and that the frequency of the oscillations was correlated with the behavioral state of the subjects. When they kept their eyes closed, a slow-frequency (~10 Hz) oscillation of large amplitude was particularly prominent in the occipital region of the brain, which he named alpha-wave. In the contrary, when the subjects had their eyelids open, the cerebral activity was dominated by a more rapid fluctuation of smaller amplitude, which he defined as beta-wave (Berger, 1929). Since then, the oscillatory character of cerebral electrical activity has been documented in the brain of numerous mammalian species during wakefulness but also during sleep (Buzsaki et al., 2013). Typically, cerebral oscillations have been classified according to their frequency band, but also as a function of the behavioral or cognitive process they are correlated with or of the underlying excitatory and inhibitory cellular interactions generating them in specific part of the brain (Steriade et al., 1990; Penttonen, 2003; Buzsáki, 2006; Uhlhaas et al., 2009). Briefly and ordered from low to high frequency, one can distinguish “ultra-slow” oscillations (< 0.1 Hz), “slow” oscillations (< 1 Hz) predominant during sleep, theta oscillations (4-12 Hz), whose mechanisms are best known in the septum-hippocampus-enthorinal circuit, alpha oscillations (8-10 Hz, or 8-20 Hz in the somatosensory system, also known as μ rhythm), beta oscillations (12-30 Hz) related to aspects of the absence of movements, gamma oscillations (30-90 Hz) related to various cognitive processes and ripples (> 150 Hz). We will focus here on the slow oscillations. Not only are they a defining feature of the different sleep phases, but they are also the dominating pattern of spontaneous neocortical activity in the anesthetized state. In addition, they are particularly relevant to the rodent somatosensory cortex and related motor areas, where a similarly slow oscillation (though its frequency can extend up to ~ 4 Hz) occurs during wakefulness in periods of behavioral quiescence (Petersen et al., 2003b; Crochet and Petersen, 2006; Gentet et al., 2010; Gentet et al., 2012; Poulet et al., 2012).

1.3.1 SLOW OSCILLATIONS

Slow oscillations were first identified as a distinct rhythmic pattern in the cat neocortex (Steriade et al., 1993a; Steriade et al., 1993b, c). Under natural sleep conditions as well as under certain types of anesthesia, the electroencephalogram displayed slow (< 1 Hz) oscillations. At the single cell level, the subthreshold membrane potential of excitatory and inhibitory neurons varied between a hyperpolarized state with no action potentials and a depolarized state with significant action potential firing lasting 0.1-3s. Notably, the presence of these oscillations was independent of the presence of the thalamic afferents, though thalamic activation could transform them into faster oscillations. Comparable low-frequency oscillations of the membrane potential of individual corticostriatal neurons and striatal spiny neurons had been measured in the rat under anesthesia but also during wakefulness

(Cowan and Wilson, 1994; Wilson and Kawaguchi, 1996). From these latter studies stemmed the now widely used nomenclature of UP and DOWN states, to describe the depolarized and hyperpolarized state of the single cell membrane potential respectively.

Though such slow oscillations have been detected in a large number of species (including humans), the exact mechanism at the basis of their generation, as well as their functional role is still the subject of ongoing investigations. However, their occurrence in preparations where thalamic and callosal axonal projections are cut (Steriade et al., 1993b) as well as in slabs (Timofeev et al., 2000) or even in slices and slice cultures of neocortex in vitro (Plenz and Aertsen, 1996; Sanchez-Vives and McCormick, 2000) seems to indicate that they originate from within the neocortex. More specifically, the precise location of the oscillation source is likely to be located in infragranular layers, probably in layer 5 (Sanchez-Vives and McCormick, 2000; Chauvette, 2007; Sakata and Harris, 2009; Beltramo et al., 2013). The exact mechanism by which they occur is assumed to be due to network effects, where recurrent excitatory and inhibitory connectivity underlie the fluctuations between the UP and the DOWN state. Excitatory and inhibitory neurons, especially the fast-spiking PV inhibitory neurons, were both shown to increase and decrease their firing rate during UP and DOWN state respectively (Contreras et al., 1996; Lampl et al., 1999; Steriade et al., 2001; Timofeev et al., 2001; Cunningham et al., 2006; Haider et al., 2006; Mateo et al., 2011; Tahvildari et al., 2012), which is translated at the single cell level by a simultaneous increase of excitatory and inhibitory synaptic conductances during UP state and a simultaneous decrease during DOWN state (Destexhe et al., 2003; Shu et al., 2003; Haider et al., 2006; Rudolph et al., 2007). However, in the rodent barrel cortex, the increase of firing rate during UP state compared to DOWN state is not always accompanied by a large conductance change (Zou et al., 2005; Waters and Helmchen, 2006; Mateo et al., 2011). As transitions to UP state are therefore likely to be correlated with recurrent excitation, whose amplitude is bounded by the amount of recurrent inhibition, transition to DOWN state are underlain by disfacilitation, a form of inhibition independent of the activity of inhibitory neurons, resulting from the lack of synaptic inputs (Contreras et al., 1996; Sanchez-Vives and McCormick, 2000; Timofeev et al., 2001; Shu et al., 2003). Several mechanisms could be at the origin of the transition to the UP state (reviewed in Bazhenov and Timofeev, 2007). Spontaneous neurotransmitter release in a large population of neurons during DOWN state leading to the summation of mini-EPSP, eventually bringing the membrane potential of excitatory neurons close to spike threshold (potentially involving the activation of persistent Na^+ currents) is one of them. Homeostatic plasticity driven excitation to counterbalance the domination of the DOWN state by hyperpolarizing influences (likely mediated by K^+ currents) is another one. Finally, intrinsically bursting layer 5 neurons could be lead to burst firing during DOWN state via the induction of a hyperpolarization-activated cation current, I_h . In comparison, the mechanisms at the origin of the termination of the UP state are less understood. Initially, synaptic depression as well as intrinsic cellular events such as activation of Na^+ or Ca^{2+} -dependent K^+ currents were thought to be at the origin of the cessation of action potential firing, leading to a decrease in synaptic inputs (Bazhenov

et al., 2002; Compte et al., 2003). However, these processes are highly cell or synapse-dependent, and are therefore likely to happen at different times in different neurons, which is in opposition to the very synchronous termination of UP states observed in vivo (Volgushev et al., 2006), therefore suggesting a possible network mechanism involved in the return to the DOWN state. Alternatively, GABA_B receptors mediated slow inhibition has been found to be critical in the termination of the UP state (Mann et al., 2009).

Functionally, the occurrence of such periods of high neuronal activity interspersed with moments of complete quiescence has been related to memory consolidation phenomena, known to occur during certain phases of sleep (Ji and Wilson, 2007). As the UP state of the slow oscillations resembles the active state of the neocortex during wakefulness (Steriade et al., 2001; Destexhe et al., 2007; Constantinople and Bruno, 2011), it might be involved in the replay of information having been processed during wakefulness (Destexhe et al., 1999). In anesthetized animals, UP and DOWN states are known to modulate synaptic transmission (Crochet et al., 2005; Crochet et al., 2006; Reig and Sanchez-Vives, 2007), the active nature of dendritic integration (Waters and Helmchen, 2004), as well as sensory responses to external stimuli (Petersen et al., 2003b; Sachdev et al., 2004; Bruno and Sakmann, 2006; Haider et al., 2007; Hasenstaub et al., 2007; Reig and Sanchez-Vives, 2007).

1.4 RATIONALE AND AIMS OF THE PHD THESIS

Most of the knowledge about neocortical functional connectivity and the physiology of neocortical synaptic transmission has been obtained from measurements performed in vitro in acute brain slices (Yamamoto and McIlwain, 1966; Edwards et al., 1989) using diverse techniques including electrophysiological and optical means of presynaptic neuron stimulation and postsynaptic potential or postsynaptic action potential recording (reviewed in Thomson and Lamy, 2007).

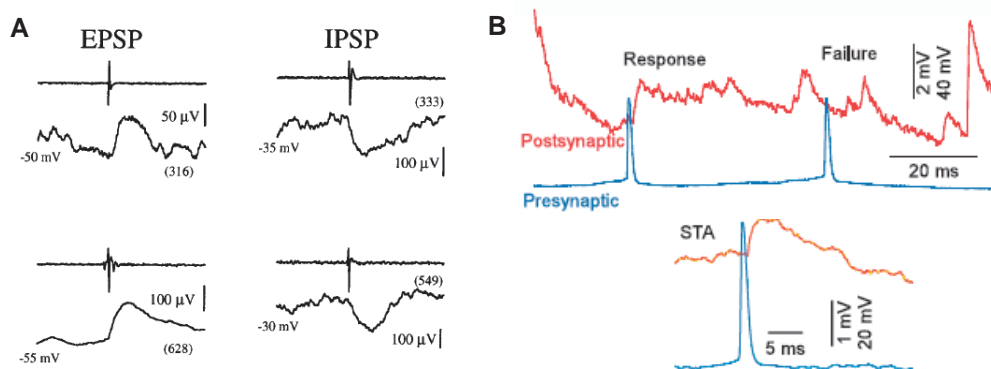


Figure 1.5 In vivo postsynaptic potentials. (A) Mean excitatory postsynaptic potentials (EPSP) (*left*) and mean inhibitory postsynaptic potentials (IPSP) (*right*). (Modified from Matsumura et al., 1996) (B) Simultaneous dual intracellular recording of presynaptic excitatory action potentials (blue) and membrane potential of postsynaptic neuron (red) (*above*). Mean excitatory postsynaptic potential (orange) (*bottom*). (Modified from Crochet et al., 2005)

Applying such techniques to the quantification of neocortical synaptic transmission *in vivo* has proven challenging, mainly due to the thickness of the intact neocortical tissue and to breathing and movement-related motion. Less than a handful of studies have therefore successfully been able to directly investigate synaptic transmission in the intact neocortex. The first one was performed in the motor cortex of the anesthetized or awake macaque monkey (Matsumura et al., 1996). Excitatory and inhibitory synaptic transmission was measured by using a combination of extracellular recordings to register action potential timing of individual presynaptic neurons with intracellular recordings of putative postsynaptic neurons (Figure 1.5A). The second one investigated excitatory synaptic transmission in L2/3 of the parietal cortex of the cat kept under anesthesia, by blindly targeting dual intracellular recordings to neurons identified through their electrophysiological properties (Figure 1.5B) (Crochet et al., 2005). Finally a more recent study reported some data about neocortical excitatory synaptic transmission between L4 and L2/3 excitatory neurons of the visual cortex of the cat kept under anesthesia using dual whole-cell patch-clamp recordings (Yu and Ferster, 2013). Though these initial studies provided a first insight about the physiology of synaptic transmission in the intact neocortex, they often lacked a rigorous identification of the recorded pre- and postsynaptic neurons. In addition, due to blind targeting of the electrophysiological recordings and therefore to the heterogeneity of the type of synapses investigated, the number of sampled putative connections was not always optimal to estimate synaptic connectivity. Lastly, the lack of comparable measurements performed *in vitro* within the same neocortical area and between the same neuron types made it sometimes difficult to assess the relevance of the *in vivo* findings.

The first aim of this thesis was thus to implement a method allowing reliable and repetitive measurement of synaptic transmission between identified neuron types *in vivo*. The second aim was to apply it to some defined synapses (excitatory synapses) in order to characterize synaptic connectivity and the physiology of synaptic transmission in a localized and anatomically definite neocortical area. The last aim was to investigate the influence of spontaneous network activity, to which individual pre- and postsynaptic neurons are exposed *in vivo*, on synaptic transmission.

CHAPTER 2: MATERIALS AND METHODS

All experiments were carried out with 4-8 week old female and male PV-IRES-Cre (Hippenmeyer et al., 2005) or Sst-IRES-Cre (Taniguchi et al., 2011) mice crossed with CAG-Lox-STOP-Lox-tdTomato (Ai9) reporter mice (Madisen et al., 2010) (referred to as PV-tdTomato and Sst-tdTomato in the rest of the text) in accordance with protocols approved by the Swiss Federal Veterinary Office.

2.1 ANIMAL IMPLANTATION

To allow localized, reproducible and stable measurements, animals were routinely implanted with a small light-weight head-holder directly on their skull. During surgery, animals were kept under constant 1-2% isoflurane anesthesia while body temperature was monitored and maintained at 37°C using a heating system (FHC), and eye ointment (Viscotears, Alcon) was applied to prevent dehydration and irritation. To diminish post-operative pain, animals were injected with Carprofen (0.3 ml at 0.5 mg/ml, i.p.) (Rimadyl, Pfizer) at the beginning of the surgery and ibuprofen (2.5 ml at 20 mg/ml) (Algifor, Vifor) was added to the drinking water (250 ml) of their home cage for two subsequent days. Skin was cut above the skull, uncovering both cerebral hemispheres as well as the cerebellum. Connective tissues were scraped off and adhesive (Loctite, Henkel) was applied over the bone. A custom-made aluminum head-holder (Figure 2.1A) covering the cerebellum and part of the right cerebral hemisphere was then glued to the skull. Finally, dental cement (Paladur, Heraeus Kulzer) was added to embed part of the holder and to create a recording chamber (Figure 2.1B). A silicone elastomer (Kwik-Cast, WPI) was used to temporarily fill the chamber and protect the exposed skull while animals were returned to their home cages.

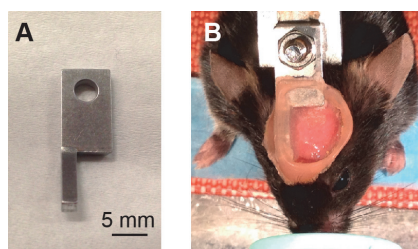


Figure 2.1 Implantation for head-fixation. (A) Custom-made, light-weight aluminum head-holder. (B) Anesthetized head-fixed mouse with head-holder glued directly to the skull, embedded in dental cement to create a recording chamber (pink).

2.2 INTRINSIC SIGNAL OPTICAL IMAGING (ISI)

Most of the electrophysiological measurements were targeted to the C2 column of the left barrel cortex. Its location was mapped by imaging the intrinsic signal elicited on the cortical surface following a repeated deflection of the corresponding right C2 whisker (Masino et al., 1993). The nature of the local intrinsic signal is thought to be multifaceted. At least three different sources have been identified, whose contributions can be isolated to some extent due to the wavelength of the light

chosen for imaging (Grinvald et al., 1986; Pouratian, 2002). The first component underlying the local intrinsic signal is a change in blood volume. An increase in neuronal electrical activity is thought to drive recruitment of the local capillaries and blood vessel dilation leading to a decrease in light reflectance, best measured at 550 -570 nm wavelengths. The second component is a change in hemoglobin oxygenation level. Increased local neuronal electrical activity, and thus local metabolism is thought to lead to a biphasic change in deoxyhemoglobin concentration (a fast initial increase followed by a slow decrease). Imaging at wavelengths at which deoxyhemoglobin light absorbance is significantly higher than oxyhemoglobin light absorbance, i.e. between 600 and 630 nm, is thought to resolve this process. The third component is a change in the brain tissue's light scattering properties. Electrical neuronal activation is thought to correlate with cellular, extracellular and vascular morphological changes leading to an overall decrease in light reflectance. Though such light scattering occurs at every imaging wavelength, it can be best imaged at wavelengths above 630 nm, where deoxy- and oxyhemoglobin absorbances are negligible.

ISI was performed either following implantation or immediately before performing craniotomy. Animals were maintained under light 0.5-1% isoflurane anesthesia, while body temperature was monitored and maintained at 37°C, both of which were critical factors for obtaining an intrinsic signal. ISI was carried out through the intact glue-covered skull, with the dental cement chamber filled with warmed Ringer's solution (in mM: 135 NaCl, 5 KCl, 5 HEPES, 1 MgCl₂, 1.8 CaCl₂, pH 7.3) and covered by a coverslip (#1 thickness, Menzel-Gläser). All whiskers but C2 whisker were trimmed at their base. C2 whisker was inserted in a small glass capillary attached to a piezo bender actuator (PL127.11, PICMA, PI Ceramic), which was driven in the antero-posterior direction at a repetition frequency of 10 Hz. Intrinsic signal was acquired at 10 Hz by a CMOS camera (PhotonFocus) coupled to a binocular stereomicroscope (Leica MZ9.5) with a magnification of 3.2x corresponding to a field of view of 3.5 mm x 3.5 mm (1024 x 1024 pixels).

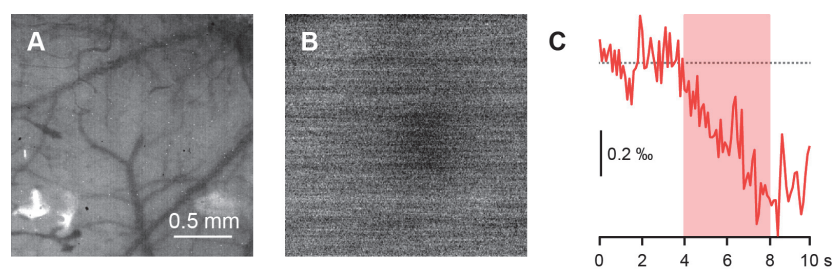


Figure 2.2 Intrinsic signal optical imaging. (A) 525 nm illumination allows imaging of the cortical blood vasculature pattern, used as reference for further targeted surgery and recordings. (B) Mean intrinsic signal averaged over 6s of C2 whisker stimulation imaged at 630 nm representing a relative decrease in light reflectance in the C2 area (darker pixels). (C) Time course of the relative intrinsic signal, during baseline (0-4s) and whisker stimulation (4-10s).

Constant illumination for functional imaging was provided by 630 nm LEDs (KingBright), while 525 nm LEDs (Kingbright) were used to obtain a reference image of the blood vasculature pattern (Figure 2.2A). Image acquisition was controlled by a custom-made script running under LabView (National Instruments). Intrinsic signal was estimated by averaging responses from 7 trials of whisker

stimulation, delivered with an inter-trial interval of 30 s. Each trial lasted 10 s and consisted of 4 s of baseline with no whisker stimulation, 4 s of whisker stimulation and 2 s with no stimulation. Relative change in light reflectance was computed by subtracting the mean reflectance value averaged over the baseline period (R_0) from the reflectance value measured during whisker stimulation (R) and dividing the difference by the mean baseline reflectance ($(R-R_0)/R_0$) (Figure 2.2B and C).

2.3 CRANIOTOMY AND DUROTOMY

To gain physical access to the cortex, the skull and dura mater need to be removed above the location of the C2 barrel column. Craniotomy and durotomy were performed under similar anesthesia conditions as during implantation. To keep the skull constantly moist, the dental cement chamber was filled with warmed Ringer solution, which was removed just before drilling of the skull and was re-applied afterwards. A dental drill (EXL-M40, Osada) was used to thin the bone over a 0.5-1 mm circular area. The thinned bone was perforated at the edge of the craniotomy with a small needle (30 gauge, BD Biosciences) and the loose bone flap was removed. To remove the dura mater, a slit was made parallel to the direction of its main fibers by cutting it with a small needle. Both sides of the slit were pushed apart as much as necessary to uncover cortical tissue.

2.4 IN VIVO SINGLE-CELL ELECTROPORATION

In order to gain control of the action potential firing of a single L2/3 barrel cortex excitatory neuron in vivo, we applied the previously described method of DNA delivery to single neurons by electroporation (Haas et al., 2001; Bestman et al., 2006; Kitamura et al., 2008; Judkewitz et al., 2009) to deliver channelrhodopsin-2 (ChR2) encoding gene to a single excitatory tdTomato-negative cell per animal. Applying an electrical field to a lipid bilayer, such as the one constituting the cellular membrane of neurons, is known to make it permeable to a wide range of normally impermeable large, lipophilic or charged molecules, such as dyes, proteins, oligonucleotides, RNA and DNA. The microscopic mechanism underlying the lipid bilayer permeabilization process is usually assumed to be the creation of transient nanopores in a restricted portion of the cell membrane, through which molecules can passively diffuse or migrate via electrophoresis (Neumann et al., 1982; Ho and Mittal, 1996; Escoffre et al., 2009). Though this mechanism seems to hold true for the transfection of small oligonucleotides of a few base pairs, larger DNA plasmids appear to penetrate the cell cytoplasm by a different and slower process likely involving endocytosis. During electrical field application, DNA plasmids are electrophoretically transported towards the cell membrane, where they possibly aggregate. Upon termination of the electrical stimulation, they seem to stay for several minutes at the surface of the cell membrane, before being internalized (Golzio et al., 2002; Rathenberg et al., 2003).

Electroporation was performed through a craniotomy with an intact dura mater under 1-1.5% isoflurane anesthesia with body temperature control. A localized electrical field was delivered between

an Ag/AgCl wire enclosed in a glass micropipette placed in close contact with the cellular membrane of the neuron soma to be transfected. Micropipettes had a resistance of 10-17 M Ω and a tip diameter of \sim 1 μ m and were made of borosilicate capillaries (OD = 2 mm, ID = 1.16 mm, Hilgenberg) using a P-97 puller (Sutter Instrument). A ground Ag/AgCl pellet electrode (WPI) was positioned in the Ringer filled dental cement chamber. A pulse generator (Axoparator 800A, Molecular Devices) was used to deliver a train of 50 square voltage pulses (-12 V, 0.5 ms) at 50 Hz. Micropipettes contained the same solution as used for whole-cell patch-clamp recordings (see Section 2.5.2), to which Alexa 488 dye (50-100 μ M) (Invitrogen), pCAG-eGFP (100 ng/ μ l) (Addgene plasmid #11150)(Matsuda and Cepko, 2004) and pCI-hSynapsin-ChR2(E123T/T159C) (200 ng/ μ l) (kindly provided by Thomas Oertner) (Berndt et al., 2011) DNA plasmids were added. Positive pressure was applied to the micropipettes while they were advanced through the dura mater and lowered to L2/3 under visual control with a two-photon microscope (Prairie Technologies) (see Section 2.5 for microscope details) (Figure 2.3A). Through the diffusion of the micropipette internal solution into the extracellular space, tdTomato-negative cells appeared as dark shadows over a brighter background, which allowed their targeting in a similar fashion as performed during “shadowpatching” (Figure 2.3B) (Kitamura et al., 2008). Successful electroporation resulting in DNA plasmid expression occurred in 80-90% of the cases and was correlated with an immediate filling of the targeted neuron soma with Alexa 488 dye (Figure 2.3C), whose fluorescence stayed constant upon retraction of the micropipette. Depth as well as the antero-posterior and medio-lateral location of the neuron targeted for electroporation were measured before the craniotomy was covered with silicone elastomer (Kwik-Cast, WPI) and animals returned to their home cage for about 24 hours to permit sufficient levels of ChR2 protein and eGFP expression.

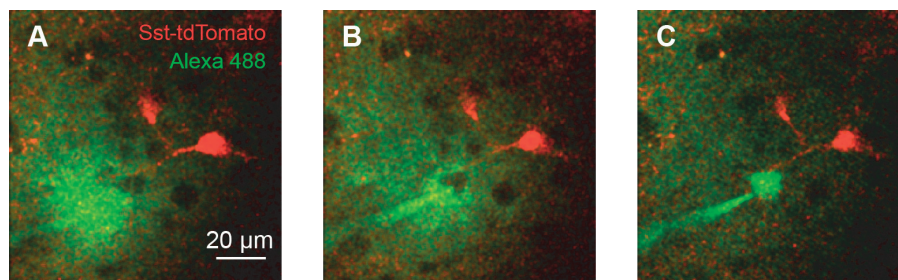


Figure 2.3 In vivo single-cell electroporation. (A) Micropipette containing ChR2- and eGFP-encoding plasmid DNAs as well as Alexa 488 dye is advanced through the brain under visual control with 2-photon microscope. (B) Due to the diffusion of Alexa 488 in the extracellular space, non-tdTomato-expressing neurons appear as dark shadows over a brighter background, which allows their specific targeting. (C) Upon application of a train of voltage pulses locally rendering the neuron membrane permeable, Alexa 488 dye immediately penetrates into the neuron’s soma and processes, followed by plasmid DNAs.

In a subset of initial experiments, DNA plasmids encoding different ChR2 variants, such as wild-type ChR2 (pCI-CMV-ChR2-EYFP (80-160 ng/ μ l), kindly provided by Michael Häusser), H134R mutant (pcDNA3.1-CMV-hChR2(H134R)-EYFP (200 ng/ μ l), Addgene plasmid #20940) (Zhang et al., 2007), T159C mutant (pCI-hSynapsin-ChR2(T159C) (200 ng/ μ l) or E123T/T159C mutant (pCI-hSynapsin-

ChR2(E123T/T159C) (200 ng/ μ l)) both kindly provided by Thomas Oertner) (Berndt et al., 2011) were introduced into individual excitatory neurons by electroporation in order to test for their ability to control action potential firing upon light stimulation.

2.5 IN VIVO ELECTROPHYSIOLOGICAL RECORDINGS

Around 24 hours after electroporation, animals were placed under 1-1.5% isoflurane anesthesia and the craniotomy was uncovered in order to remove all or part of the dura mater according to the procedure detailed in Section 2.3. This step was critical in order to visually target and obtain patch-clamp recordings in the whole-cell configuration. All recordings were performed under 0.8-1.5% isoflurane anesthesia under visual guidance with two-photon microscope (Prairie Technologies). Femtosecond pulsed infrared excitation light at the wavelength of 880 nm was generated by a MaiTai laser (SpectraPhysics) and focused into the brain via a 40x/0.8NA water immersion objective (Olympus). Backscattered infrared light was prevented from hitting the photomultiplier tubes (PMTs) by an E650SP filter (Chroma Technology). A dichroic mirror (575 nm) followed by band pass filters split emitted fluorescence into a red (607 ± 22.5 nm) PMT channel and a green (525 ± 35 nm) PMT channel. The location of the electroporated neuron was identified by the blood vasculature pattern and its excitatory nature was confirmed by its overall morphology and the presence of numerous dendritic spines. All recorded signals were amplified by a Multiclamp 700B amplifier (Axon Instruments), Bessel filtered at 10 kHz and digitized at 20 kHz by an ITC-18 (Instrutech Corporation) under the control of a custom program written on IgorPro (Wavemetrics).

2.5.1 TARGETED JUXTACELLULAR RECORDINGS

In order to measure action potential firing of the ChR2-expressing neurons in response to light stimulation, juxtacellular recordings (Pinault, 1996, 2011) were targeted to the ChR2-expressing neurons under visual control with two-photon microscope. Glass micropipettes with a resistance of 4-6 M Ω were made in the same way as for electroporation. They were filled with Ringer's solution (in mM: 135 NaCl, 5 KCl, 5 HEPES, 1 MgCl₂, 1.8 CaCl₂, pH 7.3), to which 10-25 μ M Alexa 594 dye (Invitrogen) was added.

2.5.2 TARGETED WHOLE-CELL PATCH-CLAMP RECORDINGS

To measure intracellular membrane potential of putative postsynaptic neurons, we performed targeted whole-cell recordings from tdTomato-expressing interneurons, non-tdTomato-expressing (putative excitatory) neurons (Margrie et al., 2003; Komai et al., 2006; Kitamura et al., 2008). A small number of ChR2-expressing excitatory presynaptic neurons were also recorded in the whole-cell configuration to control for any effect of ChR2 (or eGFP) expression on their basic electrophysiological properties. Glass micropipettes with a resistance of 5-7 M Ω were prepared in the same way as for electroporation. They contained an intracellular solution made of (in mM): 135 potassium gluconate, 4 KCl, 10

HEPES, 10 sodium phosphocreatine, 4 MgATP, 0.3 Na₃GTP (adjusted to pH 7.3 with KOH), to which 25-75 μM Alexa 488 dye and 3 mg/ml biocytin (Biotium) were added. All measurements were made in current-clamp mode and junction potentials were not corrected. When current was injected into the cell to measure input resistance or rheobase firing, series resistance subtraction was performed offline (see Section 2.9.2).

2.5.3 LOCAL FIELD POTENTIAL RECORDINGS

In most of the experiments, local field potential (LFP) was recorded with 2-4 MΩ glass micropipettes filled with Ringer's solution containing 10-25 μM Alexa 594 dye. Micropipettes tip was located at a depth of 150-250 μm from the pia mater and at less than 250 μm away from the area where the ChR2-expressing neuron was located.

2.6 OPTOGENETIC STIMULATION

Channelrhodopsin-2 is a cation permeable blue-light sensitive protein naturally expressed in the unicellular algae *Chlamydomonas reinhardtii*. It is part of the opsins family, which contains seven transmembrane domains proteins, whose functioning depends upon the covalent binding of the cofactor retinal, a vitamin-A derivative. Upon light exposure, photon absorption will induce retinal isomerization, which will lead to conformational changes in the opsin. Notwithstanding the opsin being an ion channel like ChR2, an ion pump (bacteriorhodopsins, halorhodopsins, sensory rhodopsins), or a G-protein-coupled receptor (eukaryotic opsins), retinal-induced changes in conformation will eventually trigger an ion flux across the cellular membrane it is embedded in, leading to a wide range of possible physiological processes (Fenno et al., 2011; Yizhar et al., 2011). ChR2 can be functionally expressed in mammalian neurons in vitro and in vivo, whereupon blue light stimulation leads to rapid and repeated action potential firing (Boyden et al., 2005; Li et al., 2005; Arenkiel et al., 2007). Several mutations have progressively been introduced into the wild type ChR2 gene in order to change protein expression level, channel current amplitude and kinetics, ion selectivity as well as light absorption spectrum (reviewed in: Fenno et al. 2011; Yizhar et al. 2011; Mattis et al., 2012). The E123T/T159C double mutant ChR2 protein used here is characterized by a larger steady photocurrent amplitude, a voltage-independent deactivation time constant and a smaller recovery time constant compared to wild-type ChR2 (Berndt et al., 2011; Mattis et al., 2012).

Since only one single excitatory neuron per animal was electroporated in L2/3 barrel cortex with the E123T/T159C double mutant encoding DNA plasmid, we used a 470 nm superbright LED (Luxeon, Philips) coupled to a 6° collimator (Polymer Optics) placed at the back of the two-photon 40x/0.8NA objective to generate wide field optical stimulation. The optogenetic stimulus consisted of either a single square pulse of light of 1 ms duration (11- 66 mW/mm², measured at the objective tip), delivered with an interval of 1 s, or of a 20 or 50 Hz train of five 1 ms light pulses of the same intensities, delivered with a minimum interval of 5 s under the control of a custom program in IgorPro

(Wavemetrics). In a subset of initial experiments testing the ability of different ChR2 variants to control action potential firing of excitatory neurons upon light stimulation, longer single square pulses of minimum 3 ms duration were delivered. A constant blue background illumination made of an array of 470 nm LEDs (Everlight Electronics) was placed in front of the animal during some of the recording sessions to prevent spread of direct visual cortical activation driven by the repeated light pulses.

2.7 TISSUE FIXATION AND HISTOLOGY

Following termination of the electrophysiological recordings, some animals were injected with pentobarbital (500 μ l at 7.5 mg/ml) (Esconarkon, Streuli) before transcardiac perfusion with 10 ml 0.9% saline solution followed by 70 ml 4% paraformaldehyde solution (32% solution (EMS) diluted in 0.1 M PBS). The brain was dissected out of the skull and post-fixed for 2 hours at room temperature in the same paraformaldehyde solution, which was then replaced by 0.1 M PBS. 50 μ m thick coronal sections were cut using a semi-automated vibratome (VT1000S, Leica) and rinsed 3 times (5 min / 10 min / 10 min) in 0.1 M PBS. Blocking in 10% normal donkey serum (NDS) in 0.1 M PBS for 1 hour preceded incubation with rabbit primary antibody against eGFP (1:5000, Abcam, Ab290) in a 5% NDS, 0.3% Triton-X in 0.1 M PBS solution for 24 hours at room temperature. Sections were rinsed 4 times (1 min / 5 min / 10 min / 10 min) and incubated with donkey anti-rabbit secondary antibody coupled to Alexa 488 (1:200, Invitrogen) and streptavidin coupled to Alexa 647 (1:2000, Invitrogen) in a 3% NDS, 0.3% Triton-X in 0.1M PBS solution for 4 hours at room temperature. Sections were rinsed in 0.1 M PBS 4 times again (1 min / 5 min / 10 min / 10 min) and incubated for 15 min in a 1:500 DAPI (AppliChem) solution in 0.1 M PBS before a final rinse (5 min / 5 min / 5 min). Sections were subsequently mounted in DABCO-based mounting medium on SuperFrost slides (Menzel-Gläser), covered with a coverslip (0.17 \pm 0.01 mm thickness, Hecht) and sealed with nail polish. Immunostaining against eGFP enhanced fluorescence of the ChR2- and eGFP-expressing excitatory presynaptic neuron in order to visualize fine axonal branches. Streptavidin-Alexa 647, through binding of biocytin, revealed the morphology of the recorded postsynaptic neuron. Sections were imaged with a laser scanning confocal microscope (LSM 700, Zeiss) equipped with an oil-immersion 40x/1.3NA objective. Images were visualized and adjusted for brightness and contrast with ImageJ.

2.8 MORPHOLOGY RECONSTRUCTION

A subset of the best-stained ChR2-biocytin neuron pairs were imaged at a high resolution with an oil-immersion 63x/1.4NA objective (voxel size: 0.12 μ m x 0.12 μ m x 1 μ m) using the same laser scanning confocal microscope as described in Section 2.7. Fluorescent image stacks from one to three 50 μ m sections were used as a basis for three-dimensional reconstruction of axon and dendrites in NeuroLucida (MBF Bioscience).

2.9 DATA ANALYSIS

Data analysis was carried out in IgorPro (Wavemetrics) and Matlab (Mathworks), and statistical analysis was performed in Matlab.

2.9.1 OPTOGENETIC CONTROL OF CHR2-EXPRESSING NEURON ACTION POTENTIAL FIRING

FIRING

To assess state-specific optogenetic control of action potential firing in the ChR2-expressing excitatory neurons, UP and DOWN states were identified either directly from the juxtacellular recording (initial experiments) or using the simultaneously recorded LFP (later experiments) (Figure 2.4B).

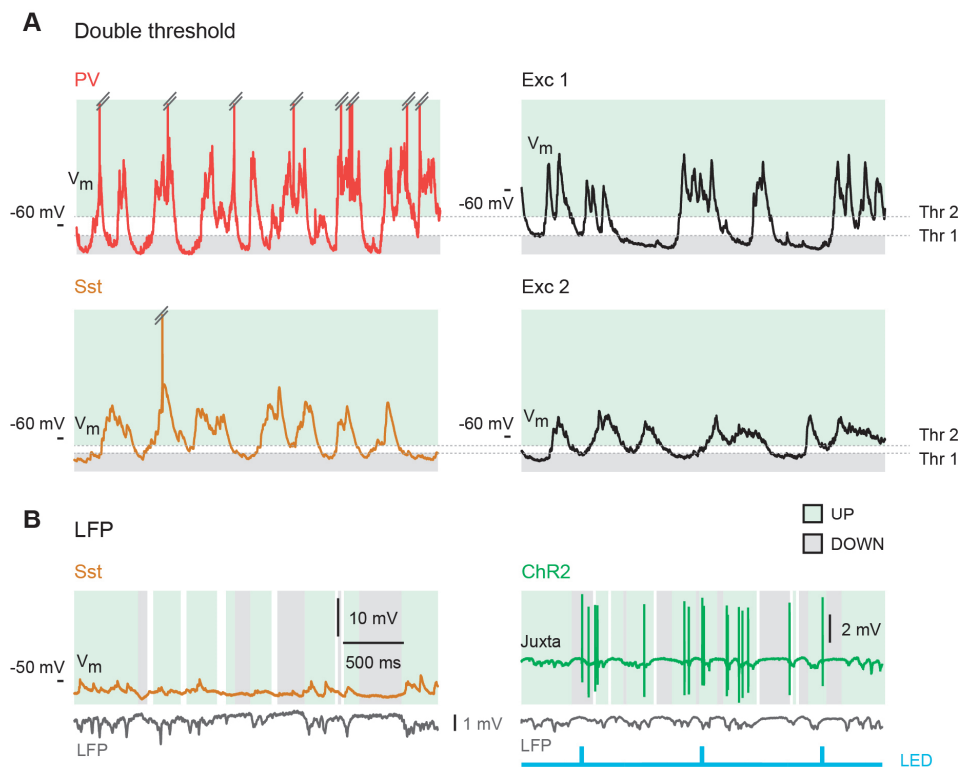


Figure 2.4 UP and DOWN state identification. (A) Double-threshold method applied on the membrane potential (V_m) of individually recorded putative postsynaptic neurons. Periods of recording where V_m is more hyperpolarized than threshold 1 (Thr 1) are classified as DOWN states, while periods of recording where V_m is more depolarized than threshold 2 (Thr 2) are classified as UP states. Different values of Thr 1 and Thr 2 are used for PV (red), Sst (brown) and excitatory neurons (black). (B) LFP (grey) frequency features-based method is used for a subset of Sst neurons displaying minimal V_m amplitude fluctuations (left) and for juxtacellular recordings of the ChR2-expressing presynaptic excitatory neuron (green) (right).

LFP was band pass filtered between 0.1 and 200 Hz and a sliding Fast Fourier Transform (FFT) (window size: 150 ms, overlap: 125 ms) was computed. Principal component analysis of the real part of the FFT followed by a Gaussian mixture model were used to extract and classify the twenty-five most relevant LFP frequency features of each window into three clusters, corresponding to UP, DOWN and transitions between these two states. An optogenetic stimulus was considered as occurring during DOWN state if the window before it and the second one after it were classified as belonging to

the DOWN cluster. Similarly, a stimulus was considered as occurring during UP state if the window before it and the second one after it were classified as belonging to the UP cluster. Action potentials were regarded as light-evoked if their peak happened within 20 ms of the end of the 1 ms light stimulus. AP latency was defined as the time elapsed between light stimulus onset and action potential peak time. AP jitter was defined as the standard deviation of action potential latency. Each metric was computed separately for DOWN and UP states, apart for [Figure 3.3](#) comparing different ChR2 protein variants, where data from optogenetic stimulations across all states (DOWN, UP, transitions) were pooled together.

2.9.2 ELECTROPHYSIOLOGICAL PROPERTIES OF POSTSYNAPTIC NEURONS

Input resistance and membrane time constant (τ) were measured by repeated current injections (-100 pA, 500 ms) immediately after establishing whole-cell configuration. Average traces of membrane potential (V_m) were fitted offline with a double exponential from 0.4 ms to 50 ms after the onset of the current injection to determine and subtract the early fast component due to series resistance. Input resistance was calculated as the difference in the corrected mean V_m averaged over two 100 ms periods (one immediately before current injection and the other at the end of current injection) divided by the amount of injected current. τ was determined by fitting the V_m with a single exponential from 1 ms to 60 ms after the onset of current injection. Action potential (AP) threshold was defined as the V_m at which the slope of rise of the voltage crossed 50 V/s (Kole and Stuart, 2008). AP half-width was computed as the full width of the AP at half of its maximum amplitude measured from threshold to peak. AP peak-to-trough ratio was computed as the ratio of the peak of the voltage first derivative to the trough of the voltage first derivative. Mean V_m and V_m FFT amplitude were computed across 20 s sweeps of recording encompassing both UP and DOWN states. A median filter was applied to sweeps where APs were present before computing the FFT. Spontaneous AP rate was computed across UP and DOWN states for the whole duration of the recording. To compute V_m vs LFP cross-correlation, V_m was offset by its average value and normalized by its standard deviation, and LFP was band pass filtered between 0.3 and 200 Hz.

2.9.3 CONNECTION IDENTIFICATION

To infer a connection between a presynaptic ChR2-expressing excitatory neuron and a given putative postsynaptic neuron, postsynaptic V_m was analyzed only when the optogenetic stimulus occurred in the DOWN states. For most neurons, DOWN and UP states were identified using a double-threshold method applied directly on the membrane potential of individually recorded putative postsynaptic neurons ([Figure 2.4A](#)). For parvalbumin (PV) neurons, the two thresholds were defined as the most hyperpolarized membrane potential (V_m) value of the given recording sweep plus 5 mV, and plus 10 mV for threshold 1 and threshold 2 respectively. For somatostatin (Sst) neurons, 3.5 mV and 5.5 mV were added to the most hyperpolarized V_m value of the given recording sweep to define threshold 1

and threshold 2. PV or Sst neurons threshold values were used for non-tdTomato neurons, according to the amplitude of their UP-DOWN V_m fluctuations. An optogenetic stimulus was considered as occurring during DOWN state if both the mean V_m averaged during the 10 ms preceding light onset and the mean V_m averaged during a time window ranging from 30 to 40 ms after light onset were smaller than threshold 1. Similarly, an optogenetic stimulus was considered as occurring during UP state if both average V_m values were larger than threshold 2. A subset of Sst neurons displayed minimal spontaneous V_m fluctuations, precluding the use of the double-threshold method. In such cases, DOWN and UP state identification was performed using the simultaneously recorded LFP as described in Section 2.9.1 (Figure 2.4B).

A stimulus-triggered V_m average was obtained for all optogenetic stimuli occurring during DOWN states (PV: 56 ± 45 trials, Sst: 41 ± 28 trials, Exc: 64 ± 33 trials, mean \pm SD) and was compared with averaged spontaneous DOWN state V_m fluctuations, measured at four different time points spanning the 150 ms preceding the light stimulus. If a clear difference between the two averages was found in a given post stimulus peak-search window, then the presence of a synaptic connection was confirmed. Peak-search was set as the timing from “AP latency – AP jitter + 1 ms” to “AP latency + AP jitter + 3 ms” after light onset for PV neurons (peak-search window size: 3.2 ± 1.5 ms, mean \pm SD) and that from “AP latency – AP jitter + 1 ms” to “AP latency + AP jitter + 5 ms” for Sst and non-tdTomato neurons (peak-search window size: 4.8 ± 0.6 ms, mean \pm SD).

2.9.4 PROPERTIES OF SYNAPTIC TRANSMISSION

A stimulus-triggered V_m average was used to quantify unitary excitatory postsynaptic potential (uEPSP) amplitude and rise-time. The amplitude of uEPSP was calculated as the difference between the mean V_m averaged over a 0.5 ms window centered at the peak of the uEPSP and the mean baseline V_m averaged over a 1 ms window taken after the end of the optogenetic stimulus. The uEPSP rise time corresponded to the time elapsed from 20% to 80% of the amplitude on the rising phase of the averaged uEPSP. The uEPSP half-width and decay time constant (Tau decay) were extracted from a stimulus-triggered V_m average made of a subset of trials elicited during DOWN states, which contained no major spontaneous V_m fluctuations from 10 to 20 ms after light stimulus onset. The uEPSP half-width was calculated as the full width duration of the uEPSP at half of its maximum amplitude. Tau decay was determined by fitting a single exponential on the decaying phase of the averaged uEPSP, starting 1 ms after the peak and 2 ms after the peak for PV neurons and Sst neurons respectively.

To compute uEPSP amplitude coefficient of variation (CV) including failures, single trial uEPSP amplitude was measured as the difference between the mean V_m averaged over a 0.5 ms window centered at the peak of the uEPSP detected within the peak-search window (as described in Section 2.9.3) and the mean baseline V_m averaged over a 1 ms window taken after the end of the optogenetic stimulus. The standard deviation of a similarly computed amplitude distribution for four

DOWN state time points at which no light stimuli were applied was subtracted from the standard deviation of the obtained uEPSP amplitude distribution before dividing it by its mean in order to correct for spontaneous V_m fluctuations occurring during DOWN states (Feldmeyer et al., 1999; Lefort et al., 2009). The synaptic transmission failure rate was defined as 1- synaptic transmission success rate. Success rate was estimated by quantifying the fraction of trials occurring during DOWN state where a clear uEPSP could be visually detected within the same peak-search window as described in Section 2.9.3. An alternate value for the amplitude of the evoked uEPSP was computed as the amplitude of the mean light-evoked uEPSP response encompassing successes only.

2.9.5 SHORT-TERM SYNAPTIC PLASTICITY

To measure short-term synaptic dynamics, five photo-stimuli were applied at 20 or 50 Hz and postsynaptic V_m traces were analyzed only when all five stimuli occurred during the DOWN states. Amplitudes of uEPSPs during the stimulus train were analyzed as described in Section 2.9.4, except for the second to fifth uEPSPs in SSt neurons, where baseline V_m was extracted from the value taken by a single exponential fit of the decaying phase of the preceding uEPSP (fit start 2 ms after uEPSP peak) at the time of the current uEPSP peak.

2.9.6 STATE MODULATION OF SYNAPTIC TRANSMISSION

For UP – DOWN state comparison of uEPSP amplitude, a light stimulus-triggered average of the V_m was obtained for UP (PV: 57 ± 40 trials, Sst: 62 ± 49 trials) and DOWN (PV: 86 ± 48 , Sst: 50 ± 31 trials (mean \pm SD)) states separately. UP state trials where postsynaptic APs were present during a 30 ms (PV neurons) or a 50 ms (Sst neurons) time window starting 10 ms before light stimulus onset were omitted from the light triggered average. UP state uEPSP amplitude was computed as described for DOWN state uEPSP amplitude (Section 2.9.4). Peak-search window size was adjusted to match presynaptic ChR2-expressing neuron light-evoked action potential firing properties during UP states.

The probability of eliciting an AP in the postsynaptic neuron in response to a single optogenetic stimulus across all cortical states was computed using the same peak-search window as used for uEPSP peak detection during UP states (PV: 250 ± 125 trials, Sst: 175 ± 122 trials (mean \pm SD)).

2.9.7 INTERSOMATIC DISTANCES AND NEURON DEPTH MEASUREMENT

Euclidean distance as well as depth difference and 2D horizontal distance difference between the center of the soma of the ChR2-expressing excitatory presynaptic neuron and the center of the soma of the putative postsynaptic neuron were computed from two-photon image stacks acquired in vivo. The depth of the ChR2-expressing presynaptic excitatory neuron was recorded immediately after electroporation.

2.9.8 STATISTICAL ANALYSIS

Population data are represented as mean \pm SD, unless otherwise stated. The Wilcoxon rank-sum test was used to compare two or more groups of unpaired data. When more than two groups were compared, Bonferroni correction was applied. The Wilcoxon signed-rank test was used to compare two groups of paired data. The χ^2 test was used to assess significant differences in connectivity rate. Spearman's ρ was used to quantify monotonic correlations.

2.10 PARVALBUMIN AND SOMATOSTATIN IMMUNOHISTOCHEMISTRY

To verify the specificity of the tdTomato labeling of parvalbumin- (PV) and somatostatin-expressing (Sst) neurons in PV-tdTomato and Sst-tdTomato transgenic animals respectively, we performed immunohistochemistry against each protein individually (single immunohistochemistry) or simultaneously (double immunohistochemistry). Confocal microscope image stacks adjusted for brightness and contrast in ImageJ were used to manually quantify colocalization of tdTomato protein in L2/3 barrel cortex. Barrel cortex was identified by DAPI-stained L4 barrels or by anatomical landmarks and L2/3 was estimated as spanning 250 μ m from its border with L1. A 250 μ m x 380 μ m area in one 50 μ m coronal section out of every four was selected for counting, which ensured uniform sampling of L2/3 barrel cortex in the antero-posterior direction. This procedure resulted in 92 ± 11 (mean \pm SD) tdTomato neurons per brain being included in the analysis for PV-tdTomato mice and 58 ± 6 tdTomato neurons per brain for Sst-tdTomato mice.

2.10.1 SINGLE IMMUNOHISTOCHEMISTRY

50 μ m thick coronal sections were obtained from three 8-week old PV-tdTomato mice and three 8-week old Sst-tdTomato mice after similar perfusion, post-fixation and slicing procedures as described in Section 2.7. After initial washes in 0.1 M PBS (5 min / 10 min / 10 min), sections were blocked in 10% normal goat serum (NGS) in 0.1 M PBS for 1hr, before incubation with either rabbit primary antibody against PV (1:1000, Swant, PV28) or rat primary monoclonal antibody against Sst (1:200, Millipore, Mab354) in a 5% NGS, 0.3% Triton-X in 0.1 M PBS solution for 24 hours at room temperature. Sections were rinsed 4 times (1 min / 5 min / 10 min / 10 min) and incubated with goat anti-rabbit secondary antibody coupled to Alexa 647 (1:500, Invitrogen) or goat anti-rat secondary antibody coupled to Alexa 647 (1:500, Invitrogen) in a 3% NDS, 0.3% Triton-X in 0.1M PBS solution for 4 hours at room temperature. Sections were rinsed in 0.1 M PBS 4 times again (1 min / 5 min / 10 min / 10 min) and incubated for 15 min in a 1:500 DAPI (AppliChem) solution in 0.1 M PBS before a final rinse (5 min / 5 min / 5 min). Sections were mounted and imaged with the same laser-scanning confocal microscope and objective as described in Section 2.7.

2.10.2 DOUBLE IMMUNOHISTOCHEMISTRY

50 µm thick coronal sections were obtained from three 7-week old Sst-tdTomato mice after similar perfusion, post-fixation and slicing procedures as described in Section 2.7. After initial washes in 0.1 M PBS (5 min / 10 min / 10 min), sections were blocked in 10% normal goat serum (NGS) in 0.1 M PBS for 1 hour, before incubation with rat primary monoclonal antibody against Sst (1:200, Millipore, Mab354) in a 5% NGS, 0.3% Triton-X in 0.1 M PBS solution for 24 hours at room temperature. Sections were rinsed 4 times (1 min / 5 min / 10 min / 10 min) and incubated with goat anti-rat secondary antibody coupled to Alexa 647 (1:500, Invitrogen) in a 3% NDS, 0.3% Triton-X in 0.1M PBS solution for 4 hours at room temperature. Sections were rinsed in 0.1 M PBS four times again (1 min / 5 min / 10 min / 10 min) and incubated with rabbit primary antibody against PV (1:1000, Swant, PV28) in a 5% NGS, 0.3% Triton-X in 0.1 M PBS solution for 24 hours at room temperature. After another round of rinses (1 min / 5 min / 10 min / 10 min), sections were incubated with goat anti-rabbit secondary antibody coupled to Alexa 405 (1:200, Invitrogen) in a 3% NDS, 0.3% Triton-X in 0.1M PBS solution for 4 hours at room temperature before three final rinses (5 min / 10 min / 10 min). Sections were mounted and imaged with the same laser-scanning confocal microscope as described in Section 2.7 using either a 40x/1.3NA (multiple cells imaging) or a 63x/1.4NA (single cell imaging) oil-immersion objective. Excitation wavelength for tdTomato, Alexa 647 (for Sst) and Alexa 405 (for PV) was 555 nm, 639 nm and 405 nm, respectively. A 450 nm dichroic mirror followed by a 490 nm short pass filter were used to collect Alexa 405 fluorescence. A 500 nm dichroic mirror followed by a 505-600 nm band pass filter were used to collect tdTomato fluorescence. Alexa 647 fluorescence was collected using a 630 nm dichroic mirror followed by a 640 nm long pass filter.

CHAPTER 3: RESULTS

To study unitary excitatory synaptic transmission in the intact and spontaneously active mammalian brain, we combined optogenetics with electrophysiology. Simultaneous ChR2 protein and eGFP expression in single presynaptic excitatory neurons enabled minimally invasive and long-lasting optical control of action potential firing while at the same time providing detailed anatomical information on dendritic and axonal morphology. Postsynaptic whole-cell patch-clamp recordings allowed direct and stable measurement of spontaneous and light-evoked supra- and subthreshold membrane potential fluctuations at single cell resolution. Taking advantage of two-photon microscopy (Denk et al., 1990; Zipfel et al., 2003) together with transgenic mouse lines expressing tdTomato fluorescent protein in distinct classes of inhibitory neurons, we further enhanced the specificity of our investigations by targeting them to visually, genetically and electrically identified putative pre- and postsynaptic neurons in the upper portion of L2/3 barrel cortex of the anesthetized mouse.

On day 1 of a typical experiment, ChR2 and eGFP encoding DNA plasmids were delivered to a single L2/3 barrel cortex non-tdTomato neuron by electroporation performed under visual guidance with a two-photon microscope (Figure 3.2A and B) (see Chapter 2: Materials and Methods, Section 2.4 for details). After 24 hours (day 2), the successfully electroporated neuron was located via its strong eGFP expression, allowing confirmation of its excitatory nature by visualization of its overall dendritic morphology and the presence of numerous dendritic spines (Figure 3.2B). In a few rare cases that were not considered for subsequent analysis, the electroporated neuron proved to be non-excitatory, as was obvious mostly from its lack of dendritic spines and sometimes from its very dense axonal arbor extending within L2/3 (Figure 3.1).

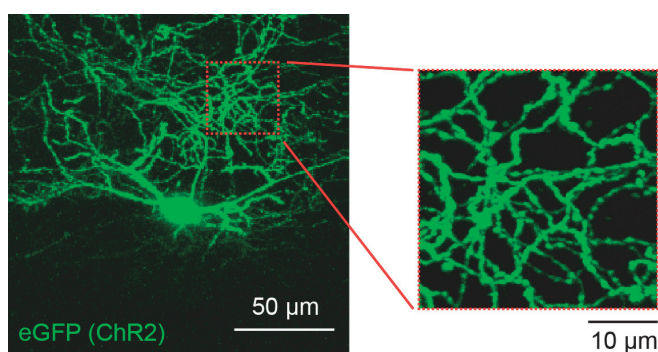


Figure 3.1 eGFP expression in a non-excitatory L2/3 neuron. In vivo two-photon image showing a putative inhibitory neuron 24 hours after electroporation of eGFP- and ChR2-encoding DNA plasmids. This particular neuron bears no obvious spines and displays a very dense local axonal arbor.

In order to investigate unitary excitatory synaptic transmission, it was critical to be able to optically elicit reliable and time-locked single APs in the ChR2-expressing excitatory neuron. We therefore performed juxtacellular recording of the ChR2-expressing neuron at the beginning of each experiment while adjusting the power of the 470 nm LED used to deliver a single 1 ms square light stimulus (see Chapter 2: Materials and Methods, Section 2.6 for details) to induce mainly single light-

evoked APs (Figure 3.2A and C). The range of light power necessary to reliably elicit single APs extended from 11 to 66 mW/mm² (mean ± SD: 30.8 ± 23.0 mW/mm²) and likely reflected different amounts of DNA plasmids transfected into the target excitatory neuron at the time of electroporation. Subthreshold membrane potential fluctuations in response to such optogenetic stimulation of the excitatory ChR2-expressing neuron delivered at 1 Hz were then sequentially recorded in whole-cell configuration in individual tdTomato-expressing inhibitory neurons (Figure 3.2A, D and E) as well as in non-tdTomato-expressing putative excitatory neurons (1 to 7 neurons recorded per experiment in total, mean ± SD: 2.5 ± 1.5).

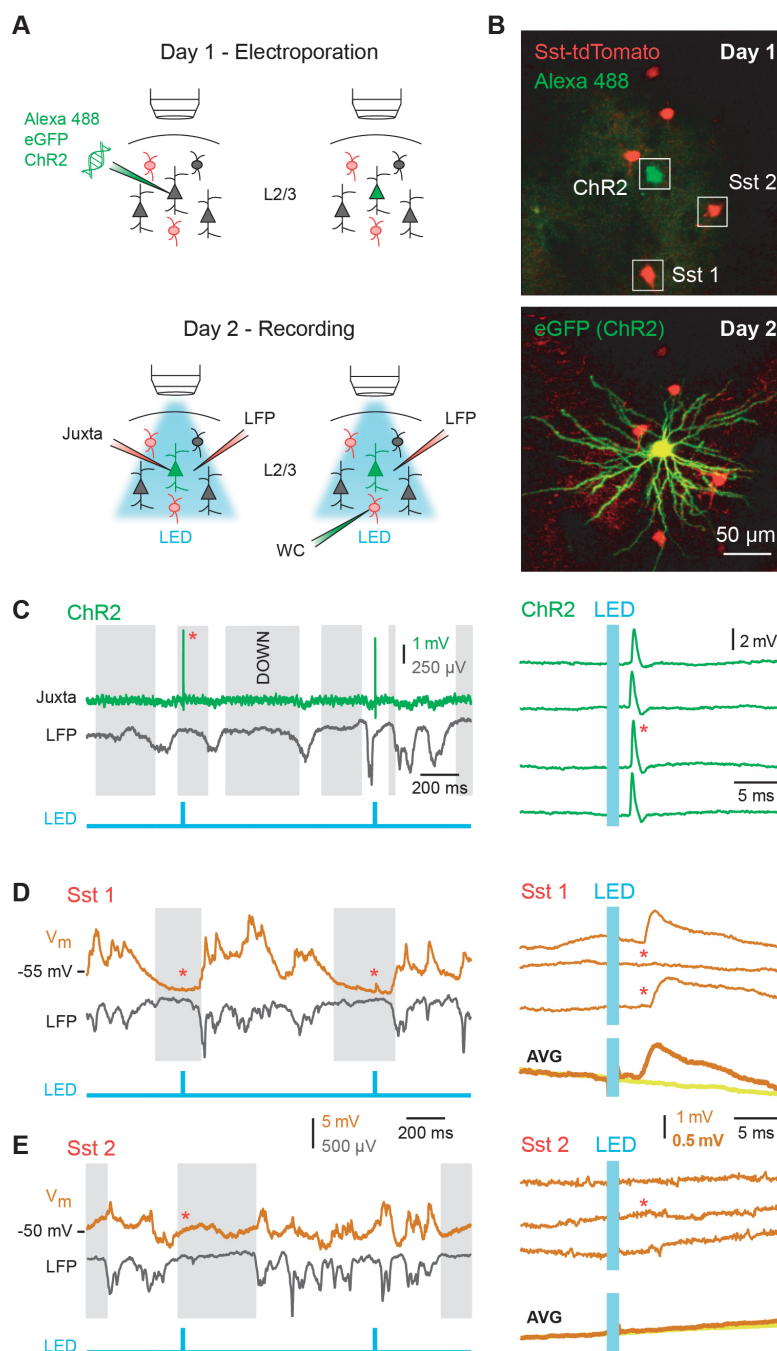


Figure 3.2 In vivo measurement of unitary excitatory postsynaptic potentials. (A) On day 1, eGFP- and ChR2-encoding DNA plasmids together with Alexa 488 dye are electroporated into a single excitatory neuron in L2/3 of the mouse barrel cortex. On day 2, juxtacellular recording of the ChR2-expressing excitatory neuron is carried out first to assess AP firing under optogenetic control. Whole-cell (WC) recordings of nearby tdTomato and non-tdTomato neurons are then performed sequentially to measure synaptic potentials. Local field potential (LFP) is recorded simultaneously. (B) Example in vivo two-photon images of a single L2/3 excitatory neuron filled with Alexa 488 dye in a Sst-tdTomato mouse taken immediately after electroporation (above) and 24 hours later showing eGFP expression in both soma and dendrites (below). (C) Juxtacellular recording of the AP firing response to a single 1 ms light pulse delivered at 1 Hz of the ChR2-expressing neuron in (B). LFP recording allowed DOWN (grey) state identification (left). A single AP is elicited with precise timing by each light pulse during DOWN states (right). (D) Whole-cell recording of a synaptically connected neuron (Sst 1 in (B)), with simultaneous LFP recording (left). Example single trial uEPSPs and synaptic failures (right, above) and average uEPSP recorded during DOWN states (right, below). Average spontaneous activity recorded during DOWN states is shown superimposed in yellow. (E) Same as (D), but for an unconnected Sst neuron (Sst 2 in (B)).

To maximize the likelihood of detecting light-evoked unitary excitatory postsynaptic potentials (uEPSPs) amongst spontaneously ongoing membrane potential fluctuations characteristic of the intact cortex, we initially restricted our connectivity analysis to periods of relative neural network quiescence (DOWN states). To infer the presence (Figure 3.2D) or absence (Figure 3.2E) of a connection between the presynaptic ChR2-expressing excitatory neuron and a given putative postsynaptic neuron we compared the mean membrane potential depolarization obtained in a defined time window after optogenetic stimulation with the average spontaneous membrane fluctuation occurring in the absence of any light stimulus (see Chapter 2: Materials and Methods, Section 2.9 for details on DOWN and UP state identification and connectivity analysis).

3.1 OPTOGENETIC CONTROL OF SINGLE EXCITATORY NEURON AP FIRING IN VIVO

3.1.1 CHR2 VARIANT SELECTION

To trigger reliable single action potentials with minimal jitter over light stimulation repetitions, we initially electroporated DNA plasmids encoding different ChR2 protein mutants in single L2/3 excitatory neurons together with an eGFP-encoding DNA plasmid. 24 hours later we performed juxtacellular recordings of the eGFP-expressing neurons while optically stimulating them with single 3 ms square pulses of blue light at maximal intensity (66 mW/mm^2), delivered at a frequency of 1 Hz. We compared four different ChR2 protein variants: wild-type ChR2 (wt), T159C single mutant (TC), E123T/T159C double mutant (ET/TC) and H134R single mutant (HR), whose gene expression was controlled by different promoters, enclosed in different DNA plasmid backbones (Figure 3.3A).

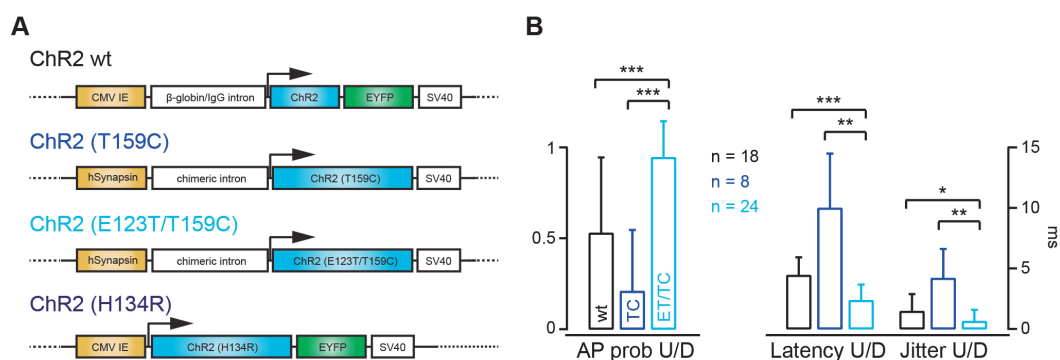


Figure 3.3 ChR2 mutants for in vivo single neuron optogenetic AP firing control. (A) Schematic of the four tested DNA plasmids encoding different ChR2 protein variants. The promoter is depicted in yellow and the origin of transcription is indicated by an arrow. (B) Light-evoked AP probability, peak latency and jitter computed across both DOWN and UP states (U/D) for an optogenetic stimulus made of a single 3 ms light pulse. ET/TC-expressing excitatory neurons display a higher probability of light-evoked AP firing and a smaller peak latency and jitter compared to wt and TC-expressing excitatory neurons. AP could not be elicited in HR-expressing excitatory neurons. Population data are represented as mean \pm SD, *** $p < 0.001$, ** $p < 0.01$, * $p < 0.05$.

A previous study has shown that when expressed under the same Camk2a promoter in lentivirus-transfected cultured hippocampal neurons, these four ChR2 protein variants displayed similar peak photocurrent amplitudes (1-1.5 nA) in response to single 1s square 470 nm light pulses. Moreover, upon stimulation with a shorter 3 ms square light pulse, wt protein and ET/TC mutants displayed a faster deactivation time constant (10-15 ms) after light stimulus offset than HR and TC mutants (> 20 ms) (Mattis et al., 2012). Under our experimental conditions, HR-expressing excitatory neurons ($n=2$) consistently failed in firing action potentials, independently of local network activity state, while TC-expressing excitatory neurons ($n=8$) fired APs with a $21 \pm 34\%$ probability and wt-expressing excitatory neurons ($n=18$) fired APs with a $53 \pm 42\%$ probability. Only ET/TC-expressing excitatory neurons ($n=24$) showed a reliable AP probability of $94 \pm 20\%$ (Figure 3.3B). Similarly, ET/TC-expressing excitatory neurons displayed the lowest AP jitter (0.6 ± 1.0 ms) and shortest AP peak latency (2.3 ± 1.3 ms) compared to excitatory neurons expressing wt or TC mutant protein (Jitter: wt: 1.4 ± 1.4 ms, TC: 4.2 ± 2.4 ms / Peak latency: wt: 4.4 ± 1.5 ms, TC: 10.0 ± 4.5 ms) (Figure 3.3B). We therefore selected the ChR2 ET/TC double mutant protein to optically control AP firing of single excitatory L2/3 barrel cortex neurons in vivo.

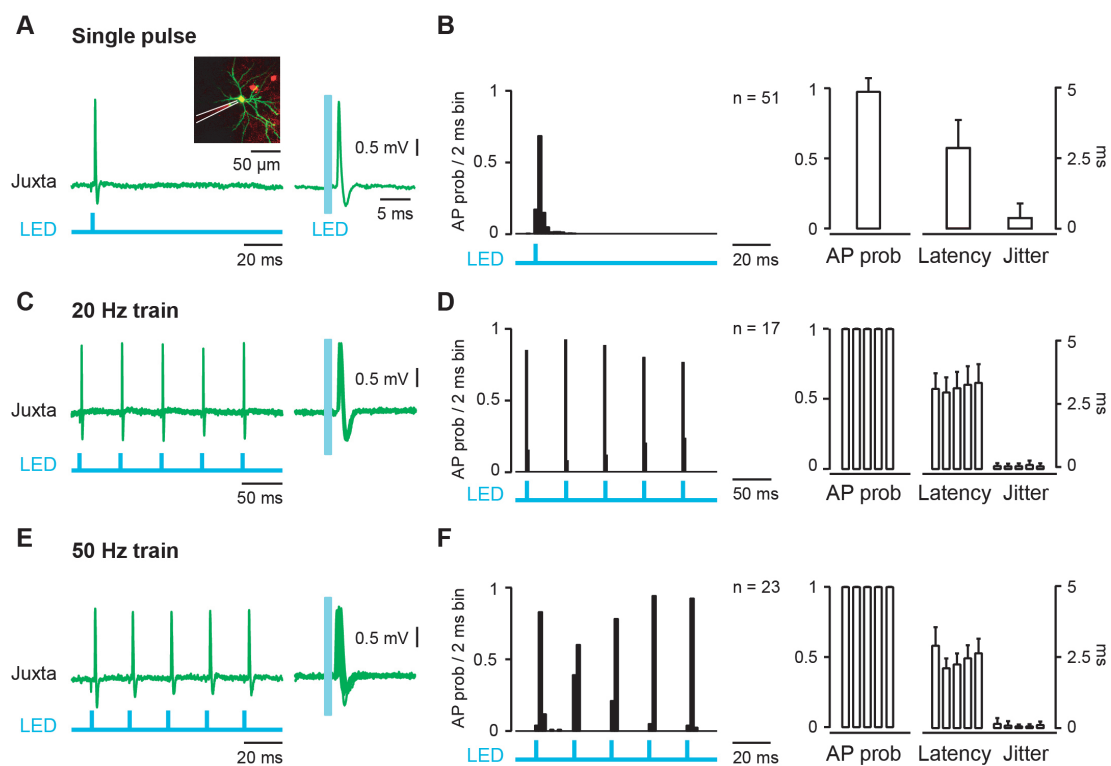


Figure 3.4 Optogenetic control of single neuron AP firing at different frequencies. (A) Example single action potential elicited by a single 1 ms light pulse recorded juxtacellularly in a L2/3 ChR2-expressing excitatory neuron. (B) Population peristimulus time histogram of light-evoked AP peak time (left) and light-evoked AP probability, peak latency and jitter (right) for an optogenetic stimulus made of a single 1 ms light pulse. (C, D) Same as (A) and (B) but for an optogenetic stimulus made of a 20 Hz train of five 1 ms light pulses. (E, F) Same as (A) and (B) but for an optogenetic stimulus made of a 50 Hz train of five 1 ms light pulses. Single 1 ms light pulse as well as 20 and 50 Hz light train elicit reliable and time-locked APs.

3.1.2 PROPERTIES OF IN VIVO LIGHT-EVOKED ACTION POTENTIAL FIRING

In order to prevent masking of putative light-evoked uEPSP in postsynaptic neurons by an artifact consistently occurring at the onset and offset of the optogenetic stimulus, we reduced the duration of the light pulse to 1 ms. In response to such brief optogenetic stimulations delivered at a frequency of 1 Hz with light intensity adjusted to elicit mainly single APs, ChR2-expressing excitatory neurons (n=51) produced APs during DOWN state with a probability of $98 \pm 9\%$, a peak latency of 2.9 ± 1.0 ms and a jitter of 0.4 ± 0.5 ms (Figure 3.4A and B). In addition, when stimulated with a 20 Hz train (Figure 3.4C and D) or a 50 Hz train (Figure 3.4E and F) of five 1 ms light pulses, ChR2-expressing excitatory neurons elicited APs with equally high probability and low jitter (20 Hz: AP probability: $100 \pm 0\%$, Jitter: 0.2 ± 0.1 ms, n=17 / 50 Hz: AP Probability: $100 \pm 0\%$, Jitter: 0.3 ± 0.1 ms, n=23).

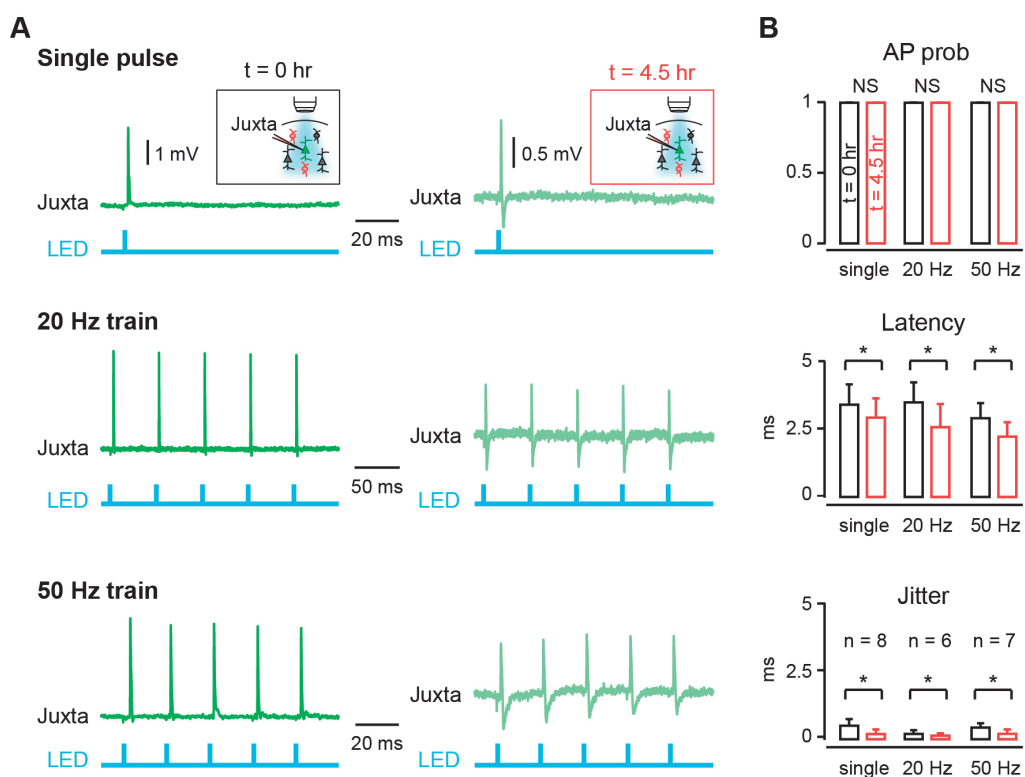


Figure 3.5 Temporal consistency of optogenetic single neuron AP firing control. (A) Example single action potentials elicited by a single 1 ms light pulse (*above*), a 20 Hz train (*middle*) and a 50 Hz train (*below*) recorded juxtacellularly in the same L2/3 ChR2-expressing excitatory neuron at the beginning (*left*) and end (*right*) of the experimental session. (B) Light-evoked AP probability, peak latency and jitter for all three types of optogenetic stimuli at the beginning (black, t=0 hr) and end (red, t=4.5 hr) of the experimental session. Probability of light-evoked AP stays constant, while AP peak latency and jitter decrease over the course of the experiment.

In a subset of experiments, we juxtacellularly recorded light-evoked APs elicited in the ChR2-expressing neuron twice, while delivering the three same types of optogenetic stimuli in order to verify the stability of the optogenetic stimulation over time. The first recording took place at the beginning of the experiment and the second at the end, after the termination of whole-cell recordings from putative postsynaptic neurons (Figure 3.5A). 4.5 hours on average elapsed between the first and

second juxtacellular recording (from 3 to 5.5 hours). Over this time period, the probability of AP firing during DOWN state in response to a single 1 ms light pulse ($n=8$) as well as to a 20 Hz ($n=6$) and 50 Hz train ($n=7$) was consistently of $100 \pm 0\%$. However, both AP peak latency and AP jitter were smaller at the time of the second recording, independently of the nature of the optogenetic stimulus (Figure 3.5B). This could be explained by a constant increase of ChR2 protein concentration in the electroporated neuron due to continuous plasmid DNA expression over the course of the experiment. In the context of synaptic connection detection and characterization, reduced jitter in presynaptic action potentials is beneficial as it minimizes potential smoothing and widening of the putative uEPSP. Also, even though the width of the uEPSP peak search window was in part based on presynaptic AP peak latency and jitter measured at the beginning of the experiment (see Chapter 2: Materials and methods, Section 2.9.3), the extent of their decrease over time (single 1 ms light pulse: AP peak latency: -0.5 ± 0.4 ms, AP jitter: -0.3 ± 0.3 ms) was much smaller than the overall window size.

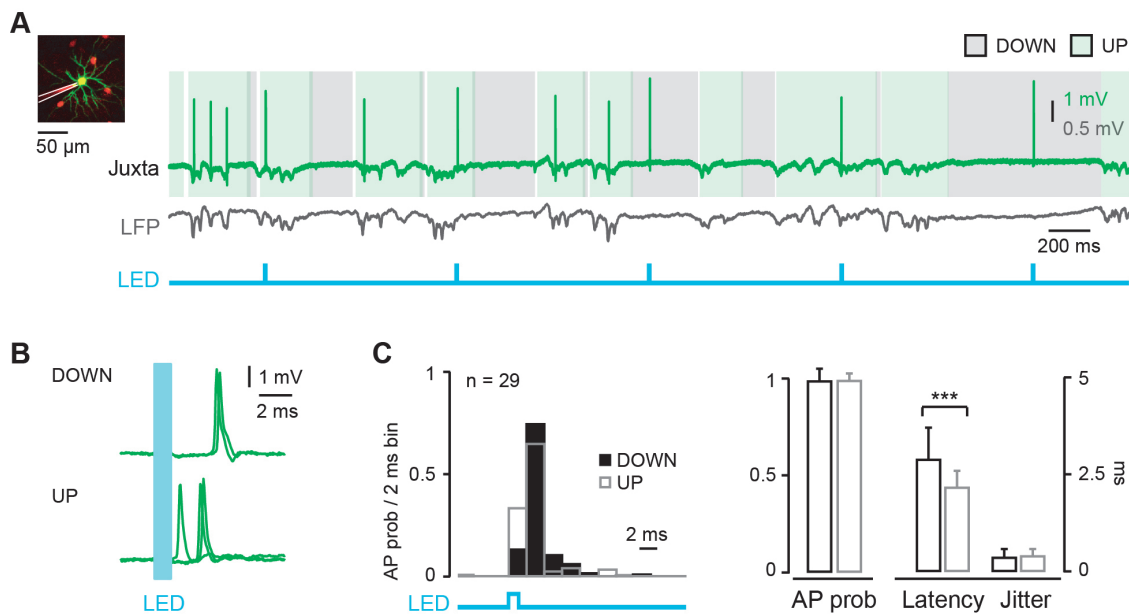
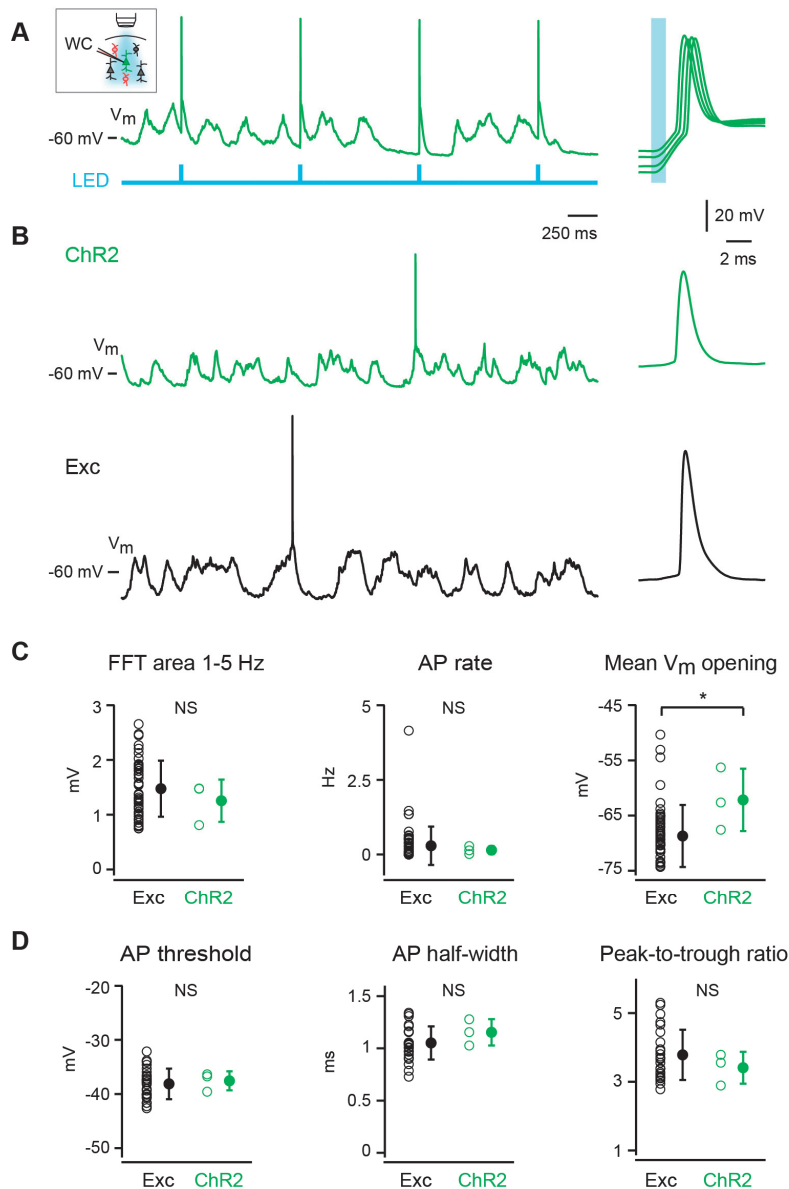


Figure 3.6 Local network state impact on optogenetic single neuron AP firing control. (A) Example action potentials elicited by a single 1 ms light pulse delivered at 1 Hz recorded juxtacellularly during DOWN (grey) and UP (green) states in a L2/3 ChR2-expressing excitatory neuron. (B) Higher magnification of the light-evoked APs shown in (A) grouped according to their occurrence during either DOWN (above) or UP states (below) (C) Population peristimulus time histogram of light-evoked AP peak time (left) and light-evoked AP probability, peak latency and jitter (right) for a single pulse optogenetic stimulus occurring in DOWN (black) and UP state (grey). Optogenetic stimuli occurring during UP state elicit APs with similar reliability and jitter compared to DOWN state. Population data are represented as mean \pm SD, *** $p < 0.001$.

After establishing the suitability of optogenetics for controlling AP generation during periods of little incoming synaptic inputs (DOWN state), we investigated the ability to elicit time-locked single APs during periods of already dense incoming synaptic inputs (UP state) (Figure 3.6A) (see Chapter 2: Materials and Methods, section 2.9 for details on DOWN and UP state identification). We found an equally high light-evoked AP probability in UP ($99 \pm 3\%$) compared to DOWN state ($99 \pm$

6%, $p > 0.05$) and equally low AP jitter (UP: 0.4 ± 0.2 ms, DOWN: 0.4 ± 0.2 ms, $p > 0.05$). The only change in the characteristics of the light-evoked APs concerns their latency, with APs occurring sooner after light stimulation in UP compared to DOWN states (UP: 2.2 ± 0.4 ms, DOWN: 2.9 ± 0.8 ms, $p < 0.001$ ($n = 29$)) (Figure 3.6B). Similar results were found in a previous study using wild-type ChR2 virally expressed in a population of excitatory neurons in L2/3 barrel cortex of mice kept under urethane anesthesia (Mateo et al., 2011).



Finally, we performed whole-cell patch-clamp recordings of ChR2-expressing excitatory neurons in order to quantify their spontaneous activity pattern as well as their action potential properties (Figure 3.7A and B). No difference was found when comparing ChR2-expressing excitatory neurons ($n=3$) with other L2/3 non-transfected excitatory neurons in the amplitude of their low-frequency oscillations or in their spontaneous AP rate, though their membrane potential just after the

establishment of the whole-cell configuration was slightly more depolarized (Figure 3.7C). Action potential threshold, half-width and first derivative peak-to-trough ratio were also similar between ChR2-expressing and wild-type excitatory neurons (Figure 3.7D). ChR2-expressing excitatory neurons are thus overall not affected by the expression of ChR2 (Boyden et al., 2005) and eGFP proteins, though more recordings could resolve the small difference ($p=0.0485$) in resting membrane potential compared to wild-type excitatory neurons

In summary, delivering ChR2 through single-cell targeted electroporation proved to be an efficient, fast, and reliable way of controlling individual L2/3 barrel cortex excitatory neuron action potential firing in vivo. Moreover, reliability and temporal precision of light-evoked single APs could be achieved for different types of optogenetic stimulations delivered at various frequencies across different levels of local network activity typical of the intact cortex.

3.2 POSTSYNAPTIC CELL TYPES

L2/3 barrel cortex putative excitatory neurons as well as parvalbumin (PV) and somatostatin expressing (Sst) inhibitory neurons were chosen as putative postsynaptic targets. We took advantage of the existence of Sst-Cre driver (Taniguchi et al., 2011) and PV-Cre driver (Hippenmeyer et al., 2005) transgenic mouse lines, which we crossed with a CAG-lox-STOP-lox-tdTomato reporter line (Madisen et al., 2010) to obtain tdTomato protein expression in Sst-expressing neurons (Sst-tdTomato mice) and PV-expressing neurons (PV-tdTomato mice) respectively. Putative excitatory neurons were non-tdTomato neurons sampled from both transgenic mice.

3.2.1 MOLECULAR SPECIFICITY OF TDTOMATO-EXPRESSING GABAERGIC NEURONS

We tested the accuracy of the tdTomato labeling of both mouse lines by performing single immunohistochemistry against either somatostatin or parvalbumin on fixed adult (7-8 weeks old) mouse brain sections (Figure 3.8A and B). In L2/3 barrel cortex of PV-tdTomato mice, colocalization of tdTomato with PV immunostain was almost complete ($95.6 \pm 7.6\%$, $n = 334$ neurons across 3 mice), while colocalization with Sst immunostain was absent ($0.8 \pm 0.7\%$, $n = 284$ cells across 3 mice) (Figure 3.8D). Although PV-tdTomato mice proved to be highly specific in labeling PV-expressing L2/3 neurons exclusively, they did not represent the whole PV-expressing neuronal population since we detected a subset ($20.0 \pm 2.9\%$) of PV-immunopositive L2/3 neurons that did not express tdTomato. In L2/3 barrel cortex of Sst-tdTomato mice, colocalization of tdTomato with Sst immunostain was $80.0 \pm 6.5\%$ ($n = 157$ cells across 3 mice), while colocalization with PV immunostain was $23.0 \pm 9.5\%$ ($n = 181$ cells across 3 mice) (Figure 3.8D). To clarify further the molecular identity of tdTomato-expressing neurons in Sst-tdTomato transgenic mice, we performed simultaneous immunohistochemistry against PV and Sst (Figure 3.8C). $68.4 \pm 1.8\%$ of tdTomato protein expression colocalized with Sst immunostain only, while $10.7 \pm 5.3\%$ colocalized solely with PV immunostain. Lastly, $9.4 \pm 3.1\%$ of tdTomato expression colocalized with both Sst and PV

immunostains and $11.5 \pm 8.2\%$ did not colocalize with any of the two markers ($n = 244$ cells across 3 mice) (Figure 3.8D).

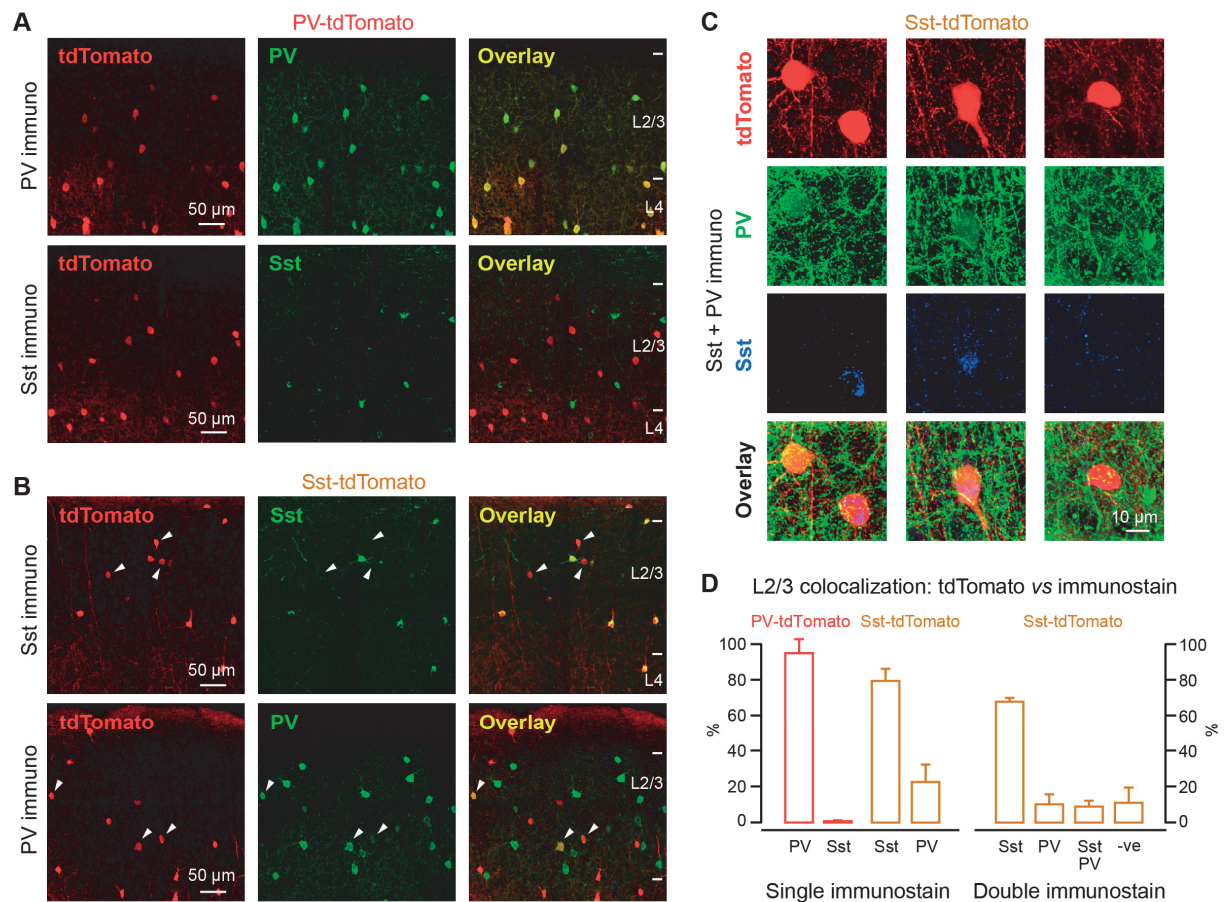


Figure 3.8 Immunostaining against PV and Sst in barrel cortex of PV-tdTomato and Sst-tdTomato adult mice. (A) Example of single immunostaining against PV or Sst (green) in barrel cortex upper layers of a PV-tdTomato mouse (red). **(B)** Same as in (A) but for a Sst-tdTomato mouse. Some L2/3 tdTomato-expressing neurons are not positive for Sst (*above*, arrows) while some L2/3 tdTomato-expressing neurons are positive for PV (*below*, arrows). **(C)** Example of double immunostaining against both PV (green) and Sst (blue) in a Sst-tdTomato mouse (red). Some L2/3 tdTomato-expressing neurons are positive only for Sst while some are positive only for PV (*left*), some are positive for both Sst and PV (*middle*) and some are negative for both PV and Sst (*right*). **(D)** Quantification of colocalization between tdTomato-protein and either or both PV and Sst immunostain in L2/3 barrel cortex of PV-tdTomato and Sst-tdTomato mice. The PV-tdTomato transgenic mouse is highly specific in labeling PV-expressing neurons. The Sst-tdTomato mouse is less specific as it labels not only Sst-expressing neurons but also PV-expressing neurons. Population data are represented as mean \pm SD.

Thus, in L2/3 barrel cortex, in addition to mostly labeling Sst-expressing neurons, Sst-tdTomato mice also showed labeled PV-expressing neurons as well as a third type of unidentified neuron expressing neither of the two markers. Similar results suggesting a lower specificity of the Sst-tdTomato mouse than initially claimed (Taniguchi et al., 2011) have recently been shown in the somatosensory cortex as well as other cortical areas; varying by different extents in different cortical areas (Hu et al., 2013; but see Pfeffer et al., 2013; Polack et al., 2013). Based on immunohistochemistry quantification, PV-expressing and Sst-expressing neuronal populations have so far been shown to be mutually exclusive in various cortical areas of the mouse brain (Kubota and Kawaguchi, 1994; Gonchar et al., 2007; Xu et al., 2010). However, *in situ* hybridization experiments have revealed that about 10% of neurons in primary somatosensory cortex are positive for both PV and Sst mRNA (Lee et al., 2010). The non-

negligible fraction of neurons positively immunostained for both Sst and PV proteins could be due to the inclusion in our analysis of low-level PV- and Sst-expressing neurons. Overall, PV-tdTomato and Sst-tdTomato transgenic mice proved to be appropriate for identifying molecularly different GABAergic neuron subtypes, though additional electrophysiological characterization helped strengthen further the classification of PV-expressing and Sst-expressing neurons into two non-overlapping groups.

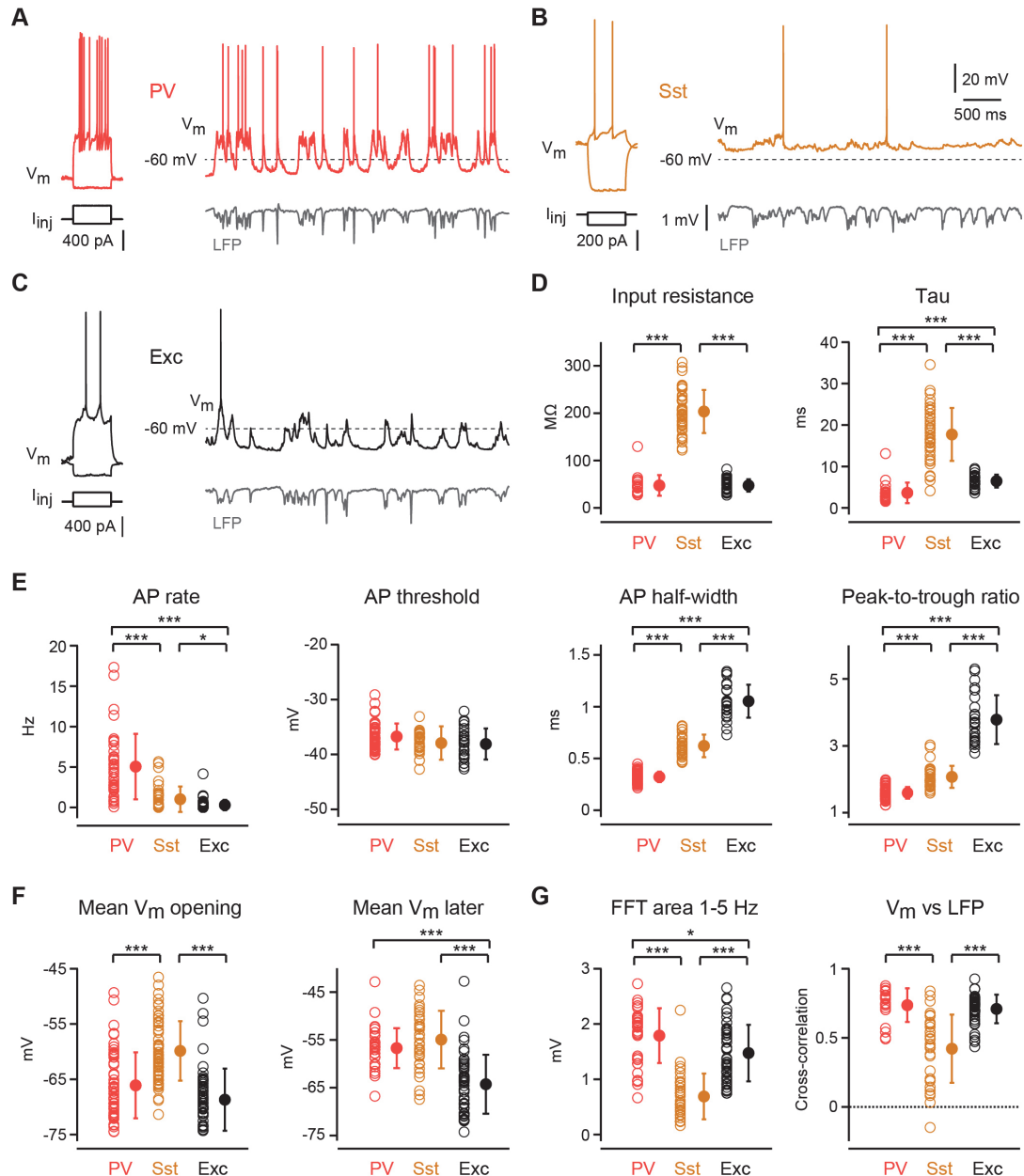


Figure 3.9 Distinct in vivo electrophysiological properties of PV, Sst and excitatory neurons in L2/3 mouse barrel cortex. (A) Example whole-cell recording of rheobase AP firing and spontaneous V_m dynamics together with LFP recording for a PV neuron. (B) Same as in (A) but for a Sst neuron. (C) Same as in (A) but for an excitatory neuron. (D) Input resistance and membrane time constant (Tau). (E) Spontaneous AP rate, AP threshold, AP half-width and peak-to-trough ratio of AP first derivative (F) Mean V_m just after establishing whole-cell configuration (left) and a few minutes into the recording (right). (G) V_m FFT integrated over the 1-5 Hz frequency band and cross-correlation between V_m and LFP at zero-time-lag. The three neuron populations display different passive membrane properties, action potential shapes and distinct spontaneous activity patterns. Population data are represented as mean \pm SD. *** $p < 0.0003$, ** $p < 0.003$, * $p < 0.017$. See also Table 3.1.

3.2.2 ELECTROPHYSIOLOGICAL PROPERTIES

We characterized in vivo passive membrane properties as well as action potential features and spontaneous membrane potential (V_m) activity of PV, Sst and putative excitatory L2/3 barrel cortex neurons by performing targeted patch-clamp recordings of tdTomato-expressing neurons and shadow patch-clamp recordings of unlabeled neurons under isoflurane anesthesia (Figure 3.9A, B and C). Under our recording conditions, Sst neurons had a larger input resistance and slower membrane time constant (τ) than PV and excitatory neurons (measured during DOWN states, (see Chapter 2: Materials and Methods, Section 2.9.2) (Figure 3.9D, Table 3.1). Action potential threshold was similar between the three cell types, while spontaneous AP firing rate, AP half-width and peak-to-trough ratio of AP first derivative were different. PV neurons displayed the highest AP firing rate, followed by Sst and excitatory neurons. They also showed the thinnest and fastest repolarizing AP, followed by Sst and excitatory neurons (Figure 3.9E, Table 3.1). Mean membrane potential was more depolarized in Sst neurons compared to PV and excitatory neurons immediately after establishing the whole-cell configuration and remained so later during the recording, when PV neurons became similarly depolarized (Figure 3.9F, Table 3.1). Finally, Sst neurons showed smaller amplitude slow-frequency oscillations in the 1-5 Hz frequency band compared to both PV and excitatory neurons, while simultaneously being less correlated with the nearby LFP (Figure 3.9G, Table 3.1). We therefore confirmed previously established differences in the in vitro (Lefort et al., 2009; Avermann et al., 2012) and in vivo electrical membrane properties as well as in vivo spontaneous patterns of activity (Gentet et al., 2010; Mateo et al., 2011; Gentet et al., 2012) between PV, Sst, and excitatory neurons of L2/3 barrel cortex.

We recorded a small fraction (3/66) of L2/3 tdTomato-expressing neurons in the Sst-tdTomato mouse exhibiting numerous spontaneous brief APs riding on large amplitude slow subthreshold membrane potential fluctuations, reminiscent of the membrane potential recorded in PV-expressing neurons (Figure 3.10A, see Figure 3.9A for comparison). These neurons (Sst*) had low input resistance (Figure 3.10B), small AP half-width and small AP's first derivative peak-to-trough ratio (Figure 3.10C). Their mean membrane potential was relatively hyperpolarized, with large amplitude 1-5 Hz frequency oscillations and high correlation with the LFP (Figure 3.10D), as measured in PV neurons. Similarly, in somatosensory cortex L3 to L5 of the same Sst-Cre driver mouse as used here crossed with a comparable CAG-floxed-tdTomato reporter (Ai14) (Madisen et al., 2010), 18% of tdTomato-expressing neurons have been shown in vitro to exhibit electrophysiological characteristics typical of PV-expressing fast-spiking neurons (Hu et al., 2013). Considering the obvious electrophysiological differences quantified between these Sst* tdTomato neurons and other L2/3 Sst tdTomato neurons in addition to the fact that immunohistochemistry revealed a subset of tdTomato neurons in the Sst-tdTomato mouse expressing PV and not Sst, we decided to exclude these particular Sst* neurons from the overall Sst population analyses. We therefore targeted our in vivo investigations

on synaptic transmission to three clearly distinct postsynaptic neuronal populations, excitatory neurons, PV neurons and Sst neurons, as identified by their chemical and electrical profiles.

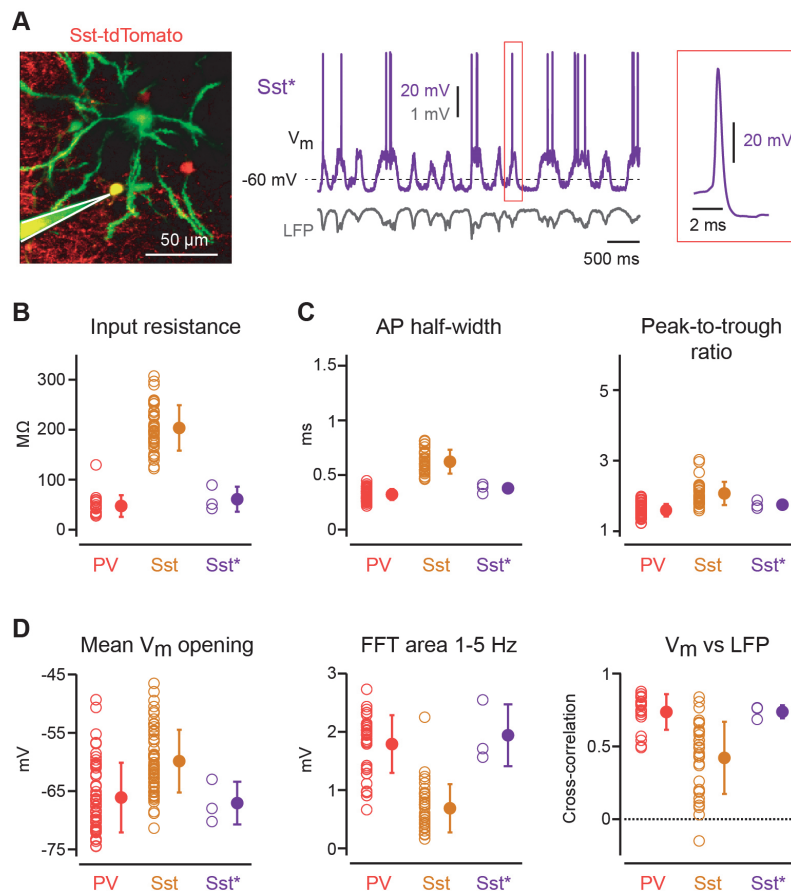


Figure 3.10 A subset of L2/3 tdTomato neurons ($n=3$) in the Sst-tdTomato transgenic mouse exhibits electrophysiological characteristics typical of PV neurons. (A) Example whole-cell recording of spontaneous V_m dynamics together with LFP recording for a tdTomato-expressing neuron in the Sst-tdTomato mouse (Sst*) showing unusual large V_m slow-wave oscillation amplitude and a relatively high firing rate with a narrow and fast AP waveform. (B) Input resistance of Sst* neurons ($n=3$) similar to the one displayed in (A) as well as of PV and Sst neurons for comparison. (C) AP half-width and AP first derivative peak-to-trough ratio. (D) Mean V_m just after establishing whole-cell configuration as well as V_m FFT integrated over the 1-5 Hz frequency band and cross-correlation between V_m and LFP at zero-time-lag. Sst* neurons exhibit electrophysiological properties different from other Sst neurons, that are more similar to PV neurons' properties. Population data are represented as mean \pm SD.

3.3 PROPERTIES OF UNITARY EXCITATORY SYNAPTIC TRANSMISSION IN VIVO

3.3.1 CONNECTIVITY RATE, CONNECTION AMPLITUDE, RELIABILITY AND KINETICS

The membrane potential of 52 PV neurons, 63 Sst neurons and 54 excitatory neurons (19 in PV-tdTomato mice, 35 in Sst-tdTomato mice) was recorded in whole-cell configuration to establish the presence or absence of postsynaptic light-evoked responses. Average light-evoked postsynaptic responses were mainly computed from single 1 ms square light pulses stimulations of the ChR2-expressing excitatory neuron, delivered at a repetition frequency of 1 Hz and selected offline for their occurrence solely during DOWN states (PV: $n = 36$, Sst: $n = 35$, Exc: $n = 54$ neurons). In a subset of putative postsynaptic neurons, average light-evoked postsynaptic responses were taken as the average response to the first pulse of a 20 or 50 Hz train of five 1 ms square pulses of light delivered at a maximal repetition frequency of 0.2 Hz and selected for their occurrence during DOWN states only

(PV: $n = 13$, Sst: $n = 26$, Exc: $n = 0$ neurons). Finally, in a few rare cases, average light-evoked postsynaptic responses were computed from responses to both types of optogenetic stimuli (PV: $n = 3$, Sst: $n = 2$, Exc: $n = 0$ neurons). The presence of a connection between neurons was inferred by comparing the average light-evoked postsynaptic response happening during DOWN state with the average spontaneous DOWN state V_m fluctuations (see Chapter 2: Materials and Methods, Section 2.9.3 for details) (Figure 3.11).

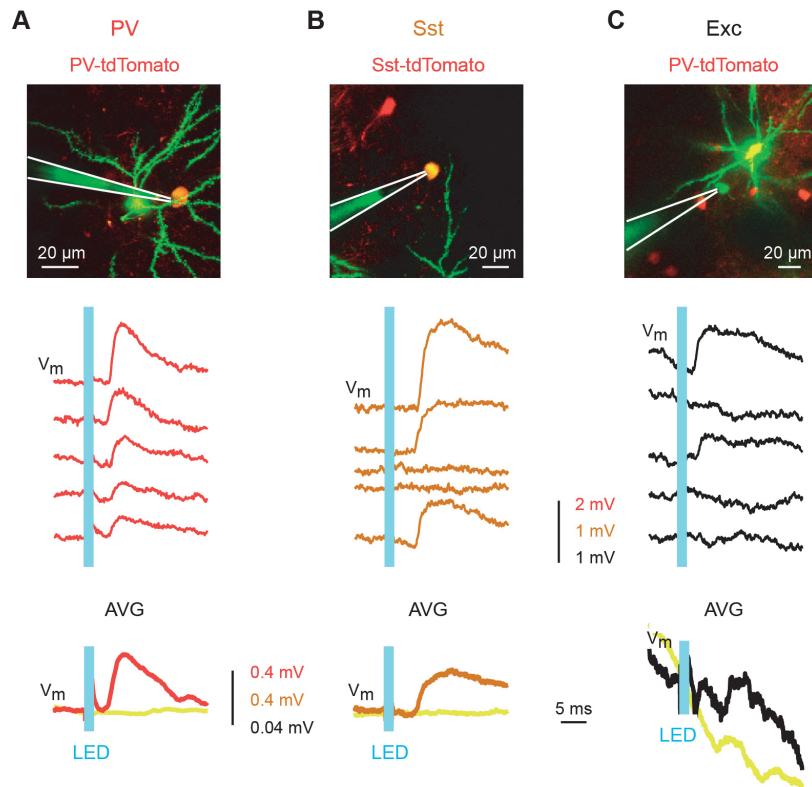


Figure 3.11 Representative light-evoked uEPSPs in postsynaptic PV, Sst and excitatory neurons in vivo. (A) Example in vivo two-photon image of a whole-cell recording pipette (Alexa 488 dye, green) targeted to a L2/3 PV neuron (yellow) in a PV-tdTomato mouse (red) with part of nearby eGFP and ChR2-expressing presynaptic excitatory neuron (above). Individual V_m responses evoked in the PV neuron during DOWN states by repeated stimulation of the ChR2-expressing neuron with a 1 ms square pulse of light. uEPSPs are visible in response to each light stimulus (middle). Average light-evoked uEPSP and average DOWN state spontaneous V_m fluctuation (yellow) (below). (B) Same as in (A) but for a postsynaptic Sst neuron. (C) Same as in (A) but for a postsynaptic excitatory neuron. Individual uEPSPs are not always elicited in response to single 1 ms light pulse stimulation in the Sst neuron and the excitatory neuron.

Light-evoked uEPSPs were detected in 25 PV neurons yielding a connectivity rate of 48% (25/52) and in 19 Sst neurons yielding a connectivity rate of 30% (19/63), both of which were larger than the connectivity rate of 7% (4/54) measured for excitatory neurons (Figure 3.12A and Figure 3.13). Overall, in vivo uEPSP size was rather small, with 74% of the light-evoked uEPSPs having amplitude smaller than 0.5 mV (PV: 64%, Sst: 82%, Exc: 100%) (Figure 3.12B and Figure 3.13). Mean uEPSP amplitude was similar in PV and Sst neurons and smaller in excitatory neurons (PV: 0.5 ± 0.4 mV ($n = 25$), Sst: 0.5 ± 0.9 mV ($n = 17$), Exc: 0.09 ± 0.07 mV ($n = 4$), PV vs Sst: $p > 0.017$, PV vs Exc: $p < 0.003$, Sst vs Exc: $p > 0.017$) (Figure 3.12C, Table 3.2). Due to the small size of uEPSPs elicited in postsynaptic excitatory neurons (max uEPSP amplitude: 0.18 mV), as well as to their small number they were not considered for further analysis.

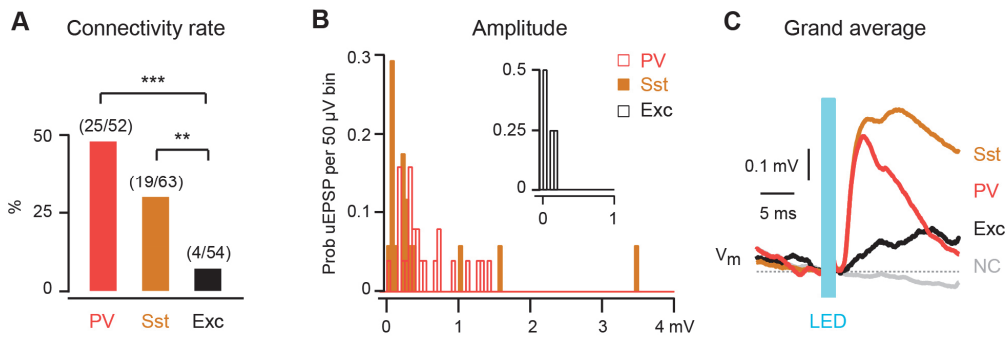


Figure 3.12. Connection probability and amplitude. (A) Connectivity rate is larger for PV and Sst neurons compared to excitatory neurons. (B) PV and Sst neurons uEPSP amplitude distribution. Inset represents amplitude distribution for excitatory neurons (C) Grand average uEPSPs computed from uEPSPs recorded in all connected PV, Sst and excitatory neurons respectively as well as from all non-connected (NC) neurons (grey). *** $p < 0.0003$, ** $p < 0.003$. See also Table 3.2.

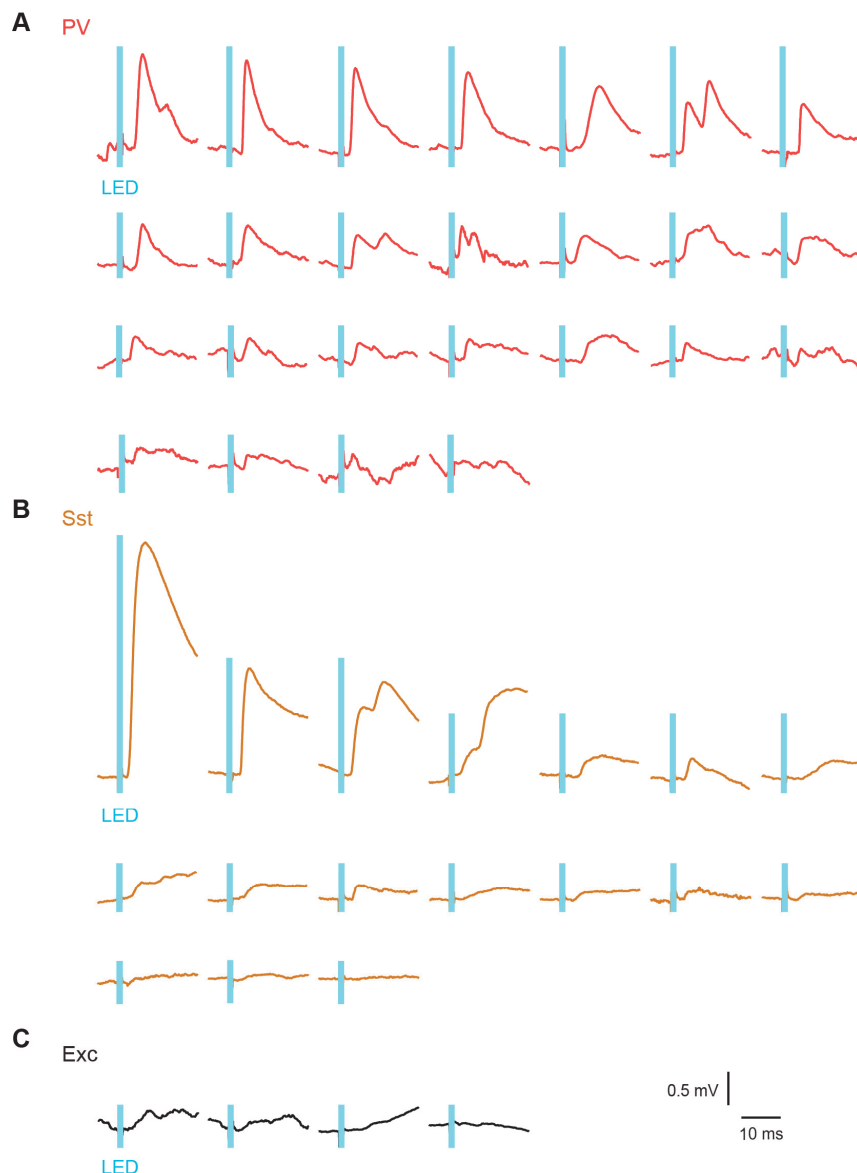


Figure 3.13 Diversity of light-evoked uEPSPs in postsynaptic PV, Sst and excitatory neurons. (A) Average DOWN state light-evoked uEPSPs recorded in 25 different PV neurons arranged in order of decreasing amplitude (B) Same for 17 Sst neurons. Average DOWN state uEPSPs from 2 connected Sst neurons are not shown here as DOWN state identification was not possible (C) Same for 4 excitatory neurons.

Individual light stimulations of the Chr2-expressing excitatory presynaptic neuron did not always elicit a uEPSP in postsynaptic connected neurons, particularly in Sst neurons (Figure 3.11B). To quantify the reliability of excitatory synaptic transmission *in vivo* we computed its coefficient of variation (CV) (Figure 3.14A, Table 3.2) as well as its failure rate (Figure 3.14B, Table 3.2) (see Chapter 2: Materials and Methods, Section 2.9.4 for details). Both CV and failure rate were larger for excitatory synaptic connections made on Sst neurons ($n = 16$) than for synaptic connections targeting PV neurons ($n = 22$) (failure rate: Sst: $68 \pm 29\%$, PV: $27 \pm 16\%$, $p < 0.001$) (CV: Sst: 0.9 ± 0.5 , PV: 0.4 ± 0.3 , $p < 0.01$), likely indicating a smaller release probability and/or smaller number of synaptic release sites. For both synapse types, failure rate was inversely correlated with the size of the uEPSP measured in the postsynaptic neuron (PV: Spearman's $\rho = -0.79$ ($p < 0.001$), Sst: Spearman's $\rho = -0.83$ ($p < 0.001$)), with large amplitude uEPSPs corresponding to low synaptic failure rates and small amplitude uEPSPs corresponding to high synaptic failure rates (Figure 3.14B). In addition, when computing an average uEPSP excluding synaptic failures, there was a non-significant trend towards smaller uEPSP amplitude for PV neurons compared to Sst neurons (PV: 0.7 ± 0.3 mV, Sst: 1.1 ± 0.8 mV, $p > 0.05$) (Figure 3.14C).

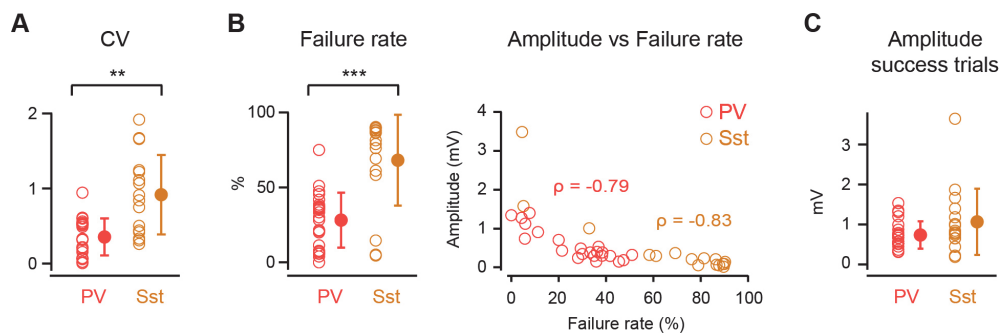


Figure 3.14 Reliability of synaptic transmission. (A) uEPSP amplitude coefficient of variation (CV) (B) Synaptic transmission failure rate. Both are larger for synaptic connections onto Sst neurons compared to synaptic connections onto PV neurons (*left*). Failure rate is anti-correlated with average uEPSP amplitude for both postsynaptic neuron types (*right*). (C) Average uEPSP amplitude excluding failures is not different between PV and Sst neurons. Population data are represented as mean \pm SD. *** $p < 0.001$, ** $p < 0.01$.

Finally we quantified uEPSP kinetics by computing uEPSP rise time (time elapsed between 20 and 80% of the peak uEPSP V_m) (Figure 3.15A, Table 3.2), uEPSP half-width (full width at half - maximal amplitude) (Figure 3.15B, Table 3.2) and time constant of the uEPSP V_m decay (Tau decay) (Figure 3.15C, Table 3.2). uEPSPs elicited in Sst neurons had a slower rise time (Sst: 1.8 ± 1.4 ms ($n=17$), PV: 0.7 ± 0.3 ms ($n=25$), $p < 0.001$), a larger width (Sst: 11.6 ± 6.7 ms ($n=13$), PV: 4.0 ± 1.4 ms ($n=24$), $p < 0.001$) and a slower decay (Sst: 16.0 ± 8.5 ms ($n=9$), PV: 5.2 ± 3.0 ms ($n=21$), $p < 0.001$) than uEPSPs elicited in PV neurons. Moreover, we observed that membrane time constant (Tau) (Figure 3.9D) was positively correlated (Spearman's $\rho = 0.63$, $p < 0.01$) with the time constant of the uEPSP V_m decay (Tau decay) across the PV and Sst neuron population (Figure 3.15D).

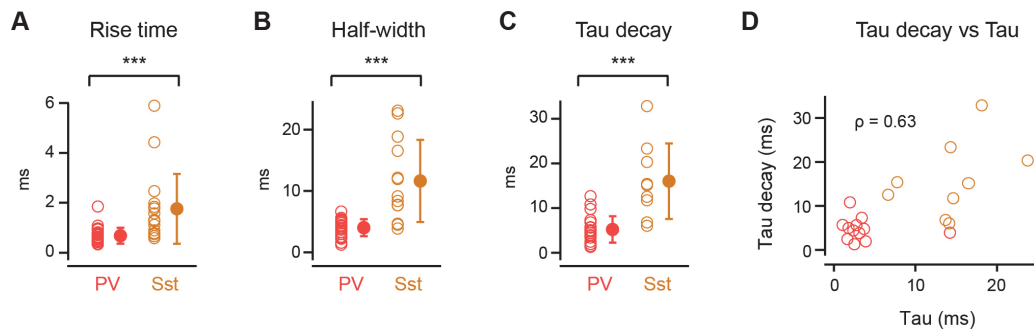


Figure 3.15 uEPSP kinetics. (A) uEPSP 20 to 80% rise time (B) uEPSP full-width at half-maximum amplitude (C) uEPSP decay time constant (Tau decay). The three metrics are larger in Sst neurons compared to PV neurons (D) Positive correlation between membrane time constant (Tau) and Tau decay. Population data are represented as mean \pm SD. *** $p < 0.001$

In summary, within L2/3 mouse barrel cortex in vivo, single excitatory neurons connected to inhibitory neurons more frequently and more strongly than to other excitatory neurons. PV and Sst interneurons received local excitatory inputs of similar amplitude, but of differing reliability and kinetics. Excitatory synaptic connections made on PV neurons had a lower failure rate and showed less trial-to-trial variability than did excitatory synapses targeting Sst neurons. Light-evoked uEPSPs occurring in Sst neurons were slower in their rising and decaying phases and had larger widths compared to uEPSPs evoked in PV neurons.

3.3.2 DISTANCE DEPENDENCE OF CONNECTIVITY

Due to intrinsic signal imaging, the majority of the presynaptic ChR2-expressing excitatory neurons and putative postsynaptic recorded neurons were located within the perimeter of the C2 barrel column. However, no post-hoc anatomical staining of the barrels was performed to further confirm the position of the pre- and post-synaptic partners of a pair relative to barrel core, wall or septa. All distances and depth quantifications were performed on two-photon fluorescence image stacks acquired in vivo. Euclidean distance between the soma of the presynaptic excitatory neuron and the soma of the postsynaptic inhibitory neuron was similar for PV ($68 \pm 25 \mu\text{m}$, range: 30-122 μm , $n = 47$) and Sst neurons (67 ± 27 , range: 18-117 μm , $n = 61$) ($p > 0.05$). We found no differences between the intersomatic distances of connected (C) and unconnected pairs (NC), neither for PV (C: $65 \pm 28 \mu\text{m}$ ($n = 21$), NC: $71 \pm 23 \mu\text{m}$ ($n = 26$), $p > 0.05$), nor for Sst neurons (C: $57 \pm 27 \mu\text{m}$ ($n = 19$), NC: $71 \pm 27 \mu\text{m}$ ($n = 42$), $p > 0.05$) (Figure 3.16A). When considering only connected pairs, no correlation existed between intersomatic distance and uEPSP amplitude for either PV (Spearman's $\rho = -0.05$, $p > 0.05$), or for Sst neurons (Spearman's $\rho = -0.003$, $p > 0.05$) (Figure 3.16B). Presynaptic ChR2-expressing excitatory neurons were located at depths ranging from 130 to 250 μm from the pia (mean \pm SD: $186 \pm 26 \mu\text{m}$), while recorded putative postsynaptic Sst neurons were located more superficially compared to PV neurons (Sst: $165 \pm 30 \mu\text{m}$, PV: $192 \pm 36 \mu\text{m}$, $p < 0.001$), probably owing to their natural spatial distribution in the Sst-tdTomato and PV-tdTomato transgenic mice respectively.

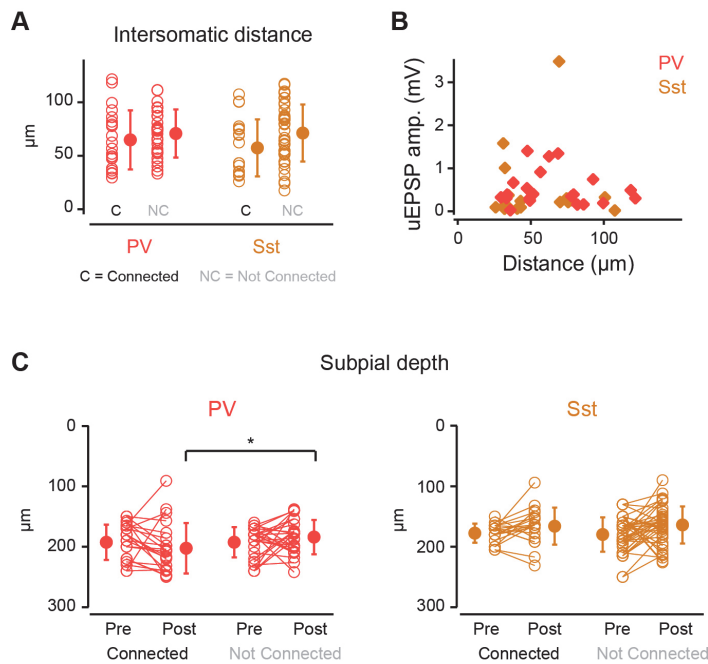


Figure 3.16 Link between pre- and postsynaptic neuron location and synaptic connectivity. (A) Intersomatic distance between connected (C) and unconnected (NC) pairs of neurons is not different, neither for PV, nor for Sst neurons. (B) No correlation exists between uEPSP amplitude and the intersomatic distance between connected pairs. (C) Subpial depth for both the pre- and postsynaptic neurons of a pair. No difference in depth is observed between presynaptic neurons that are part of a connected pair and presynaptic neurons that are part of an unconnected pair. Depth of postsynaptic Sst neurons is not different in connected pairs compared to unconnected ones, but connected PV neurons are located more deeply within L2/3 than unconnected PV neurons. Population data are represented as mean \pm SD. * $p < 0.05$.

No difference was measured between the depth of presynaptic neurons when comparing connected versus unconnected pairs, independently of the postsynaptic neuron type. However, a depth difference was found for postsynaptic PV neurons that was absent for the Sst neurons, with connected PV neurons being deeper than unconnected ones (C: $203 \pm 42 \mu\text{m}$, NC: 184 ± 28 , $p < 0.05$) (Figure 3.16C). In conclusion no connectivity principle could be established based solely on the absolute and relative positions of the pre- and postsynaptic neuron somas, though such an organizational principle was showed to exist in layer 5 of the mouse visual cortex in vitro (Kozloski et al., 2001).

3.3.3 OTHER INFLUENCES ON CONNECTIVITY AND CONNECTION AMPLITUDE

Aside from examining the relationship between connectivity and neuron position within L2/3 or intersomatic distance between the two neurons of the pair, we aimed at investigating other properties of either the pre- or postsynaptic neurons that could be linked to the presence or absence of a light-evoked uEPSP recorded at the interneuron soma. We first explored characteristics representative of spontaneous activity and network activity-related properties of the postsynaptic neuron, such as spontaneous AP firing rate, the amplitude of 1-5 Hz V_m oscillations and V_m vs LFP cross-correlation. Only the spontaneous AP rate in Sst neurons exhibited differing values between connected and unconnected pairs (Figure 3.17A, Table 3.3). Indeed, unconnected Sst neurons had a higher spontaneous AP firing rate than unconnected ones (NC: $1.3 \pm 1.7 \text{ Hz}$, C: $0.2 \pm 0.5 \text{ Hz}$, $p < 0.05$). Similarly, neither input resistance, nor mean membrane potential differed between connected and unconnected pairs (Figure 3.17B, Table 3.3). Finally, the spontaneous action potential firing rate of the presynaptic ChR2-expressing neuron in the absence of any light stimulation proved to be similar between neurons that were part of a connected or an unconnected pair (Figure 3.17C, Table 3.3).

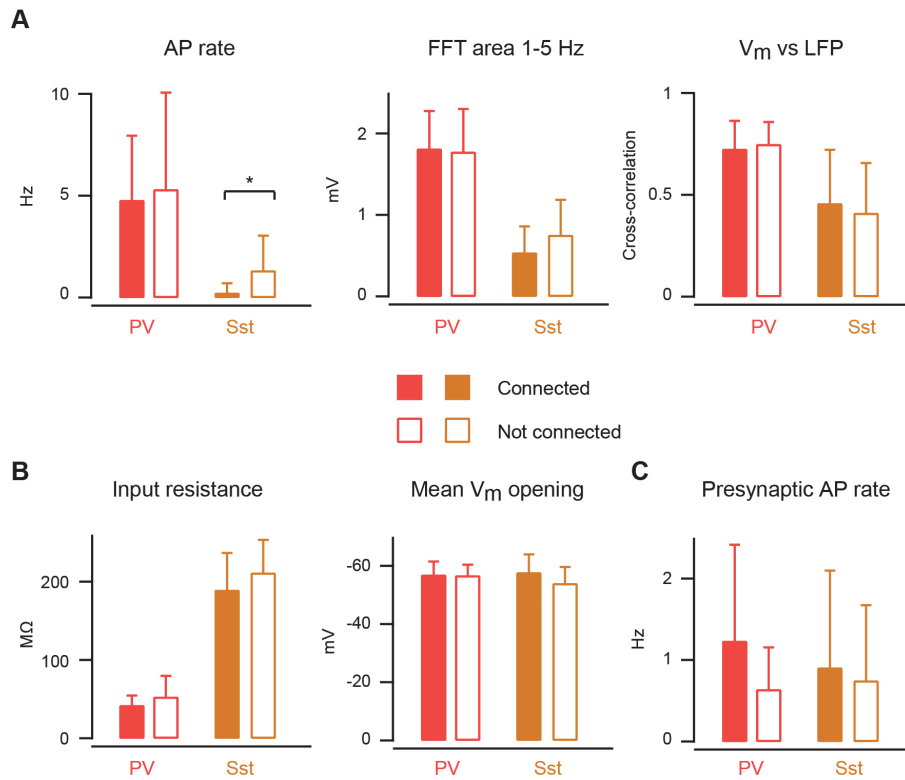


Figure 3.17 Relationship between electrophysiological properties and connectivity. (A) Spontaneous AP firing rate, V_m FFT integrated over the 1-5 Hz frequency band and V_m vs LFP cross-correlation at zero time-lag. None are different in connected postsynaptic PV and Sst neurons compared to unconnected ones except for AP rate that is higher in unconnected compared to connected Sst neurons. (B) Input resistance and mean V_m just after establishing whole-cell configuration are similar in connected and unconnected pairs (C) Presynaptic spontaneous AP firing rate is not different for ChR2-expressing excitatory neurons being part of a connected versus an unconnected pair. Population data are represented as mean \pm SD. * $p < 0.05$. See also Table 3.3

In an analogous manner, we checked for a possible monotonic correlation between uEPSP amplitude and the amplitude of 1-5 Hz V_m oscillations, spontaneous AP firing rate, membrane potential at uEPSP onset (baseline V_m) and input resistance (Figure 3.18A and B).

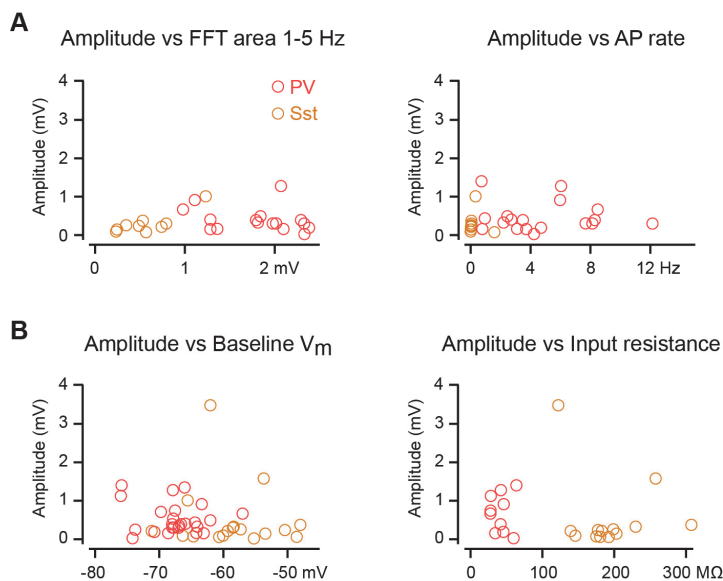


Figure 3.18 Relationship between uEPSP amplitude and electrophysiological properties. (A) V_m FFT integrated over the 1-5 Hz frequency band and spontaneous AP firing rate versus uEPSP amplitude. (B) Baseline V_m at uEPSP onset and input resistance versus uEPSP amplitude. None are correlated with PV or Sst uEPSP amplitude.

For both PV and Sst neurons, there were no significant correlations with uEPSP amplitude. The overall absence of a correlation between the different electrophysiological properties reported above and the presence or absence of a single uEPSP of small amplitude (~ 0.5 mV on average in both PV and Sst neurons) is likely due to the fact that a single cortical neuron receives thousands of such excitatory inputs (as well as inhibitory ones) (DeFelipe et al., 2002), which are likely to contribute only to a small part of the neuron's spontaneous activity levels.

3.4 SHORT-TERM SYNAPTIC DYNAMICS

After having examined postsynaptic responses to single presynaptic action potentials we were interested in quantifying the responses to multiple presynaptic action potentials elicited at various frequencies. We stimulated the ChR2-expressing neuron with a train of five 1 ms light pulses delivered at 20 Hz (Figure 3.19A) or 50 Hz (Figure 3.19B) while recording uEPSPs evoked in connected PV and Sst neurons. Trials where all five optogenetic stimuli occurred during DOWN state were used to compute an average light-evoked membrane potential response, which was used for subsequent quantifications.

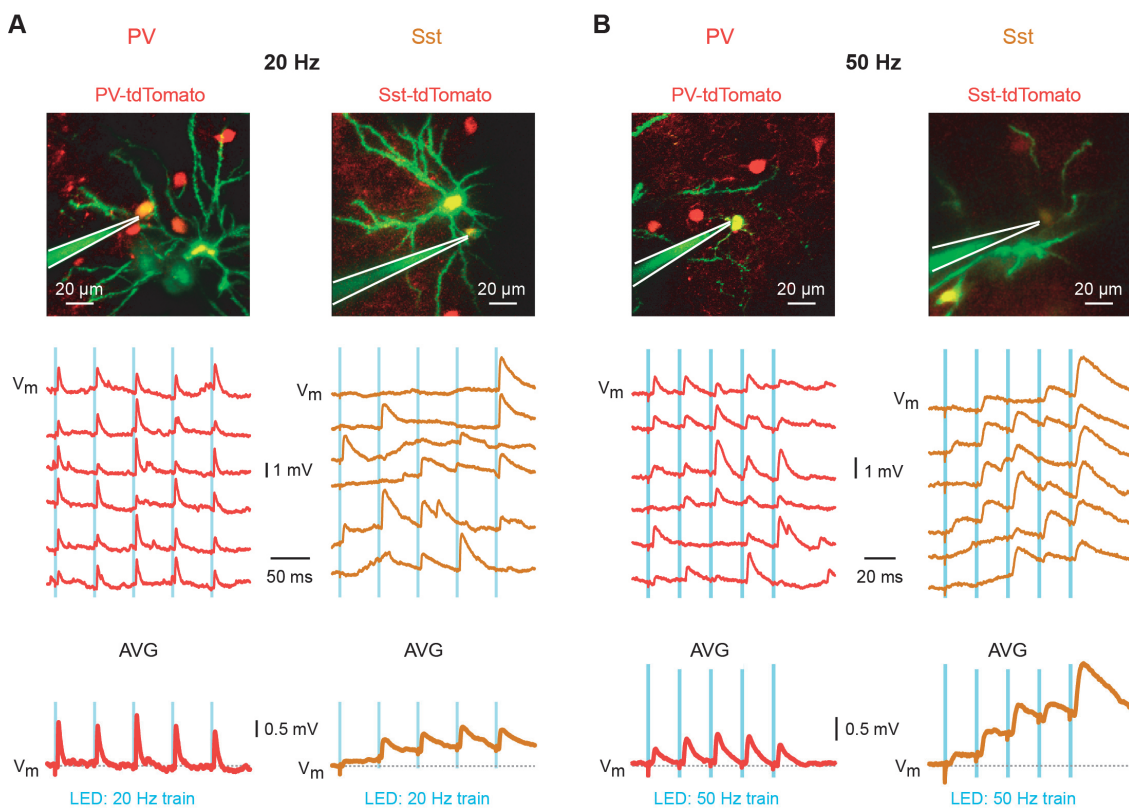


Figure 3.19 Representative short-term dynamics in PV and Sst neurons. (A) Example whole-cell recordings of uEPSPs elicited in a PV and a Sst neuron during DOWN state by optogenetic stimulation of the ChR2-expressing presynaptic neuron with a 20 Hz train of five 1 ms light pulses. Single trial uEPSPs are shown above and average uEPSPs below. (B) Same as in (A) but for an optogenetic stimulation made of a 50 Hz train of five 1 ms light pulses. A different PV neuron and a different Sst neuron than in (A) are represented. The in vivo two-photon images show the whole-cell recording pipette (Alexa 488 dye, green), the recorded tdTomato-expressing neuron (yellow) and part of the presynaptic eGFP- and ChR2-expressing neuron (green).

We measured the amplitude of each light-evoked uEPSP in the train as well as the membrane potential at its onset (baseline V_m) and compared them with the amplitude, respectively baseline V_m , of the first uEPSP of the train. uEPSP amplitude in Sst neurons increased significantly over the course of the 50 Hz train (uEPSP1: 0.8 ± 1.2 mV, uEPSP5: 1.5 ± 1.8 mV, one tail $p < 0.05$, $n=9$), while it did not change in PV neurons (uEPSP1: 0.7 ± 0.4 mV, uEPSP5: 0.7 ± 0.6 mV, $p > 0.05$, $n=10$) (Figure 3.20A and D) leading to a larger amplitude ratio between the fifth and the first uEPSP of the train for Sst neurons than for PV neurons (PV: 1.04 ± 0.51 (SEM: 0.16), Sst: 9.24 ± 15.09 (SEM: 5.03), $p < 0.05$) (Figure 3.20E).

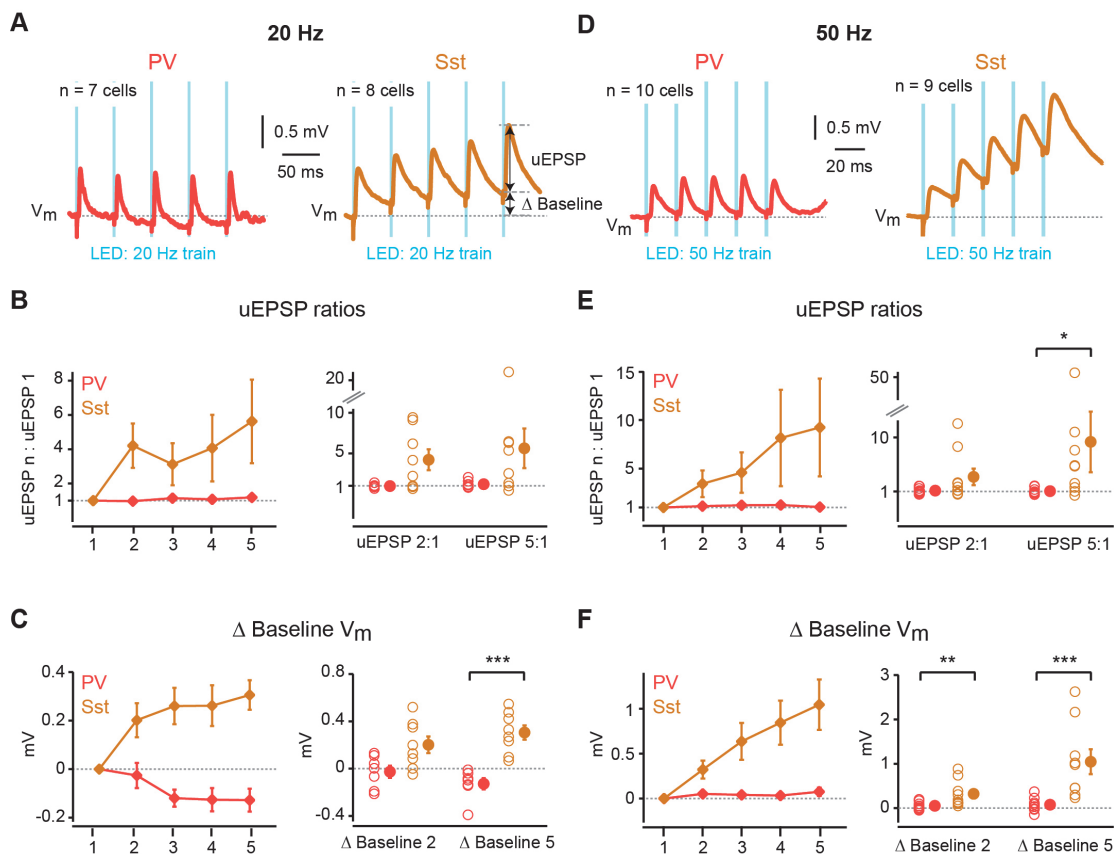


Figure 3.20 Cell type-specific short-term dynamics in vivo. (A) Grand average uEPSPs for PV and Sst neurons elicited during DOWN state in response to stimulation of the presynaptic ChR2-expressing neuron with a 20 Hz train of five 1 ms light pulses. (B) Population uEPSP amplitude ratios comparing the amplitude of each uEPSP in the train to the amplitude of the first uEPSP for PV and Sst neurons (left). Individual neurons uEPSP amplitude ratios for uEPSP2 and uEPSP5 (right). (C) Population difference in baseline V_m at onset of the uEPSP comparing baseline V_m of each uEPSP in the train to the baseline V_m of the first uEPSP for PV and Sst neurons (left). Individual neurons' differences in baseline V_m at the onset of uEPSP2 and uEPSP5 (right). (D-F) Same as in (A-C) but for stimulation of the presynaptic ChR2-expressing neuron with a 50 Hz train of five 1 ms light pulses. Excitatory synaptic connections onto Sst neurons exhibit larger uEPSP amplitude ratio indicative of short-term facilitation compared to connections made onto PV neurons, which show little short-term dynamics. Sst neurons display larger difference in baseline V_m underlying uEPSP summation compared to PV neurons. Data are represented as mean \pm SEM. *** $p < 0.001$, ** $p < 0.01$, * $p < 0.05$.

A comparable tendency was observed at a presynaptic stimulation frequency of 20 Hz (Figure 3.20B). Similarly, the baseline V_m recorded at the uEPSP's onset became more depolarized in Sst neurons over the course of the 50 Hz train (-57.4 ± 5.1 mV, -56.4 ± 5.5 mV, one tail $p < 0.05$), while it remained

hyperpolarized in PV neurons (uEPSP1: -68.0 ± 4.4 mV, uEPSP5: -68.0 ± 4.3 mV, $p > 0.05$). The baseline V_m difference between fifth and first uEPSP was thus larger in Sst neurons than in PV neurons at both stimulation frequencies (20 Hz: PV: -0.1 ± 0.1 mV (SEM: 0.05 mV), Sst: 0.3 ± 0.2 mV (SEM: 0.06 mV), $p < 0.001$ / 50 Hz: PV: 0.08 ± 0.1 mV (SEM: 0.05 mV) Sst: 1.0 ± 0.8 mV (SEM: 0.3 mV), $p < 0.001$) (Figure 3.20C and F). In summary, in response to multiple closely timed presynaptic action potentials, excitatory synaptic connections targeting Sst neurons showed short-term facilitation while those targeting PV neurons showed no distinct short-term dynamics. In addition, Sst neurons displayed summation of incoming uEPSPs, leading to an even further enhanced depolarization of their membrane potential, which was absent in PV neurons. These two phenomena were more evident at a higher frequency of presynaptic excitatory neuron stimulation and are likely related to the high-failure rate and high coefficient of variation as well as to the slow uEPSP kinetics observed in Sst neurons compared to PV neurons (see Section 3.3.1).

3.5 MODULATION OF SYNAPTIC TRANSMISSION BY NETWORK STATE

The results about in vivo excitatory synaptic transmission presented so far were all obtained from pre- and postsynaptic events occurring during the quiescent phase (DOWN) of the cortical slow oscillations typical of anesthesia. We then focused on analyzing light-evoked uEPSPs elicited in PV and Sst neurons during the more active UP states. Considering single 1 ms pulse optogenetic stimuli occurring during UP states only, we measured the amplitude of the average light-evoked uEPSP in 13 PV and 8 Sst neurons, which were previously classified as connected based on their responses to light stimulation during DOWN states (Figure 3.21A). On average, no difference was found between the mean amplitude of uEPSP evoked during UP states compared to uEPSP evoked during DOWN states for both PV (UP: 0.53 ± 0.49 mV, DOWN: 0.55 ± 0.39 mV, $p > 0.05$) and Sst neurons (UP: 0.31 ± 0.34 mV, DOWN: 0.33 ± 0.36 , $p > 0.05$), though some individual neurons seemed to display apparent decrease in uEPSP amplitude in UP compared to DOWN states, while others showed seemingly increased uEPSP amplitude in UP compared to DOWN states (Figure 3.21B). Due to the high spontaneous membrane potential fluctuations characterizing the more depolarized UP state (Figure 3.21C) in both PV and Sst neurons, we did not attempt at any quantifications involving the detection of single trial uEPSPs, such as those estimating the reliability of synaptic transmission. We nonetheless tried to measure short-term plasticity during the UP state, but due to an insufficient number of trials we could not conclude to any potential modulation of short-term dynamic by network state. As trials where postsynaptic action potentials occurred around the time of the optogenetic stimulation were excluded from the calculation of the average UP state uEPSP, we performed a separate analysis estimating the likelihood of a postsynaptic action potential occurring in response to a single presynaptic action potential.

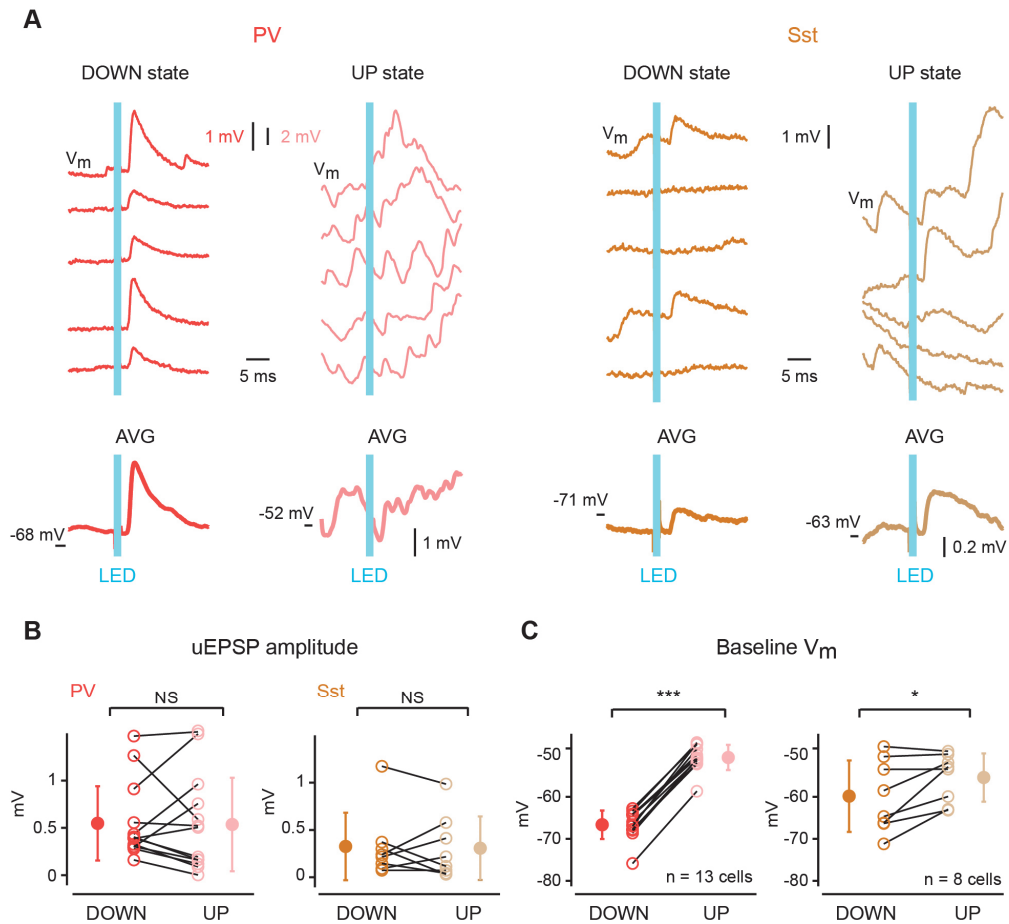


Figure 3.21 Modulation of uEPSP amplitude by local network activity. (A) Individual V_m responses evoked in a PV and a Sst neuron during DOWN (left) and UP (right) state by repeated stimulation of the Chr2-expressing neuron with a 1 ms square pulse of light (above). DOWN and UP average light-evoked uEPSPs (below). uEPSP amplitude is larger in DOWN compared to UP state for the PV neuron, while the opposite is true for the Sst neuron, with a larger uEPSP amplitude in UP compared to DOWN state. (B) At the population level, uEPSP amplitude is similar when comparing UP and DOWN states for both PV and Sst neurons. (C) Membrane potential at uEPSP onset is more depolarized during UP compared to DOWN state for both PV and Sst neurons. Data are represented as mean \pm SD. *** $p < 0.001$, * $p < 0.05$

Considering all optogenetic stimuli delivered across both UP and DOWN states we did not find a different postsynaptic action potential probability in a given post-stimulus time window compared to the spontaneous action potential probability computed in the absence of any light stimulation neither in PV neurons (Light: $1.57 \pm 1.2\%$, Spontaneous: $1.44 \pm 1.53\%$, $n = 11$, $p > 0.05$) nor in Sst neurons (Light: $0.16 \pm 0.44\%$, Spontaneous: $0.05 \pm 0.13\%$, $n = 8$, $p > 0.05$) (Figure 3.22).

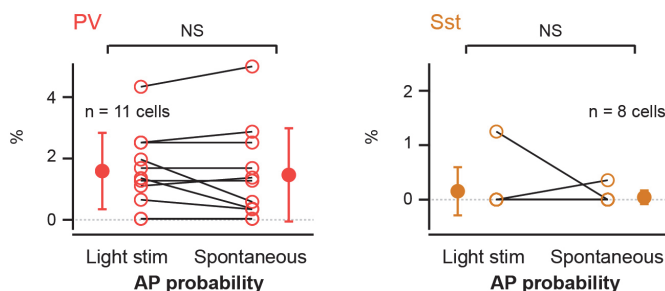


Figure 3.22 Light-evoked postsynaptic APs. Postsynaptic action potential probability in response to optogenetic stimulation of the presynaptic Chr2-expressing excitatory neuron compared to spontaneous postsynaptic action potential probability for PV and Sst neurons. No additional action potentials are elicited in the postsynaptic neuron in response to light. Data are represented as mean \pm SD.

Therefore, the likelihood that an individual light-evoked action potential elicited in a single excitatory presynaptic neuron could generate an action potential in a connected postsynaptic neuron is very low. Upon numerous repetitions of the optogenetic stimulus, it could however eventually lead to a postsynaptic AP (London et al., 2010). Though we only examined this phenomenon in PV and Sst neurons, it seems reasonable to assume that an analogous conclusion can be drawn for less connected postsynaptic excitatory neurons, thus making it rather unlikely that we recorded any polysynaptic uEPSPs at any point in our experiments. Finally, as there is a high intra-population variability in uEPSP amplitude modulation by network state that results in an overall absence of changes in uEPSP amplitude between DOWN and UP state, additional data points might help to further refine our understanding of the impact of a change in network state upon synaptic transmission.

3.6 MORPHOLOGY OF RECORDED NEURON PAIRS

As the number and location of excitatory synaptic contacts could be related to the size of the uEPSP elicited in the postsynaptic neurons *in vivo*, we attempted to recover the morphologies of both the presynaptic excitatory neuron and the postsynaptic neuron. Electroporation of eGFP-encoding plasmid DNA allowed an amount of protein to be expressed in 24 hours that was sufficient to clearly visualize excitatory neuron local dendritic and proximal axonal branches *in vivo* and in fixed tissue without further enhancement of the fluorescent signal. By performing immunohistochemistry on fixed sections and adjusting plasmid DNA expression time, the finer axonal branches could be identified regardless of whether they were restricted to the barrel cortex (Figure 3.23A) or extended millimeters away towards and within other cortical areas (Figure 3.23B) (Yamashita et al., 2013). Biocytin filling of the whole-cell recorded postsynaptic neurons allowed recovery of their soma and dendrites, which permitted reconstruction of the overall local morphology of the pre- and postsynaptic partners of a connected pairs (Figure 3.23C). However, due to the very small number of properly filled postsynaptic neurons, we were unable to conduct a quantitative analysis of the morphological parameters potentially correlated with subtypes of PV and Sst neurons as well as to identify the number and location of putative contacts between pre- and postsynaptic neurons.

In conclusion, by using a combination of single-cell optogenetics with whole-cell patch-clamp recordings targeted to three different cell types in L2/3 mouse barrel cortex, we obtained novel evidence on synaptic connectivity and synaptic transmission within the intact and spontaneously active brain. We chose a ChR2 protein mutant that was able to reliably elicit time-locked single action potentials in individual excitatory neurons at various frequencies and across different cortical states over long period of time. It allowed us to estimate the probability of synaptic connection and to characterize synaptic transmission between excitatory neurons, as well as between excitatory neurons and two chemically and electrically distinct GABAergic neuron types, namely PV-expressing and Sst-expressing neurons. In upper L2/3 barrel cortex, GABAergic neurons were found to receive more

frequent and larger excitatory inputs than excitatory neurons, with little dependency on intersomatic distances or other cell-type specific electrophysiological properties. Comparing excitatory synaptic transmission onto PV and Sst neurons, we found more reliable and faster inputs in PV neurons compared to Sst neurons. In a related fashion, synaptic connections onto PV neurons exhibited little short-term dynamics with no summation of the uEPSPs, while Sst neurons displayed strong short-term facilitation with clear uEPSP summation. Finally, in investigating the effect of different levels of spontaneous cortical activity on synaptic transmission, we did not find any significant modulation of uEPSP amplitude in neither PV nor Sst neurons.

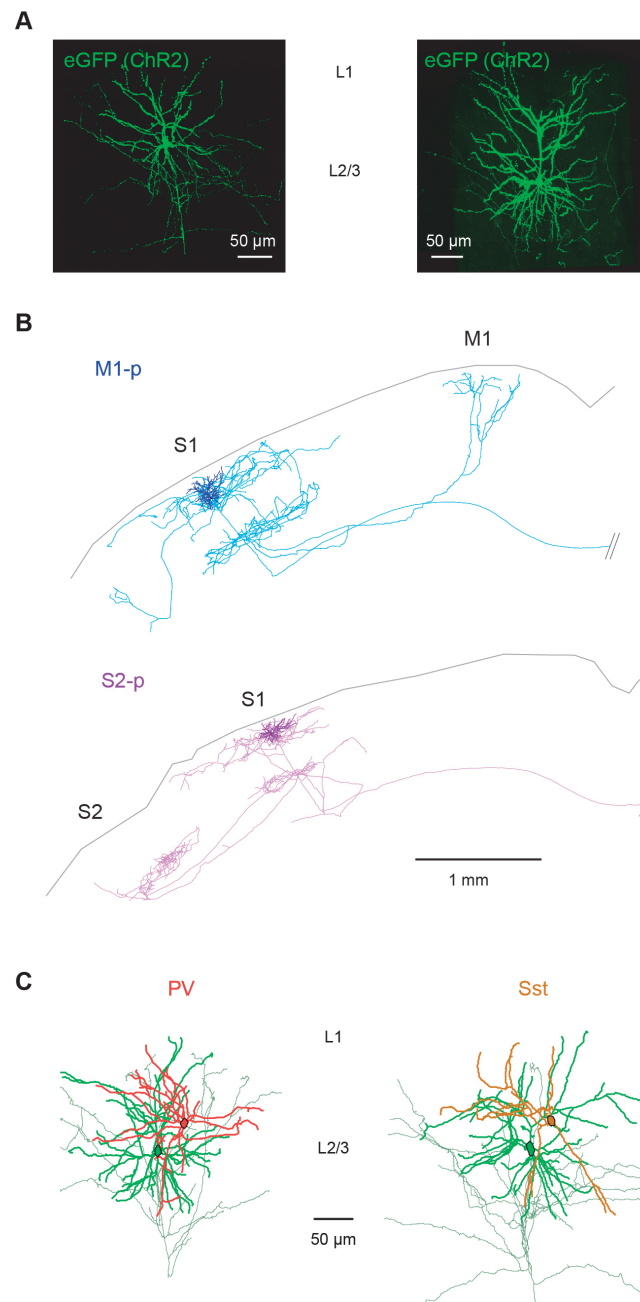


Figure 3.23 Morphological identification of pre- and postsynaptic neurons. (A) eGFP-expressing presynaptic excitatory neurons located in the upper part (left) and lower part (right) of L2/3 barrel cortex. (B) Single cell electroporation of eGFP in individual excitatory neurons allows recovery of local and long-range axonal arborisations (modified from Yamashita et al. 2013). S2: secondary somatosensory cortex, M1: primary motor cortex (C) Reconstruction of the morphology of the pre- and postsynaptic neurons for a connected excitatory-PV pair (left) and a connected excitatory-Sst pair (right).

3.7 TABLES

Properties	PV	Sst	Exc
Input resistance (MΩ)	47 ± 22 (n = 21)	203 ± 45 (n = 43)	47 ± 13 (n = 27)
Tau (ms)	3.6 ± 2.5 (n = 21)	17.7 ± 6.4 (n = 45)	6.5 ± 1.6 (n = 27)
Mean V _m opening (mV)	-66.1 ± 6.0 (n = 52)	-59.9 ± 5.4 (n = 63)	-68.7 ± 5.6 (n = 54)
Mean V _m later (mV)	-56.7 ± 4.2 (n = 35)	-54.9 ± 6.0 (n = 36)	-64.3 ± 6.2 (n = 50)
AP rate (Hz)	5.05 ± 4.05 (n = 38)	1.02 ± 1.56 (n = 37)	0.29 ± 0.64 (n = 54)
AP threshold (mV)	-36.7 ± 2.4 (n = 51)	-37.9 ± 3.0 (n = 33)	-38.1 ± 2.8 (n = 25)
AP half-width (ms)	0.32 ± 0.05 (n = 51)	0.62 ± 0.11 (n = 33)	1.05 ± 0.16 (n = 25)
Peak-to-trough ratio	1.6 ± 0.2 (n = 51)	2.1 ± 0.3 (n = 33)	3.8 ± 0.7 (n = 25)
FFT area 1-5 Hz (mV)	1.79 ± 0.50 (n = 35)	0.69 ± 0.41 (n = 35)	1.47 ± 0.51 (n = 49)
V _m vs LFP Cross-correlation	0.74 ± 0.12 (n = 19)	0.42 ± 0.25 (n = 33)	0.71 ± 0.10 (n = 45)

Table 3.1 Electrophysiological properties. Data are represented as mean ± SD.

uEPSP properties	PV	Sst	uEPSP properties	PV	Sst
Amplitude (mV)	n = 25	n = 17	Rise time (ms)	n = 25	n = 17
mean ± SD	0.53 ± 0.39	0.50 ± 0.86	mean ± SD	0.68 ± 0.32	1.76 ± 1.40
median	0.39	0.21	median	0.61	1.31
range	0.03 - 1.40	0.02 - 3.48	range	0.33 - 1.85	0.58 - 5.89
Failure rate (%)	n = 22	n = 16	Half-width (ms)	n = 24	n = 13
mean ± SD	27.4 ± 15.5	68.0 ± 29.1	mean ± SD	4.0 ± 1.4	11.6 ± 6.7
median	31.7	80.2	median	4.3	9.1
range	0 - 51.0	4.5 - 90.3	range	1.2 - 6.6	3.9 - 23.1
Coefficient of variation	n = 22	n = 16	Tau decay (ms)	n = 21	n = 9
mean ± SD	0.35 ± 0.25	0.92 ± 0.53	mean ± SD	5.2 ± 3.0	16.0 ± 8.5
median	0.33	0.88	median	4.8	15.2
range	0.01 - 0.94	0.26 - 1.92	range	1.3 - 12.7	6.0 - 32.9

Table 3.2 uEPSP properties

PV

Properties	Connected	Not Connected
AP rate (Hz)	4.8 ± 3.2	5.3 ± 4.8
FFT area 1-5 Hz (mV)	1.81 ± 0.47	1.77 ± 0.53
V _m vs LFP	0.72 ± 0.14	0.75 ± 0.11
Input resistance (MΩ)	42 ± 13	53 ± 27
Mean V _m opening (mV)	-56.8 ± 4.7	-56.6 ± 3.8
Presynaptic AP rate (Hz)	1.2 ± 1.2	0.6 ± 0.5

Sst

Properties	Connected	Not Connected
AP rate (Hz)	0.2 ± 0.5	1.3 ± 1.7
FFT area 1-5 Hz (mV)	0.53 ± 0.32	0.75 ± 0.44
V _m vs LFP	0.47 ± 0.26	0.41 ± 0.25
Input resistance (MΩ)	189 ± 48	211 ± 42
Mean V _m opening (mV)	-57.6 ± 6.3	-53.9 ± 5.7
Presynaptic AP rate (Hz)	0.9 ± 1.2	0.7 ± 0.9

Table 3.3 Electrophysiological properties of connected and not connected neurons. Data are represented as mean ± SD.

CHAPTER 4: DISCUSSION

In this thesis, I showed that by using a combination of single-cell optogenetics and electrophysiological recordings I could directly assess unitary excitatory synaptic transmission in the neocortex of the mouse *in vivo*. I found cell-type specific properties of excitatory synaptic transmission within the neuronal population of L2/3 barrel cortex *in vivo*. GABAergic neurons received stronger excitation than excitatory neurons. The excitatory input on PV neurons was fast and reliable, with little short-term dynamics. In contrast, Sst neurons received slow and rather unreliable excitatory input that facilitated. Finally, spontaneous changes in local network activity, as found in the intact neocortex under anesthesia, did not affect synaptic transmission.

4.1 SINGLE-CELL OPTOGENETICS FOR MEASURING SYNAPTIC TRANSMISSION IN VIVO

Due to the probabilistic nature of chemical synaptic transmission, its measurement requires repeated generation of single time-locked action potentials (APs) in the presynaptic neuron, while measuring subthreshold membrane potential fluctuations in the postsynaptic neuron by intracellular recording or patch-clamp recording. *In vivo*, this has been achieved by juxtacellular or intracellular injection of positive current at the presynaptic neuron soma (Crochet et al., 2005; Bruno and Sakmann, 2006; Yu and Ferster, 2013) or by simply monitoring spontaneous or sensory stimulation-triggered presynaptic APs (Matsumura et al., 1996; Bruno and Sakmann, 2006; Constantinople and Bruno, 2013). Here, we used optogenetics as an alternate method to control presynaptic AP firing *in vivo*. Using single-cell electroporation of ChR2 with wide-field optical stimulation, we succeeded in controlling single AP firing in a single neuron per animal over long time periods, at various frequencies and across different levels of network activity. As electroporation enables multiple DNA plasmids to be simultaneously delivered, it allowed us to express a non-fused version of the ChR2 protein, which likely optimizes its insertion and functioning at the plasma membrane, together with a cytoplasmic fluorescent protein (eGFP), which rendered possible the recovery of the full morphology of the presynaptic neuron, including its axonal tree. In addition, being able to stimulate the same presynaptic neuron while sequentially recording its putative postsynaptic targets would ideally permit to estimate the connection probability of individual presynaptic neurons. In practice however, due to the limited number of possible recordings made during a typical experimental session this quantification lacks resolution. It would be interesting to examine uEPSPs elicited in neurons sharing the same presynaptic partner *in vivo*, as short-term dynamics and by extension the overall probability of neurotransmitter release across synaptic contacts arising from the same axon has been shown to be dependent of the postsynaptic cell type *in vitro* (Markram et al., 1998; Reyes et al., 1998; Scanziani et al., 1998).

Moreover, it would be interesting to investigate the spontaneous pattern of activity as well as the receptive field properties of neurons sharing the same presynaptic partner.

We took advantage of the recent development of ChR2-mutants, exhibiting various kinetics and conductances, to select the ET/TC double mutant in light of its relatively fast deactivation time constant (Berndt et al., 2011; Mattis et al., 2012). Such a parameter is critical in minimizing the purely ChR2-mediated depolarization occurring during the repolarizing phase of a light-evoked AP. Indeed, as we did not restrict the optical stimulus to the soma of the ChR2 neuron, and as functional ChR2 proteins are known to be present in the axonal compartment (Petreanu et al., 2007), this long-lasting depolarization might affect synaptic transmission, as it has been shown to mediate Ca^{2+} influx through activation of voltage-gated Ca^{2+} channels (Zhang and Oertner, 2007). Such a ChR2-mediated rise in intracellular Ca^{2+} concentration is linked to a higher basal probability of neurotransmitter release, which translates into a short-term synaptic dynamics skewed towards depression (Cruikshank et al., 2010). However, recent evidences seem to indicate that the presence or absence of such a ChR2-mediated change in release probability might be cell-type specific, as well as to depend on the transfection method used to express ChR2 (Jackman et al., 2014). In any case, as we conducted most of our measurements during the DOWN states, which are relatively hyperpolarized, this effect might not have been so preponderant, as the N and P/Q voltage-gated Ca^{2+} channels involved in neurotransmitter release require the membrane potential to be brought to about -20 mV for activation (Hille, 2001).

In addition, one should keep in mind that ChR2 is by default permeable to Ca^{2+} (Nagel et al., 2003). Future improvements in the use of ChR2 for investigating synaptic transmission *in vivo* could thus include reducing the Ca^{2+} permeability of the channel as well as using a different method of light stimulation. Indeed two-photon stimulation, due to its small volume of excitation and decreased scattering, could prove ideal to selectively activate individual neuron somas or even dendrites *in vivo*. ChR2 could thus be expressed in multiple neurons, via transfection by a viral vector or by using transgenic animals, and multiple presynaptic partners could be tested for each recorded postsynaptic neuron. *In vitro*, ChR2-expressing neurons were successfully triggered to fire APs by either scanning the two-photon light beam across the soma following a specific pattern (Rickgauer and Tank, 2009) or by performing conventional line-scanning on the soma of neurons expressing a slower-kinetic ChR2 mutant (Packer et al., 2012; Prakash et al., 2012). In addition, scan-free methods based on spatiotemporal shaping of the two-photon beam such that it overlaps with a portion of the somatic plasma membrane have also proven successful in eliciting AP firing *in vitro* (Andrasfalvy et al., 2010; Papagiakoumou et al., 2010; Begue et al., 2013).

4.2 IN VIVO CONNECTIVITY ANALYSIS

In order to assess connectivity between a single excitatory neuron and a putative postsynaptic neuron, we usually examined the mean postsynaptic depolarization elicited during DOWN states in response to a single light pulse of 1 ms duration, delivered every 1s. In addition, connectivity was also assessed by considering the postsynaptic response to a train of five such light stimuli, delivered at 20 Hz or 50 Hz during DOWN states, with a minimal interval between two trains of 5s. We noted that in 2 out of 9 connected Sst neurons whose excitatory input was assessed by stimulating the presynaptic ChR2-expressing excitatory neuron with the trains of light, only a small depolarization was visible in response to the first light pulse of the train, and the existence of a connection became more obvious when subsequent light pulses were considered. The number of excitatory connections onto Sst neurons might thus have been underestimated when assessed by solely stimulating presynaptic ChR2-expressing excitatory neuron with single 1 ms light pulses, as the evoked uEPSP might not have been distinguishable from spontaneous membrane potential fluctuations. This phenomenon may be especially relevant to the finding of high failure rate synaptic connections when only a small number of trials assessed the presence of a light-evoked response. In addition, it is worth noting that we did not apply a strict criterion in terms of minimal amplitude or rising slope of the evoked uEPSP in order to verify the presence of a connection; therefore, there might be a range of uEPSP amplitudes and shapes for which the certainty of the identification is likely to be less convincing. This is partially the reason why we did not pursue further the characterization of excitatory synaptic transmission targeting excitatory neurons. In addition, initial attempts at comparing single trial uEPSP amplitude distribution (as measured by subtracting baseline V_m just after light stimulus offset to V_m at uEPSP peak) with an amplitude distribution of a similarly calculated V_m difference for equally spaced time points during spontaneous periods of activity in DOWN states lead to the detection of connected PV neurons quite accurately, as confirmed by visual examination of the average evoked uEPSP. However, uEPSPs evoked in Sst neurons could not be reliably detected by this method, probably because of their higher failure rate, giving rise to an amplitude distribution that was similar to the amplitude distribution of spontaneous activity in some cases.

As we recorded the change in membrane potential evoked at the soma of the postsynaptic neuron, it is also likely that our estimate of functional connectivity is affected by the passive and active properties of the dendrites, particularly in case of connections where the synaptic contacts were located in distal dendrites. This might be especially important for excitatory neurons, as GABAergic neurons are more likely to receive their excitatory inputs on proximal dendrites and on the soma (Wang et al., 2002; Douglas, 2004; Markram et al., 2004; Feldmeyer et al., 2006). In addition, even though we conducted most of our analysis during DOWN states where spontaneous AP firing of the pre- and postsynaptic neurons is low, we cannot rule out possible effects of the history of spiking activity of both neurons during previous UP states in shaping the strength of the synapse at the time

we are probing it, since synaptic plasticity happens on such a time scale of hundreds of milliseconds to seconds. One could also wonder about the physiological relevance of the AP firing patterns we chose to elicit in the presynaptic excitatory neuron to assess synaptic connectivity. Indeed, AP firing activity of L2/3 barrel cortex excitatory neurons is low and dominated by single APs, both under anesthesia (here: 0.3 ± 0.6 Hz, see also Mateo et al. 2011), and during quiet and active wakefulness (Crochet and Petersen, 2006). However, a small percentage of the spiking activity of L2/3 excitatory neurons consists of bursts of a few APs (de Kock and Sakmann, 2008; Poulet and Petersen, 2008).

Finally, correlating the presence (or absence) of a somatic uEPSP with the presence (or absence) of physical synaptic contacts between the pre- and postsynaptic neurons could strengthen functional connectivity analysis. As we attempted here, one option is to reconstruct the cellular morphologies of the pre- and postsynaptic neurons post-recording. Another option would be to label synaptically connected neurons before targeting them for recording. In the preliminary phase of this work, we indeed tested three different trans-synaptic tracers, with little success. Protein-based tracers, including wheat germ agglutinin (WGA) fused to a Cre recombinase enzyme (Sugita and Shiba, 2005; Gradinaru et al., 2010) and the non-toxic C-fragment of tetanus toxin (TTC) fused to eGFP (Maskos et al., 2002) individually delivered to single neurons by single-cell electroporation lead to their expression in the initially transfected neurons only. Replication incompetent pseudotyped rabies virus expressing the mCherry protein (Wickersham et al., 2007) injected into L2/3 barrel cortex after electroporation into a single neuron of DNA plasmids encoding glycoprotein G (necessary for virus replication and presynaptic spread) and a plasma membrane surface receptor (necessary for virus entry inside the cell) exhibited some success in labeling a handful of neurons located in every cortical layer of S1. However, due to the scarcity and the spread of trans-synaptically labeled neurons, in addition to the potential toxicity and putative activity-dependent transfer of the virus at synapses, we did not further utilize it.

4.3 IN VIVO VS IN VITRO MEASUREMENT OF SYNAPTIC TRANSMISSION

Most of the available information about the functional synaptic organization of glutamatergic and GABAergic neurons of the neocortex comes from recordings made in brain slices in vitro (Yamamoto and McIlwain, 1966; Edwards et al., 1989). The advantages of brain slices include mechanical stability and direct visualization of the cells, allowing simultaneous recordings of multiple neurons. Moreover, the easy access and control of the extracellular medium renders pharmacological investigations possible. In studies interested mainly in connectivity, within or across layers or neocortical areas, minimal extracellular stimulation (Volgushev et al., 1995; Finnerty et al., 1999), glutamate (Callaway and Katz, 1993) or GABA uncaging (Zayat et al., 2007; Rial Verde et al., 2008) as well as optogenetics (Zhang et al., 2006; Petreanu et al., 2007) were amongst the chosen investigation methods. In addition, due to advances in microscopy techniques for optogenetic

stimulation (see Section 4.1) as well as for caged-compound stimulation (Zahid et al., 2010), single-cell resolution can be achieved. However, a large part of the data on neocortical synaptic connectivity and on the physiology of unitary synaptic transmission come from simultaneous electrophysiological recordings between two (Thomson et al., 1988) or more neurons (Perin et al., 2011). In such experiments, one micropipette is typically used to stimulate an identified presynaptic neuron, either juxtacellularly or through whole-cell recording, while another is used to record elicited PSPs in a putative postsynaptic neuron.

Though brain slice preparations have proven highly valuable, axonal and dendritic arbors are inevitably severed during slicing. In addition such procedure seems to induce rapid spines growth (Kirov et al., 1999), with new synapses potentially being formed. Together, these factors might thus affect synaptic connectivity and synaptic strength. Another drawback of the *in vitro* configuration is the lack of spontaneous network activity, which, as found *in vivo*, can affect the strength, reliability and dynamics of synapses (Boudreau and Ferster, 2005; Reig et al., 2006; Groh et al., 2008; Lorteije et al., 2009) as well as modulate the active properties of dendrites (Waters and Helmchen, 2004) and thus the propagation of the PSP to the soma. The ionic concentrations of the slice perfusion solution are also likely to be different than those estimated *in vivo*. For instance, of particular relevance to the molecular mechanisms involved in neurotransmitter release, extracellular Ca^{2+} concentration is usually higher in slices (2 mM - 2.5 mM) than *in vivo*, where it was estimated to be between 1.1 mM and 1.5 mM (Heinemann et al., 1977; Hansen, 1985; Jones and Keep, 1988), therefore potentially contributing to larger release probabilities *in vitro* than *in vivo* (Borst, 2010). The concentration of neurotransmitters in the extracellular space is also likely to be smaller *in vitro* than that found *in vivo* (Kekesi et al., 1997; Nyitrai et al., 2006). As such, these ambient neurotransmitter molecules could be sufficient to activate or desensitize postsynaptic receptors (Featherstone and Shippey, 2008), and also to activate presynaptic metabotropic receptors or extrasynaptic receptors (Glykys and Mody, 2007; Rodriguez et al., 2013), which could all directly or indirectly participate to the regulation of synaptic transmission *in vivo*. Finally, as many *in vitro* recordings are conducted in brain slices from young animals, measurements are likely to reflect characteristics of immature connections.

Knowledge about subthreshold synaptic transmission and synaptic connectivity in the intact brain is scarce, though estimates of synaptic connectivity based on correlated AP activity recorded extracellularly are common (Perkel et al., 1967; Fetz et al., 1991; Constantinidis et al., 2002; Fujisawa et al., 2008). However, this method requires the unambiguous identification of individual units in case of multi-unit recordings, as well as a certain level of spontaneous AP firing, and it does not account for correlations of suprathreshold activity occurring through shared presynaptic inputs. Using postsynaptic APs as the readout of synaptic connectivity, a recent study using Ca^{2+} imaging investigated synaptic transmission of presynaptic high-frequency presynaptic AP trains elicited in a single excitatory neuron in L2/3 mouse visual cortex. Postsynaptic AP firing in response to such presynaptic activity was detected in 30% of the recorded Sst neurons, absent in PV neurons, and very

infrequent in other excitatory neurons (Kwan and Dan, 2012). Direct measurements of EPSPs elicited in L4 barrel cortex neurons as a function of AP firing in single VPM neurons were shown to be smaller in vivo than when measured using minimal stimulation in vitro; this difference was putatively attributed to a higher spontaneous activity of thalamic neurons in vivo leading to a depression of the thalamocortical (TC) synapse (Bruno and Sakmann, 2006). Similar results were found at the mouse calyx of Held, where a lower probability of release was found in vivo compared to that measured in vitro (Lorteije et al., 2009). Finally, corticocortical synaptic transmission was directly measured in vivo in a handful of studies carried in monkey and cat neocortices (Matsumura et al., 1996; Crochet et al., 2005; Yu and Ferster, 2013).

We investigated the occurrence of uEPSPs in 54 putative excitatory neurons, 52 PV neurons and 63 Sst neurons in response to optogenetically-elicited action potentials in a single presynaptic excitatory neuron in L2/3 of the mouse barrel cortex in vivo. The connection probabilities we found for excitatory neurons (7.4%) and PV neurons (48.1%) were similar to those obtained in brain slices of young animals in vitro (Exc: 9.3%, $p > 0.05$, χ^2 test (Lefort et al., 2009); PV: 57.5%, $p > 0.05$, χ^2 test (Avermann et al., 2012)), for the same cortical area, layer and range of intersomatic distances (in vivo: $67 \pm 26 \mu\text{m}$ ($< 125 \mu\text{m}$) ; $61 \pm 39 \mu\text{m}$ ($< 150 \mu\text{m}$) in Avermann et al., 2012, mean \pm SD). Excitatory connectivity onto Sst neurons was found to be 57.1% in vitro (Fanselow and Connors, 2010) which is larger than the 30.2% probability we obtained in vivo. However their estimation comes from the sampling of a smaller (8/14) number of neuron pairs. We could have expected a larger connectivity in vivo, as all the cellular processes are intact, however, it is possible that the smaller input resistance measured in vivo during DOWN state (PV neurons R_{in} , in vivo: $47 \pm 5 \text{ M}\Omega$, in vitro: $99 \pm 3 \text{ M}\Omega$, mean Avermann et al., 2012 / Exc neurons R_{in} , in vivo: $47 \pm 3 \text{ M}\Omega$, in vitro: $188 \pm 3 \text{ M}\Omega$, Lefort et al., 2012, mean \pm SEM) might affect uEPSP size and thus renders the identification of small inputs impossible in vivo. Indeed, mean and median uEPSP amplitudes in PV neurons tended to be smaller in vivo than in vitro (PV: in vivo: $0.53 \pm 0.08 \text{ mV}$ (median: 0.39 mV), in vitro: $0.82 \pm 0.10 \text{ mV}$ (median: 0.68 mV), mean \pm SEM), while mean uEPSP amplitude in Sst neurons tended to be larger in vivo ($0.5 \pm 0.86 \text{ mV}$) than in vitro ($0.25 \pm 0.2 \text{ mV}$, mean \pm SD) as measured in L2/3 rat somatosensory cortex (Reyes et al., 1998). Considering the kinetics of the uEPSPs elicited in PV neurons, their half-widths, rise-times and decay time constants were all faster in vivo than in vitro, which could be explained by a faster membrane time constant in vivo ($5.2 \pm 0.7 \text{ ms}$, mean \pm SEM) compared to in vitro ($9.3 \pm 0.3 \text{ ms}$, mean \pm SEM). Alternatively, the recording temperature (32°C) (Avermann et al., 2012) could also play a role in the slower kinetics observed in vitro.

We found an increase in the amplitude of subsequent uEPSPs in the 20 Hz or 50 Hz train compared to the first uEPSP in Sst neurons, representative of synaptic facilitation (Figure 3.20). This is in agreement with many in vitro results obtained in different cortical areas and layers in response to diverse presynaptic AP firing frequencies (Reyes et al., 1998; Rozov et al., 2001a; Beierlein et al., 2003; Koester and Johnston, 2005; Watanabe et al., 2005; Kapfer et al., 2007; Silberberg and

Markram, 2007; Fanselow et al., 2008; Fanselow and Connors, 2010). In contrast, uEPSPs elicited in PV neurons showed rather steady amplitude during the 20 Hz and 50 Hz trains; this result is quite different from the clear decreased amplitude of subsequent uEPSPs in response to high-frequency trains measured in vitro under various conditions, and resulting from synaptic depression (Reyes et al., 1998; Galarreta and Hestrin, 1998; Rozov et al., 2001; Holmgren et al., 2003; Koester and Johnston, 2005; Watanabe et al., 2005; Kapfer et al., 2007; but see also Hofer et al., 2011 reporting little depression in mouse primary visual cortex). One could wonder whether this difference is due to the expression of the ChR2 protein in the presynaptic neuron, leading to an increased intracellular Ca^{2+} concentration. However, such an augmentation would rather result in a larger release probability, which correlates with synaptic dynamics dominated by depression. The two most likely reasons for such a difference in short-term plasticity are the variations in extracellular Ca^{2+} concentration and the animal's age difference, as we conducted our investigations in animals older than four weeks old, whereas most of the brain slices data come from animal younger than 3 weeks. As mentioned above, decreased Ca^{2+} concentration in vivo could lead to a smaller release probability, potentially reflecting a less strong contribution of depression to short-term synaptic plasticity. In addition, recordings performed in vitro in brain slices of more mature animals have shown a decreased depression of the excitatory synaptic connections onto PV neurons (Oswald and Reyes, 2011). Similar results were found for excitatory synapses targeting excitatory neurons, where a more mature circuit correlated with an attenuation of synaptic depression and sometimes even the appearance of a slight facilitation (Reyes and Sakmann, 1999; Zhang, 2004; Frick et al., 2007; Oswald and Reyes, 2008; Feldmeyer and Radnikow, 2009). In addition, as PV neurons display high spontaneous AP firing in vivo, one could hypothesize that they might regulate their excitatory inputs in an activity-dependent, retrograde manner. Such activity-dependent retrograde signaling is known to exist for GABAergic synaptic transmission onto cerebellar Purkinje cells (Llano et al., 1991) and hippocampal neurons (Pitler and Alger, 1992; Ohno-Shosaku et al., 2001). It could thus account for a lower probability of release in vivo than in vitro.

4.4 PV AND SST INHIBITORY NEURONS IN VIVO

PV and Sst neurons were previously shown to have different electrical properties in vitro and in vivo (See Chapter 1: Introduction). Under our recording conditions, PV and Sst neurons showed distinct passive membrane properties, action potential shapes and spontaneous activity patterns (Figure 3.9 and Table 3.1). Measurements in PV neurons were rather homogeneous across the population of cells sampled, while Sst neurons showed a larger variability, potentially supporting their classification into further subclasses as a function of calretinin expression (Xu et al., 2006) or of diverse axonal and dendritic morphologies (Halabisky et al., 2006; Ma et al., 2006; McGarry et al., 2010). For instance, some Sst neurons displayed thin, fast-repolarizing APs similar to those observed in PV neurons. In

addition, some Sst neurons had a depolarized membrane potential with small amplitude slow oscillations, comparable to what was observed during quiet wakefulness (Gentet et al., 2012), while others displayed clear bimodal distribution of their V_m (Figure 2.4). However, on average Sst neurons displayed smaller amplitude slow oscillations than PV neurons, although their input resistance was larger. This could in part be explained by their lower excitatory connectivity rate from local L2/3 excitatory neurons compared to PV neurons and potentially also by the presence in some neurons of an I_h current that could oppose to the DOWN state hyperpolarization. Such a lower connectivity rate, together with a high-failure rate of excitatory synaptic transmission might also explain the low correlation to the LFP we recorded under anesthesia, as well as the anticorrelation between their V_m and that of excitatory neurons under wakefulness (Gentet et al., 2012).

The mean amplitude of the uEPSP elicited in Sst and PV neurons was on average similar, though the median amplitude was different, suggesting a different distribution of uEPSP amplitudes across the two populations of neurons (Table 3.2), which could be better resolved with more data points. In any case, excitatory inputs onto PV and Sst neurons in vivo were predominantly small, with very few large connections detected (the largest being about 3.5 mV detected in a Sst neuron). uEPSPs elicited in Sst neurons were significantly slower than those elicited in PV neurons. As excitatory synaptic currents in GABAergic neurons bear little contribution from NMDA conductances (Thomson et al., 1996; Matta et al., 2013) and are therefore mostly dominated by fast (~1 ms) AMPA conductances, the difference in uEPSP kinetics between PV and Sst neurons could be explained by their different membrane time constant (Figure 3.15D), though their dendritic morphologies as well as the location of the synaptic inputs on their dendritic trees might also contribute. uEPSPs evoked in response to single light stimuli were reliably elicited in PV neurons and they displayed a small coefficient of variation of their amplitude, therefore suggesting a rather high initial probability of neurotransmitter release. Interestingly, uEPSP amplitude was anticorrelated with failure rate in both PV and Sst neurons, suggesting a relationship between uEPSP amplitude and the probability of release (Figure 3.14). Upon high-frequency stimulation, synaptic connections targeting PV neurons displayed little overall dynamics, suggesting a possible interaction of depression and facilitation mechanisms. PV neurons thus appear to rapidly and faithfully respond to any kind of presynaptic excitatory activity pattern. On the contrary, uEPSPs elicited in Sst neurons were unreliable when occurring at low frequency, as assessed by their high coefficient of variation and high failure rate, which seem to indicate a smaller initial probability of neurotransmitter release than for PV neurons (Koester and Johnston, 2005). However, upon higher frequency presynaptic stimulation, excitatory synapses targeting Sst neurons were dominated by facilitation. It seems therefore that Sst neurons are specifically recruited by high-frequency presynaptic excitatory activity, such as that occurring in AP bursts, while responding only sparsely to excitatory suprathreshold activity in the form of single APs with large interspike intervals. As L2/3 excitatory neurons mostly fire single APs at low frequency with some rare bursts of APs in vivo (see Section 4.2), layer 2/3 PV neurons are likely to be key in

tracking excitation and balancing it across several regimes of ongoing activity through dense projections targeted to local excitatory neuron somas (Packer and Yuste, 2011). On the other hand, Sst neurons seem to specifically be recruited in case of particular high excitatory activity, which will lead to their inhibitory action onto neighboring excitatory neurons (Fino and Yuste, 2011) at the level of their distal dendrites. In addition Sst neurons recruitment can lead to inhibition of other inhibitory neurons (Pfeffer et al., 2013), including PV neurons, therefore releasing their inhibitory effect on excitatory neurons somas.

4.5 MODULATION OF uEPSP AMPLITUDE BY UP AND DOWN STATES

We took advantage of the two different levels of network activity present under anesthesia, UP and DOWN states, to investigate their effect on synaptic transmission. Under isoflurane anesthesia, the V_m of PV neurons and most of the Sst neurons (as well as excitatory neurons) fluctuated between a depolarized state (UP) and a hyperpolarized state (DOWN), at a frequency between 0.1 Hz to 4 Hz. Some Sst neurons did not show such a clear fluctuation of their membrane potential, though the frequency content of the UP states was clearly dominated by high frequencies, while the DOWN states exhibited little spontaneous V_m fluctuations (Figure 2.4). The exact frequency of these slow UP-DOWN oscillations was highly dependent of the concentration of isoflurane used. In order to ensure comparable levels of activity across experiments, we adjusted the concentration of isoflurane delivered during the recording session by monitoring the frequency of the slow oscillations in the LFP signal. Indeed, the amplitude of the LFP slow oscillations in the 1-5 Hz frequency band was not significantly different between recording carried out in the Sst-tdTomato mice and those performed in the PV-tdTomato mice (Sst: 0.033 ± 0.011 mV ($n = 34$), PV: 0.033 ± 0.017 mV ($n=19$), $p > 0.05$).

We showed that optogenetic stimulation was equally efficient in triggering single APs in UP states compared to DOWN states in ChR2-expressing excitatory neurons, with no difference in the AP jitter (Figure 3.6). However, it was sometimes the case that the optimal light intensity chosen to elicit single APs during DOWN states lead to two action potentials being triggered during UP states. Even in such configurations the peak of the uEPSP elicited in response to the first AP could be resolved. We therefore restricted our analysis to the comparison of the amplitude of the uEPSP, as any analysis involving detection of uEPSPs in single trials would have been further confounded by the high level of excitatory and inhibitory inputs received by PV and Sst neurons during UP states. At the population level, we did not find a significant difference in the uEPSP amplitude between UP and DOWN states for both PV and Sst neurons. Although certain PV and Sst neurons showed increased uEPSP amplitude in UP states, others exhibited decreased amplitude (Figure 3.21). Previous studies examining corticocortical (Crochet et al., 2005) and thalamocortical synaptic transmission (Bruno and Sakmann, 2006) found reduced uEPSP amplitude in UP compared to DOWN state. In addition, sensory-evoked EPSPs were found to be attenuated in barrel cortex during UP state (Petersen et al.,

2003b; Sachdev et al., 2004; Hasenstaub et al., 2007), while visually-evoked PSPs had similar amplitude in either UP or DOWN states (Haider et al., 2007). Though an increased dataset would surely bring further insight about the role of elevated spontaneous activity on excitatory synaptic transmission in vivo, there are nonetheless several factors, which could account for a decrease or an increase in uEPSP amplitude between UP and DOWN states. UP states being more depolarized than DOWN states for both PV (UP: -50.6 ± 3.0 mV, DOWN: -66.6 ± 3.4 mV, $p < 0.001$) and Sst neurons (UP: -55.4 ± 5.7 mV, DOWN: -59.8 ± 8.5 mV, $p < 0.05$) implies a smaller electrical driving force in UP compared to DOWN state. Based solely on this parameter one would expect uEPSPs to be reduced in amplitude in UP compared to DOWN states. A decrease in input resistance during UP state can also mediate smaller uEPSP amplitude in UP compared to DOWN states. Though input resistance has been found to be smaller in UP state compared to DOWN state in certain cases (Bernander et al., 1991; Destexhe et al., 2003; Leger et al., 2005), in others it was unchanged (Waters and Helmchen, 2006; Mateo et al., 2011). In addition, decreased neurotransmitter release probability can be another reason leading to smaller uEPSP in UP state (Crochet et al., 2005). On the other hand, UP state depolarized membrane potential can lead to activation of somatic (Bazhenov and Timofeev, 2007) and dendritic voltage-gated conductances (Waters and Helmchen, 2004), as well as to an enhanced neurotransmitter release (Shu et al., 2006), all increasing uEPSP amplitude.

Applying high-frequency trains of optogenetic stimuli during UP states could be an alternate manner to gain insight about activity-dependent regulation of short-term synaptic plasticity, as it was shown to be modulated by network activity (Crochet et al., 2006; Reig et al., 2006; Reig and Sanchez-Vives, 2007). Future investigations about synaptic transmission should also be undertaken during wakefulness, where different patterns of neocortical activity correlate with different behaviors. Finally, it will be interesting to investigate the impact of neuromodulators on synaptic transmission in the context of varying neocortical activities and behavioral states.

REFERENCES

- Adesnik, H., and Scanziani, M. (2010). Lateral competition for cortical space by layer-specific horizontal circuits. *Nature* 464, 1155-1160.
- Agmon, A., and Connors, B.W. (1992). Correlation between intrinsic firing patterns and thalamocortical synaptic responses of neurons in mouse barrel cortex. *J Neurosci* 12, 319-329.
- Alloway, K.D. (2008). Information processing streams in rodent barrel cortex: the differential functions of barrel and septal circuits. *Cereb Cortex* 18, 979-989.
- Andrasfalvy, B.K., Zemelman, B.V., Tang, J., and Vaziri, A. (2010). Two-photon single-cell optogenetic control of neuronal activity by sculpted light. *Proc Natl Acad Sci U S A* 107, 11981-11986.
- Arenkiel, B.R., Peca, J., Davison, I.G., Feliciano, C., Deisseroth, K., Augustine, G.J., Ehlers, M.D., and Feng, G. (2007). In vivo light-induced activation of neural circuitry in transgenic mice expressing channelrhodopsin-2. *Neuron* 54, 205-218.
- Armstrong-James, M., Fox, K., and Das-Gupta, A. (1992). Flow of excitation within rat barrel cortex on striking a single vibrissa. *J Neurophysiol* 68, 1345-1358.
- Aronoff, R., Matyas, F., Mateo, C., Ciron, C., Schneider, B., and Petersen, C.C. (2010). Long-range connectivity of mouse primary somatosensory barrel cortex. *Eur J Neurosci* 31, 2221-2233.
- Ascher, P., and Nowak, L. (1986). A patch-clamp study of excitatory amino acid activated channels. *Adv Exp Med Biol* 203, 507-511.
- Ashery, U., Bielopolski, N., Lavi, A., Barak, B., Michaeli, I., Ben-Simon, Y., Sheinin, A., Bar-On, D., Shapira, Z., and Gottfried, I. (2014). The molecular mechanisms underlying synaptic transmission: a view of the presynaptic terminal. In *The synapse : structure and function*, V. Pickel, and M. Segal, eds. (Academic Press), pp. 21-106.
- Atluri, P.P., and Regehr, W.G. (1996). Determinants of the time course of facilitation at the granule cell to Purkinje cell synapse. *J Neurosci* 16, 5661-5671.
- Atluri, P.P., and Regehr, W.G. (1998). Delayed release of neurotransmitter from cerebellar granule cells. *J Neurosci* 18, 8214-8227.
- Atzori, M., Lei, S., Evans, D.I., Kanold, P.O., Phillips-Tansey, E., McIntyre, O., and McBain, C.J. (2001). Differential synaptic processing separates stationary from transient inputs to the auditory cortex. *Nat Neurosci* 4, 1230-1237.
- Avermann, M., Tomm, C., Mateo, C., Gerstner, W., and Petersen, C.C. (2012). Microcircuits of excitatory and inhibitory neurons in layer 2/3 of mouse barrel cortex. *J Neurophysiol* 107, 3116-3134.
- Bacaj, T., Wu, D., Yang, X., Morishita, W., Zhou, P., Xu, W., Malenka, R.C., and Sudhof, T.C. (2013). Synaptotagmin-1 and synaptotagmin-7 trigger synchronous and asynchronous phases of neurotransmitter release. *Neuron* 80, 947-959.
- Bartho, P., Slezia, A., Varga, V., Bokor, H., Pinault, D., Buzsaki, G., and Acsady, L. (2007). Cortical control of zona incerta. *J Neurosci* 27, 1670-1681.

- Bayraktar, T., Welker, E., Freund, T.F., Zilles, K., and Staiger, J.F. (2000). Neurons immunoreactive for vasoactive intestinal polypeptide in the rat primary somatosensory cortex: morphology and spatial relationship to barrel-related columns. *J Comp Neurol* 420, 291-304.
- Bazhenov, M., and Timofeev, I. (2007). Intrinsic and synaptic mechanisms of cortical active states generation during slow wave sleep. In *Mechanisms of spontaneous active states in the neocortex*, I. Timofeev, ed. (Research Signpost), pp. 1-22.
- Bazhenov, M., Timofeev, I., Steriade, M., and Sejnowski, T.J. (2002). Model of thalamocortical slow-wave sleep oscillations and transitions to activated States. *J Neurosci* 22, 8691-8704.
- Beaulieu, C. (1993). Numerical data on neocortical neurons in adult rat, with special reference to the GABA population. *Brain Res* 609, 284-292.
- Beaulieu, C., and Colonnier, M. (1985). A laminar analysis of the number of round-asymmetrical and flat-symmetrical synapses on spines, dendritic trunks, and cell bodies in area 17 of the cat. *J Comp Neurol* 231, 180-189.
- Begue, A., Papagiakoumou, E., Leshem, B., Conti, R., Enke, L., Oron, D., and Emiliani, V. (2013). Two-photon excitation in scattering media by spatiotemporally shaped beams and their application in optogenetic stimulation. *Biomed Opt Express* 4, 2869-2879.
- Beierlein, M., Gibson, J.R., and Connors, B.W. (2003). Two dynamically distinct inhibitory networks in layer 4 of the neocortex. *J Neurophysiol* 90, 2987-3000.
- Beltramo, R., D'Urso, G., Dal Maschio, M., Farisello, P., Bovetti, S., Clovis, Y., Lassi, G., Tucci, V., De Pietri Tonelli, D., and Fellin, T. (2013). Layer-specific excitatory circuits differentially control recurrent network dynamics in the neocortex. *Nat Neurosci* 16, 227-234.
- Bennett, M.R. (2001). The Discovery of Acetylcholine and the Concept of Receptors at Synapses. In *History of the synapse*, C. Press, ed. (Hardwood academy publishers), pp. 43-64.
- Berg, R.W., and Kleinfeld, D. (2003). Rhythmic whisking by rat: retraction as well as protraction of the vibrissae is under active muscular control. *J Neurophysiol* 89, 104-117.
- Berger, H. (1929). Uber das Elektroenkephalogramm des menschen. *Arch Psychiat* 87, 527-570.
- Bernander, O., Douglas, R.J., Martin, K.A., and Koch, C. (1991). Synaptic background activity influences spatiotemporal integration in single pyramidal cells. *Proc Natl Acad Sci U S A* 88, 11569-11573.
- Berndt, A., Schoenenberger, P., Mattis, J., Tye, K.M., Deisseroth, K., Hegemann, P., and Oertner, T.G. (2011). High-efficiency channelrhodopsins for fast neuronal stimulation at low light levels. *Proc Natl Acad Sci U S A* 108, 7595-7600.
- Bestman, J.E., Ewald, R.C., Chiu, S.L., and Cline, H.T. (2006). In vivo single-cell electroporation for transfer of DNA and macromolecules. *Nat Protoc* 1, 1267-1272.
- Biro, A.A., Holderith, N.B., and Nusser, Z. (2005). Quantal size is independent of the release probability at hippocampal excitatory synapses. *J Neurosci* 25, 223-232.
- Biro, A.A., Holderith, N.B., and Nusser, Z. (2006). Release probability-dependent scaling of the postsynaptic responses at single hippocampal GABAergic synapses. *J Neurosci* 26, 12487-12496.

- Blatow, M., Caputi, A., Burnashev, N., Monyer, H., and Rozov, A. (2003). Ca²⁺ buffer saturation underlies paired pulse facilitation in calbindin-D28k-containing terminals. *Neuron* 38, 79-88.
- Blatow, M., Caputi, A., and Monyer, H. (2005). Molecular diversity of neocortical GABAergic interneurons. *J Physiol* 562, 99-105.
- Bobrov, E., Wolfe, J., Rao, R.P., and Brecht, M. (2014). The representation of social facial touch in rat barrel cortex. *Curr Biol* 24, 109-115.
- Borst, J.G. (2010). The low synaptic release probability in vivo. *Trends Neurosci* 33, 259-266.
- Boudreau, C.E., and Ferster, D. (2005). Short-term depression in thalamocortical synapses of cat primary visual cortex. *J Neurosci* 25, 7179-7190.
- Bourassa, J., Pinault, D., and Deschenes, M. (1995). Corticothalamic projections from the cortical barrel field to the somatosensory thalamus in rats: a single-fibre study using biocytin as an anterograde tracer. *Eur J Neurosci* 7, 19-30.
- Boyden, E.S., Zhang, F., Bamberg, E., Nagel, G., and Deisseroth, K. (2005). Millisecond-timescale, genetically targeted optical control of neural activity. *Nat Neurosci* 8, 1263-1268.
- Branco, T., and Staras, K. (2009). The probability of neurotransmitter release: variability and feedback control at single synapses. *Nat Rev Neurosci* 10, 373-383.
- Brecht, M., Roth, A., and Sakmann, B. (2003). Dynamic receptive fields of reconstructed pyramidal cells in layers 3 and 2 of rat somatosensory barrel cortex. *J Physiol* 553, 243-265.
- Brecht, M., and Sakmann, B. (2002). Dynamic representation of whisker deflection by synaptic potentials in spiny stellate and pyramidal cells in the barrels and septa of layer 4 rat somatosensory cortex. *J Physiol* 543, 49-70.
- Brill, J., and Huguenard, J.R. (2009). Robust short-latency perisomatic inhibition onto neocortical pyramidal cells detected by laser-scanning photostimulation. *J Neurosci* 29, 7413-7423.
- Brock, L.G., Coombs, J.S., and Eccles, J.C. (1952). The recording of potentials from motoneurons with an intracellular electrode. *J Physiol* 117, 431-460.
- Bruno, R.M., Hahn, T.T., Wallace, D.J., de Kock, C.P., and Sakmann, B. (2009). Sensory experience alters specific branches of individual corticocortical axons during development. *J Neurosci* 29, 3172-3181.
- Bruno, R.M., and Sakmann, B. (2006). Cortex is driven by weak but synchronously active thalamocortical synapses. *Science* 312, 1622-1627.
- Bruno, R.M., and Simons, D.J. (2002). Feedforward mechanisms of excitatory and inhibitory cortical receptive fields. *J Neurosci* 22, 10966-10975.
- Bureau, I., von Saint Paul, F., and Svoboda, K. (2006). Interdigitated paralemniscal and lemniscal pathways in the mouse barrel cortex. *PLoS Biol* 4, e382.
- Burkhalter, A. (2008). Many specialists for suppressing cortical excitation. *Front Neurosci* 2, 155-167.
- Butt, S.J., Fuccillo, M., Nery, S., Noctor, S., Kriegstein, A., Corbin, J.G., and Fishell, G. (2005). The temporal and spatial origins of cortical interneurons predict their physiological subtype. *Neuron* 48, 591-604.

- Buzsáki, G. (2006). *Rhythms of the brain* (Oxford University Press).
- Buzsaki, G., Logothetis, N., and Singer, W. (2013). Scaling brain size, keeping timing: evolutionary preservation of brain rhythms. *Neuron* 80, 751-764.
- Callaway, E.M., and Katz, L.C. (1993). Photostimulation using caged glutamate reveals functional circuitry in living brain slices. *Proc Natl Acad Sci U S A* 90, 7661-7665.
- Carvell, G.E., and Simons, D.J. (1990). Biometric analyses of vibrissal tactile discrimination in the rat. *J Neurosci* 10, 2638-2648.
- Caton, R. (1875). The electric currents of the brain. *Br Med J*, 2: 278.
- Catterall, W.A., and Few, A.P. (2008). Calcium channel regulation and presynaptic plasticity. *Neuron* 59, 882-901.
- Cauli, B., Audinat, E., Lambolez, B., Angulo, M.C., Ropert, N., Tsuzuki, K., Hestrin, S., and Rossier, J. (1997). Molecular and physiological diversity of cortical nonpyramidal cells. *J Neurosci* 17, 3894-3906.
- Chagnac-Amitai, Y., and Connors, B.W. (1989). Synchronized excitation and inhibition driven by intrinsically bursting neurons in neocortex. *J Neurophysiol* 62, 1149-1162.
- Chauvette, S., Volgushev, M., Mukovski, M., Timofeev, I. (2007). Local origin and long-range synchrony of active state in neocortex during slow oscillation. In *Mechanisms of spontaneous active states in the neocortex*, I. Timofeev, ed. (Research Signpost), pp. 73-92.
- Chen, J.L., Carta, S., Soldado-Magraner, J., Schneider, B.L., and Helmchen, F. (2013). Behaviour-dependent recruitment of long-range projection neurons in somatosensory cortex. *Nature* 499, 336-340.
- Christie, J.M., and Jahr, C.E. (2006). Multivesicular release at Schaffer collateral-CA1 hippocampal synapses. *J Neurosci* 26, 210-216.
- Chu, Z., Galarreta, M., and Hestrin, S. (2003). Synaptic interactions of late-spiking neocortical neurons in layer 1. *J Neurosci* 23, 96-102.
- Compte, A., Sanchez-Vives, M.V., McCormick, D.A., and Wang, X.J. (2003). Cellular and network mechanisms of slow oscillatory activity (<1 Hz) and wave propagations in a cortical network model. *J Neurophysiol* 89, 2707-2725.
- Connors, B.W., and Gutnick, M.J. (1990). Intrinsic firing patterns of diverse neocortical neurons. *Trends Neurosci* 13, 99-104.
- Constantinidis, C., Williams, G.V., and Goldman-Rakic, P.S. (2002). A role for inhibition in shaping the temporal flow of information in prefrontal cortex. *Nat Neurosci* 5, 175-180.
- Constantinople, C.M., and Bruno, R.M. (2011). Effects and mechanisms of wakefulness on local cortical networks. *Neuron* 69, 1061-1068.
- Constantinople, C.M., and Bruno, R.M. (2013). Deep cortical layers are activated directly by thalamus. *Science* 340, 1591-1594.
- Contreras, D. (2004). Electrophysiological classes of neocortical neurons. *Neural Netw* 17, 633-646.

- Contreras, D., Timofeev, I., and Steriade, M. (1996). Mechanisms of long-lasting hyperpolarizations underlying slow sleep oscillations in cat corticothalamic networks. *J Physiol* 494 (Pt 1), 251-264.
- Cowan, R.L., and Wilson, C.J. (1994). Spontaneous firing patterns and axonal projections of single corticostriatal neurons in the rat medial agranular cortex. *J Neurophysiol* 71, 17-32.
- Crochet, S., Chauvette, S., Boucetta, S., and Timofeev, I. (2005). Modulation of synaptic transmission in neocortex by network activities. *Eur J Neurosci* 21, 1030-1044.
- Crochet, S., Fuentealba, P., Cisse, Y., Timofeev, I., and Steriade, M. (2006). Synaptic plasticity in local cortical network in vivo and its modulation by the level of neuronal activity. *Cereb Cortex* 16, 618-631.
- Crochet, S., and Petersen, C.C. (2006). Correlating whisker behavior with membrane potential in barrel cortex of awake mice. *Nat Neurosci* 9, 608-610.
- Cruikshank, S.J., Urabe, H., Nurmikko, A.V., and Connors, B.W. (2010). Pathway-specific feedforward circuits between thalamus and neocortex revealed by selective optical stimulation of axons. *Neuron* 65, 230-245.
- Cunningham, M.O., Pervouchine, D.D., Racca, C., Kopell, N.J., Davies, C.H., Jones, R.S., Traub, R.D., and Whittington, M.A. (2006). Neuronal metabolism governs cortical network response state. *Proc Natl Acad Sci U S A* 103, 5597-5601.
- Curtis, D.R., and Watkins, J.C. (1960). The excitation and depression of spinal neurones by structurally related amino acids. *J Neurochem* 6, 117-141.
- Curtis, D.R., and Watkins, J.C. (1961). Analogues of glutamic and gamma-amino-n-butyric acids having potent actions on mammalian neurones. *Nature* 191, 1010-1011.
- de Kock, C.P., Bruno, R.M., Spors, H., and Sakmann, B. (2007). Layer- and cell-type-specific suprathreshold stimulus representation in rat primary somatosensory cortex. *J Physiol* 581, 139-154.
- de Kock, C.P., and Sakmann, B. (2008). High frequency action potential bursts (≥ 100 Hz) in L2/3 and L5B thick tufted neurons in anaesthetized and awake rat primary somatosensory cortex. *J Physiol* 586, 3353-3364.
- DeFelipe, J., Alonso-Nanclares, L., and Arellano, J.I. (2002). Microstructure of the neocortex: comparative aspects. *J Neurocytol* 31, 299-316.
- DeFelipe, J., and Farinas, I. (1992). The pyramidal neuron of the cerebral cortex: morphological and chemical characteristics of the synaptic inputs. *Prog Neurobiol* 39, 563-607.
- DeFelipe, J., Lopez-Cruz, P.L., Benavides-Piccione, R., Bielza, C., Larranaga, P., Anderson, S., Burkhalter, A., Cauli, B., Fairen, A., Feldmeyer, D., *et al.* (2013). New insights into the classification and nomenclature of cortical GABAergic interneurons. *Nat Rev Neurosci* 14, 202-216.
- Del Castillo, J., and Katz, B. (1954). Quantal components of the end-plate potential. *J Physiol* 124, 560-573.
- Del Castillo, J., and Katz, B. (1956). Biophysical aspects of neuro-muscular transmission. *Prog Biophys Biophys Chem* 6, 121-170.

- Denk, W., Strickler, J.H., and Webb, W.W. (1990). Two-photon laser scanning fluorescence microscopy. *Science* 248, 73-76.
- Deschênes, M., and Urbain, N. (2009). Vibrissal afferents from trigeminus to cortices. In *Scholarpedia*, p. 7454.
- Destexhe, A., Contreras, D., and Steriade, M. (1999). Spatiotemporal analysis of local field potentials and unit discharges in cat cerebral cortex during natural wake and sleep states. *J Neurosci* 19, 4595-4608.
- Destexhe, A., Hughes, S.W., Rudolph, M., and Crunelli, V. (2007). Are corticothalamic 'up' states fragments of wakefulness? *Trends Neurosci* 30, 334-342.
- Destexhe, A., Rudolph, M., and Pare, D. (2003). The high-conductance state of neocortical neurons in vivo. *Nat Rev Neurosci* 4, 739-751.
- Deuchars, J., and Thomson, A.M. (1995). Innervation of burst firing spiny interneurons by pyramidal cells in deep layers of rat somatomotor cortex: paired intracellular recordings with biocytin filling. *Neuroscience* 69, 739-755.
- Deuchars, J., West, D.C., and Thomson, A.M. (1994). Relationships between morphology and physiology of pyramid-pyramid single axon connections in rat neocortex in vitro. *J Physiol* 478 Pt 3, 423-435.
- Diamond, M.E., Armstrong-James, M., and Ebner, F.F. (1992). Somatic sensory responses in the rostral sector of the posterior group (POm) and in the ventral posterior medial nucleus (VPM) of the rat thalamus. *J Comp Neurol* 318, 462-476.
- Dittman, J.S., Kreitzer, A.C., and Regehr, W.G. (2000). Interplay between facilitation, depression, and residual calcium at three presynaptic terminals. *J Neurosci* 20, 1374-1385.
- Dittman, J.S., and Regehr, W.G. (1997). Mechanism and kinetics of heterosynaptic depression at a cerebellar synapse. *J Neurosci* 17, 9048-9059.
- Dodge, F.A., Jr., and Rahamimoff, R. (1967). Co-operative action a calcium ions in transmitter release at the neuromuscular junction. *J Physiol* 193, 419-432.
- Douglas, R., Markram, H. and Martin, K. (2004). Neocortex. In *The synaptic organization of the brain*, G.M. Shepherd, ed. (Oxford University Press), pp. 499-558.
- Douglas, R.J., and Martin, K.A. (2004). Neuronal circuits of the neocortex. *Annu Rev Neurosci* 27, 419-451.
- Dresbach, T., Qualmann, B., Kessels, M.M., Garner, C.C., and Gundelfinger, E.D. (2001). The presynaptic cytomatrix of brain synapses. *Cell Mol Life Sci* 58, 94-116.
- Eccles, J.C. (1987). Recollections on the early concepts of the synapse. *Synapse* 1, 131-132.
- Edwards, F.A., Konnerth, A., Sakmann, B., and Takahashi, T. (1989). A thin slice preparation for patch clamp recordings from neurones of the mammalian central nervous system. *Pflugers Arch* 414, 600-612.
- Egger, V., Nevian, T., and Bruno, R.M. (2008). Subcolumnar dendritic and axonal organization of spiny stellate and star pyramid neurons within a barrel in rat somatosensory cortex. *Cereb Cortex* 18, 876-889.

- Escoffre, J.M., Portet, T., Wasungu, L., Teissie, J., Dean, D., and Rols, M.P. (2009). What is (still not) known of the mechanism by which electroporation mediates gene transfer and expression in cells and tissues. *Mol Biotechnol* 41, 286-295.
- Fanselow, E.E., and Connors, B.W. (2010). The roles of somatostatin-expressing (GIN) and fast-spiking inhibitory interneurons in UP-DOWN states of mouse neocortex. *J Neurophysiol* 104, 596-606.
- Fanselow, E.E., Richardson, K.A., and Connors, B.W. (2008). Selective, state-dependent activation of somatostatin-expressing inhibitory interneurons in mouse neocortex. *J Neurophysiol* 100, 2640-2652.
- Fatt, P., and Katz, B. (1952). Spontaneous subthreshold activity at motor nerve endings. *J Physiol* 117, 109-128.
- Featherstone, D.E., and Shippy, S.A. (2008). Regulation of synaptic transmission by ambient extracellular glutamate. *Neuroscientist* 14, 171-181.
- Feldmeyer, D. (2012). Excitatory neuronal connectivity in the barrel cortex. *Front Neuroanat* 6, 24.
- Feldmeyer, D., Egger, V., Lubke, J., and Sakmann, B. (1999). Reliable synaptic connections between pairs of excitatory layer 4 neurones within a single 'barrel' of developing rat somatosensory cortex. *J Physiol* 521 Pt 1, 169-190.
- Feldmeyer, D., Lubke, J., and Sakmann, B. (2006). Efficacy and connectivity of intracolumnar pairs of layer 2/3 pyramidal cells in the barrel cortex of juvenile rats. *J Physiol* 575, 583-602.
- Feldmeyer, D., Lubke, J., Silver, R.A., and Sakmann, B. (2002). Synaptic connections between layer 4 spiny neurone-layer 2/3 pyramidal cell pairs in juvenile rat barrel cortex: physiology and anatomy of interlaminar signalling within a cortical column. *J Physiol* 538, 803-822.
- Feldmeyer, D., and Radnikow, G. (2009). Developmental alterations in the functional properties of excitatory neocortical synapses. *J Physiol* 587, 1889-1896.
- Feldmeyer, D., Roth, A., and Sakmann, B. (2005). Monosynaptic connections between pairs of spiny stellate cells in layer 4 and pyramidal cells in layer 5A indicate that lemniscal and paralemniscal afferent pathways converge in the infragranular somatosensory cortex. *J Neurosci* 25, 3423-3431.
- Fenko, L., Yizhar, O., and Deisseroth, K. (2011). The development and application of optogenetics. *Annu Rev Neurosci* 34, 389-412.
- Ferezou, I., Bolea, S., and Petersen, C.C. (2006). Visualizing the cortical representation of whisker touch: voltage-sensitive dye imaging in freely moving mice. *Neuron* 50, 617-629.
- Fetz, E.E., Toyama, K., and Smith, W. (1991). Synaptic interactions between cortical neurons. *Cerebral Cortex* 9, 1-47.
- Finnerty, G.T., Roberts, L.S., and Connors, B.W. (1999). Sensory experience modifies the short-term dynamics of neocortical synapses. *Nature* 400, 367-371.
- Fino, E., and Yuste, R. (2011). Dense inhibitory connectivity in neocortex. *Neuron* 69, 1188-1203.
- Fioravante, D., and Regehr, W.G. (2011). Short-term forms of presynaptic plasticity. *Curr Opin Neurobiol* 21, 269-274.

- Fisher, S.A., Fischer, T.M., and Carew, T.J. (1997). Multiple overlapping processes underlying short-term synaptic enhancement. *Trends Neurosci* 20, 170-177.
- Fishman, M.C. (1972). Sir Henry Hallett Dale and acetylcholine story. *Yale J Biol Med* 45, 104-118.
- Fox, K. (2008). Anatomical pathways. In *Barrel cortex* (Cambridge University Press), pp. 14-48.
- Frick, A., Feldmeyer, D., and Sakmann, B. (2007). Postnatal development of synaptic transmission in local networks of L5A pyramidal neurons in rat somatosensory cortex. *J Physiol* 585, 103-116.
- Fujisawa, S., Amarasingham, A., Harrison, M.T., and Buzsaki, G. (2008). Behavior-dependent short-term assembly dynamics in the medial prefrontal cortex. *Nat Neurosci* 11, 823-833.
- Fukuda, T. (2007). Structural organization of the gap junction network in the cerebral cortex. *Neuroscientist* 13, 199-207.
- Galarreta, M., and Hestrin, S. (1998). Frequency-dependent synaptic depression and the balance of excitation and inhibition in the neocortex. *Nat Neurosci* 1, 587-594.
- Geiger, J.R., and Jonas, P. (2000). Dynamic control of presynaptic Ca²⁺ inflow by fast-inactivating K⁺ channels in hippocampal mossy fiber boutons. *Neuron* 28, 927-939.
- Gentet, L.J. (2012). Functional diversity of supragranular GABAergic neurons in the barrel cortex. *Front Neural Circuits* 6, 52.
- Gentet, L.J., Avermann, M., Matyas, F., Staiger, J.F., and Petersen, C.C. (2010). Membrane potential dynamics of GABAergic neurons in the barrel cortex of behaving mice. *Neuron* 65, 422-435.
- Gentet, L.J., Kremer, Y., Taniguchi, H., Huang, Z.J., Staiger, J.F., and Petersen, C.C. (2012). Unique functional properties of somatostatin-expressing GABAergic neurons in mouse barrel cortex. *Nat Neurosci* 15, 607-612.
- Gil, Z., Connors, B.W., and Amitai, Y. (1997). Differential regulation of neocortical synapses by neuromodulators and activity. *Neuron* 19, 679-686.
- Glykys, J., and Mody, I. (2007). Activation of GABAA receptors: views from outside the synaptic cleft. *Neuron* 56, 763-770.
- Goda, Y., and Stevens, C.F. (1994). Two components of transmitter release at a central synapse. *Proc Natl Acad Sci U S A* 91, 12942-12946.
- Golzio, M., Teissie, J., and Rols, M.P. (2002). Direct visualization at the single-cell level of electrically mediated gene delivery. *Proc Natl Acad Sci U S A* 99, 1292-1297.
- Gonchar, Y., Wang, Q., and Burkhalter, A. (2007). Multiple distinct subtypes of GABAergic neurons in mouse visual cortex identified by triple immunostaining. *Front Neuroanat* 1, 3.
- Gottlieb, J.P., and Keller, A. (1997). Intrinsic circuitry and physiological properties of pyramidal neurons in rat barrel cortex. *Exp Brain Res* 115, 47-60.
- Gould, E. (2007). How widespread is adult neurogenesis in mammals? *Nat Rev Neurosci* 8, 481-488.
- Gradinaru, V., Zhang, F., Ramakrishnan, C., Mattis, J., Prakash, R., Diester, I., Goshen, I., Thompson, K.R., and Deisseroth, K. (2010). Molecular and cellular approaches for diversifying and extending optogenetics. *Cell* 141, 154-165.

- Gray, E.G. (1959). Axo-somatic and axo-dendritic synapses of the cerebral cortex: an electron microscope study. *J Anat* 93, 420-433.
- Grinvald, A., Lieke, E., Frostig, R.D., Gilbert, C.D., and Wiesel, T.N. (1986). Functional architecture of cortex revealed by optical imaging of intrinsic signals. *Nature* 324, 361-364.
- Groh, A., de Kock, C.P., Wimmer, V.C., Sakmann, B., and Kuner, T. (2008). Driver or coincidence detector: modal switch of a corticothalamic giant synapse controlled by spontaneous activity and short-term depression. *J Neurosci* 28, 9652-9663.
- Gulyas, A.I., Miles, R., Sik, A., Toth, K., Tamamaki, N., and Freund, T.F. (1993). Hippocampal pyramidal cells excite inhibitory neurons through a single release site. *Nature* 366, 683-687.
- Gupta, A., Wang, Y., and Markram, H. (2000). Organizing principles for a diversity of GABAergic interneurons and synapses in the neocortex. *Science* 287, 273-278.
- Haas, K., Sin, W.C., Javaherian, A., Li, Z., and Cline, H.T. (2001). Single-cell electroporation for gene transfer in vivo. *Neuron* 29, 583-591.
- Haider, B., Duque, A., Hasenstaub, A.R., and McCormick, D.A. (2006). Neocortical network activity in vivo is generated through a dynamic balance of excitation and inhibition. *J Neurosci* 26, 4535-4545.
- Haider, B., Duque, A., Hasenstaub, A.R., Yu, Y., and McCormick, D.A. (2007). Enhancement of visual responsiveness by spontaneous local network activity in vivo. *J Neurophysiol* 97, 4186-4202.
- Halabisky, B., Shen, F., Huguenard, J.R., and Prince, D.A. (2006). Electrophysiological classification of somatostatin-positive interneurons in mouse sensorimotor cortex. *J Neurophysiol* 96, 834-845.
- Hansen, A.J. (1985). Effect of anoxia on ion distribution in the brain. *Physiol Rev* 65, 101-148.
- Hasenstaub, A., Sachdev, R.N., and McCormick, D.A. (2007). State changes rapidly modulate cortical neuronal responsiveness. *J Neurosci* 27, 9607-9622.
- Hayashi, T. (1952). A physiological study of epileptic seizures following cortical stimulation in animals and its application to human clinics. *Jpn J Physiol* 3, 46-64.
- Hayashi, T. (1959). The inhibitory action of beta-hydroxy-gamma-aminobutyric acid upon the seizure following stimulation of the motor cortex of the dog. *J Physiol* 145, 570-578.
- Heinemann, U., Lux, H.D., and Gutnick, M.J. (1977). Extracellular free calcium and potassium during paroxysmal activity in the cerebral cortex of the cat. *Exp Brain Res* 27, 237-243.
- Helmstaedter, M., Sakmann, B., and Feldmeyer, D. (2009a). L2/3 interneuron groups defined by multiparameter analysis of axonal projection, dendritic geometry, and electrical excitability. *Cereb Cortex* 19, 951-962.
- Helmstaedter, M., Sakmann, B., and Feldmeyer, D. (2009b). Neuronal correlates of local, lateral, and translaminar inhibition with reference to cortical columns. *Cereb Cortex* 19, 926-937.
- Helmstaedter, M., Sakmann, B., and Feldmeyer, D. (2009c). The relation between dendritic geometry, electrical excitability, and axonal projections of L2/3 interneurons in rat barrel cortex. *Cereb Cortex* 19, 938-950.

- Helmstaedter, M., Staiger, J.F., Sakmann, B., and Feldmeyer, D. (2008). Efficient recruitment of layer 2/3 interneurons by layer 4 input in single columns of rat somatosensory cortex. *J Neurosci* 28, 8273-8284.
- Herculano-Houzel, S. (2009). The human brain in numbers: a linearly scaled-up primate brain. *Front Hum Neurosci* 3, 31.
- Hestrin, S. (1993). Different glutamate receptor channels mediate fast excitatory synaptic currents in inhibitory and excitatory cortical neurons. *Neuron* 11, 1083-1091.
- Higley, M.J., and Contreras, D. (2003). Nonlinear integration of sensory responses in the rat barrel cortex: an intracellular study in vivo. *J Neurosci* 23, 10190-10200.
- Hille, B. (2001). *Ion channels of excitable membranes* (Sinauer Associates).
- Hippenmeyer, S., Vrieseling, E., Sigrist, M., Portmann, T., Laengle, C., Ladle, D.R., and Arber, S. (2005). A developmental switch in the response of DRG neurons to ETS transcription factor signaling. *PLoS Biol* 3, e159.
- Ho, S.Y., and Mittal, G.S. (1996). Electroporation of cell membranes: a review. *Crit Rev Biotechnol* 16, 349-362.
- Hofer, S.B., Ko, H., Pichler, B., Vogelstein, J., Ros, H., Zeng, H., Lein, E., Lesica, N.A., and Mrsic-Flogel, T.D. (2011). Differential connectivity and response dynamics of excitatory and inhibitory neurons in visual cortex. *Nat Neurosci* 14, 1045-1052.
- Hollmann, M., and Heinemann, S. (1994). Cloned glutamate receptors. *Annu Rev Neurosci* 17, 31-108.
- Holmgren, C., Harkany, T., Svennenfors, B., and Zilberter, Y. (2003). Pyramidal cell communication within local networks in layer 2/3 of rat neocortex. *J Physiol* 551, 139-153.
- Hooks, B.M., Hires, S.A., Zhang, Y.X., Huber, D., Petreanu, L., Svoboda, K., and Shepherd, G.M. (2011). Laminar analysis of excitatory local circuits in vibrissal motor and sensory cortical areas. *PLoS Biol* 9, e1000572.
- Hu, H., Cavendish, J.Z., and Agmon, A. (2013). Not all that glitters is gold: off-target recombination in the somatostatin-IRES-Cre mouse line labels a subset of fast-spiking interneurons. *Front Neural Circuits* 7, 195.
- Hubel, D.H., and Wiesel, T.N. (1962). Receptive fields, binocular interaction and functional architecture in the cat's visual cortex. *J Physiol* 160, 106-154.
- Hubel, D.H., and Wiesel, T.N. (1963). Shape and arrangement of columns in cat's striate cortex. *J Physiol* 165, 559-568.
- Hutson, K.A., and Masterton, R.B. (1986). The sensory contribution of a single vibrissa's cortical barrel. *J Neurophysiol* 56, 1196-1223.
- Jackman, S.L., Beneduce, B.M., Drew, I.R., and Regehr, W.G. (2014). Achieving high-frequency optical control of synaptic transmission. *J Neurosci* 34, 7704-7714.
- Jefferys, J.G. (1995). Nonsynaptic modulation of neuronal activity in the brain: electric currents and extracellular ions. *Physiol Rev* 75, 689-723.

- Ji, D., and Wilson, M.A. (2007). Coordinated memory replay in the visual cortex and hippocampus during sleep. *Nat Neurosci* 10, 100-107.
- Jiang, X., Wang, G., Lee, A.J., Stornetta, R.L., and Zhu, J.J. (2013). The organization of two new cortical interneuronal circuits. *Nat Neurosci* 16, 210-218.
- Jonas, P., Racca, C., Sakmann, B., Seeburg, P.H., and Monyer, H. (1994). Differences in Ca²⁺ permeability of AMPA-type glutamate receptor channels in neocortical neurons caused by differential GluR-B subunit expression. *Neuron* 12, 1281-1289.
- Jones, H.C., and Keep, R.F. (1988). Brain fluid calcium concentration and response to acute hypercalcaemia during development in the rat. *J Physiol* 402, 579-593.
- Jones, M.V., and Westbrook, G.L. (1996). The impact of receptor desensitization on fast synaptic transmission. *Trends Neurosci* 19, 96-101.
- Judkewitz, B., Rizzi, M., Kitamura, K., and Hausser, M. (2009). Targeted single-cell electroporation of mammalian neurons in vivo. *Nat Protoc* 4, 862-869.
- Kang, J., Huguenard, J.R., and Prince, D.A. (1996). Two types of BK channels in immature rat neocortical pyramidal neurons. *J Neurophysiol* 76, 4194-4197.
- Kapfer, C., Glickfeld, L.L., Atallah, B.V., and Scanziani, M. (2007). Supralinear increase of recurrent inhibition during sparse activity in the somatosensory cortex. *Nat Neurosci* 10, 743-753.
- Katz, B., and Miledi, R. (1967). A study of synaptic transmission in the absence of nerve impulses. *J Physiol* 192, 407-436.
- Katz, B., and Miledi, R. (1968). The role of calcium in neuromuscular facilitation. *J Physiol* 195, 481-492.
- Katz, B., and Miledi, R. (1970). Further study of the role of calcium in synaptic transmission. *J Physiol* 207, 789-801.
- Katzel, D., Zemelman, B.V., Buettner, C., Wolfel, M., and Miesenbock, G. (2011). The columnar and laminar organization of inhibitory connections to neocortical excitatory cells. *Nat Neurosci* 14, 100-107.
- Kekesi, K.A., Dobolyi, A., Salfay, O., Nyitrai, G., and Juhasz, G. (1997). Slow wave sleep is accompanied by release of certain amino acids in the thalamus of cats. *Neuroreport* 8, 1183-1186.
- Killackey, H.P., and Belford, G.R. (1979). The formation of afferent patterns in the somatosensory cortex of the neonatal rat. *J Comp Neurol* 183, 285-303.
- Killackey, H.P., and Leshin, S. (1975). The organization of specific thalamocortical projections to the posteromedial barrel subfield of the rat somatic sensory cortex. *Brain Res* 86, 469-472.
- Killackey, H.P., and Sherman, S.M. (2003). Corticothalamic projections from the rat primary somatosensory cortex. *J Neurosci* 23, 7381-7384.
- Kirov, S.A., Sorra, K.E., and Harris, K.M. (1999). Slices have more synapses than perfusion-fixed hippocampus from both young and mature rats. *J Neurosci* 19, 2876-2886.
- Kitamura, K., Judkewitz, B., Kano, M., Denk, W., and Hausser, M. (2008). Targeted patch-clamp recordings and single-cell electroporation of unlabeled neurons in vivo. *Nat Methods* 5, 61-67.

- Koester, H.J., and Johnston, D. (2005). Target cell-dependent normalization of transmitter release at neocortical synapses. *Science* 308, 863-866.
- Kole, M.H., and Stuart, G.J. (2008). Is action potential threshold lowest in the axon? *Nat Neurosci* 11, 1253-1255.
- Komai, S., Denk, W., Osten, P., Brecht, M., and Margrie, T.W. (2006). Two-photon targeted patching (TPTP) in vivo. *Nat Protoc* 1, 647-652.
- Korngreen, A., and Sakmann, B. (2000). Voltage-gated K⁺ channels in layer 5 neocortical pyramidal neurones from young rats: subtypes and gradients. *J Physiol* 525 Pt 3, 621-639.
- Kozloski, J., Hamzei-Sichani, F., and Yuste, R. (2001). Stereotyped position of local synaptic targets in neocortex. *Science* 293, 868-872.
- Krupa, D.J., Matell, M.S., Brisben, A.J., Oliveira, L.M., and Nicolelis, M.A. (2001). Behavioral properties of the trigeminal somatosensory system in rats performing whisker-dependent tactile discriminations. *J Neurosci* 21, 5752-5763.
- Kubota, Y., and Kawaguchi, Y. (1994). Three classes of GABAergic interneurons in neocortex and neostriatum. *Jpn J Physiol* 44 Suppl 2, S145-148.
- Kwan, A.C., and Dan, Y. (2012). Dissection of cortical microcircuits by single-neuron stimulation in vivo. *Curr Biol* 22, 1459-1467.
- Lambert, N.A., and Wilson, W.A. (1994). Temporally distinct mechanisms of use-dependent depression at inhibitory synapses in the rat hippocampus in vitro. *J Neurophysiol* 72, 121-130.
- Lampl, I., Reichova, I., and Ferster, D. (1999). Synchronous membrane potential fluctuations in neurons of the cat visual cortex. *Neuron* 22, 361-374.
- Land, P.W., and Simons, D.J. (1985). Cytochrome oxidase staining in the rat SmI barrel cortex. *J Comp Neurol* 238, 225-235.
- Landis, D.M., Hall, A.K., Weinstein, L.A., and Reese, T.S. (1988). The organization of cytoplasm at the presynaptic active zone of a central nervous system synapse. *Neuron* 1, 201-209.
- Larkum, M.E., Zhu, J.J., and Sakmann, B. (1999). A new cellular mechanism for coupling inputs arriving at different cortical layers. *Nature* 398, 338-341.
- Larsen, D.D., and Callaway, E.M. (2006). Development of layer-specific axonal arborizations in mouse primary somatosensory cortex. *J Comp Neurol* 494, 398-414.
- Larsen, D.D., Wickersham, I.R., and Callaway, E.M. (2007). Retrograde tracing with recombinant rabies virus reveals correlations between projection targets and dendritic architecture in layer 5 of mouse barrel cortex. *Front Neural Circuits* 1, 5.
- Lawrence, J.J., Grinspan, Z.M., and McBain, C.J. (2004). Quantal transmission at mossy fibre targets in the CA3 region of the rat hippocampus. *J Physiol* 554, 175-193.
- Le Be, J.V., Silberberg, G., Wang, Y., and Markram, H. (2007). Morphological, electrophysiological, and synaptic properties of corticocallosal pyramidal cells in the neonatal rat neocortex. *Cereb Cortex* 17, 2204-2213.

- Lee, S., Hjerling-Leffler, J., Zagha, E., Fishell, G., and Rudy, B. (2010). The largest group of superficial neocortical GABAergic interneurons expresses ionotropic serotonin receptors. *J Neurosci* 30, 16796-16808.
- Lefort, S., Tómm, C., Floyd Sarria, J.C., and Petersen, C.C. (2009). The excitatory neuronal network of the C2 barrel column in mouse primary somatosensory cortex. *Neuron* 61, 301-316.
- Leger, J.F., Stern, E.A., Aertsen, A., and Heck, D. (2005). Synaptic integration in rat frontal cortex shaped by network activity. *J Neurophysiol* 93, 281-293.
- Li, X., Gutierrez, D.V., Hanson, M.G., Han, J., Mark, M.D., Chiel, H., Hegemann, P., Landmesser, L.T., and Herlitze, S. (2005). Fast noninvasive activation and inhibition of neural and network activity by vertebrate rhodopsin and green algae channelrhodopsin. *Proc Natl Acad Sci U S A* 102, 17816-17821.
- Llano, I., Leresche, N., and Marty, A. (1991). Calcium entry increases the sensitivity of cerebellar Purkinje cells to applied GABA and decreases inhibitory synaptic currents. *Neuron* 6, 565-574.
- London, M., and Hausser, M. (2005). Dendritic computation. *Annu Rev Neurosci* 28, 503-532.
- London, M., Roth, A., Beeren, L., Hausser, M., and Latham, P.E. (2010). Sensitivity to perturbations in vivo implies high noise and suggests rate coding in cortex. *Nature* 466, 123-127.
- Lorteije, J.A., Rusu, S.I., Kushmerick, C., and Borst, J.G. (2009). Reliability and precision of the mouse calyx of Held synapse. *J Neurosci* 29, 13770-13784.
- Lu, S.M., and Lin, R.C. (1993). Thalamic afferents of the rat barrel cortex: a light- and electron-microscopic study using Phaseolus vulgaris leucoagglutinin as an anterograde tracer. *Somatosens Mot Res* 10, 1-16.
- Lu, T., and Trussell, L.O. (2000). Inhibitory transmission mediated by asynchronous transmitter release. *Neuron* 26, 683-694.
- Lubke, J., Egger, V., Sakmann, B., and Feldmeyer, D. (2000). Columnar organization of dendrites and axons of single and synaptically coupled excitatory spiny neurons in layer 4 of the rat barrel cortex. *J Neurosci* 20, 5300-5311.
- Lubke, J., Roth, A., Feldmeyer, D., and Sakmann, B. (2003). Morphometric analysis of the columnar innervation domain of neurons connecting layer 4 and layer 2/3 of juvenile rat barrel cortex. *Cereb Cortex* 13, 1051-1063.
- Ma, Y., Hu, H., Berrebi, A.S., Mathers, P.H., and Agmon, A. (2006). Distinct subtypes of somatostatin-containing neocortical interneurons revealed in transgenic mice. *J Neurosci* 26, 5069-5082.
- MacDermott, A.B., Role, L.W., and Siegelbaum, S.A. (1999). Presynaptic ionotropic receptors and the control of transmitter release. *Annu Rev Neurosci* 22, 443-485.
- Madisen, L., Zwingman, T.A., Sunkin, S.M., Oh, S.W., Zariwala, H.A., Gu, H., Ng, L.L., Palmiter, R.D., Hawrylycz, M.J., Jones, A.R., *et al.* (2010). A robust and high-throughput Cre reporting and characterization system for the whole mouse brain. *Nat Neurosci* 13, 133-140.
- Magee, J.C., and Johnston, D. (1995). Synaptic activation of voltage-gated channels in the dendrites of hippocampal pyramidal neurons. *Science* 268, 301-304.

- Mann, E.O., Kohl, M.M., and Paulsen, O. (2009). Distinct roles of GABA(A) and GABA(B) receptors in balancing and terminating persistent cortical activity. *J Neurosci* 29, 7513-7518.
- Manns, I.D., Sakmann, B., and Brecht, M. (2004). Sub- and suprathreshold receptive field properties of pyramidal neurones in layers 5A and 5B of rat somatosensory barrel cortex. *J Physiol* 556, 601-622.
- Mao, T., Kusefoglou, D., Hooks, B.M., Huber, D., Petreanu, L., and Svoboda, K. (2011). Long-range neuronal circuits underlying the interaction between sensory and motor cortex. *Neuron* 72, 111-123.
- Margrie, T.W., Meyer, A.H., Caputi, A., Monyer, H., Hasan, M.T., Schaefer, A.T., Denk, W., and Brecht, M. (2003). Targeted whole-cell recordings in the mammalian brain in vivo. *Neuron* 39, 911-918.
- Markram, H., Lubke, J., Frotscher, M., Roth, A., and Sakmann, B. (1997). Physiology and anatomy of synaptic connections between thick tufted pyramidal neurones in the developing rat neocortex. *J Physiol* 500 (Pt 2), 409-440.
- Markram, H., Toledo-Rodriguez, M., Wang, Y., Gupta, A., Silberberg, G., and Wu, C. (2004). Interneurons of the neocortical inhibitory system. *Nat Rev Neurosci* 5, 793-807.
- Markram, H., Wang, Y., and Tsodyks, M. (1998). Differential signaling via the same axon of neocortical pyramidal neurons. *Proc Natl Acad Sci U S A* 95, 5323-5328.
- Masino, S.A., Kwon, M.C., Dory, Y., and Frostig, R.D. (1993). Characterization of functional organization within rat barrel cortex using intrinsic signal optical imaging through a thinned skull. *Proc Natl Acad Sci U S A* 90, 9998-10002.
- Maskos, U., Kissa, K., St Cloment, C., and Brulet, P. (2002). Retrograde trans-synaptic transfer of green fluorescent protein allows the genetic mapping of neuronal circuits in transgenic mice. *Proc Natl Acad Sci U S A* 99, 10120-10125.
- Mateo, C., Avermann, M., Gentet, L.J., Zhang, F., Deisseroth, K., and Petersen, C.C. (2011). In vivo optogenetic stimulation of neocortical excitatory neurons drives brain-state-dependent inhibition. *Curr Biol* 21, 1593-1602.
- Matsuda, T., and Cepko, C.L. (2004). Electroporation and RNA interference in the rodent retina in vivo and in vitro. *Proc Natl Acad Sci U S A* 101, 16-22.
- Matsumura, M., Chen, D., Sawaguchi, T., Kubota, K., and Fetz, E.E. (1996). Synaptic interactions between primate precentral cortex neurons revealed by spike-triggered averaging of intracellular membrane potentials in vivo. *J Neurosci* 16, 7757-7767.
- Matta, J.A., Pelkey, K.A., Craig, M.T., Chittajallu, R., Jeffries, B.W., and McBain, C.J. (2013). Developmental origin dictates interneuron AMPA and NMDA receptor subunit composition and plasticity. *Nat Neurosci* 16, 1032-1041.
- Mattis, J., Tye, K.M., Ferenczi, E.A., Ramakrishnan, C., O'Shea, D.J., Prakash, R., Gunaydin, L.A., Hyun, M., Fenno, L.E., Gradinaru, V., *et al.* (2012). Principles for applying optogenetic tools derived from direct comparative analysis of microbial opsins. *Nat Methods* 9, 159-172.
- Matveev, V., Zucker, R.S., and Sherman, A. (2004). Facilitation through buffer saturation: constraints on endogenous buffering properties. *Biophys J* 86, 2691-2709.

- McCormick, D.A., Connors, B.W., Lighthall, J.W., and Prince, D.A. (1985). Comparative electrophysiology of pyramidal and sparsely spiny stellate neurons of the neocortex. *J Neurophysiol* 54, 782-806.
- McGarry, L.M., Packer, A.M., Fino, E., Nikolenko, V., Sippy, T., and Yuste, R. (2010). Quantitative classification of somatostatin-positive neocortical interneurons identifies three interneuron subtypes. *Front Neural Circuits* 4, 12.
- Meldrum, B.S. (2000). Glutamate as a neurotransmitter in the brain: review of physiology and pathology. *J Nutr* 130, 1007S-1015S.
- Mercier, B.E., Legg, C.R., and Glickstein, M. (1990). Basal ganglia and cerebellum receive different somatosensory information in rats. *Proc Natl Acad Sci U S A* 87, 4388-4392.
- Meyer, H.S., Egger, R., Guest, J.M., Foerster, R., Reissl, S., and Oberlaender, M. (2013). Cellular organization of cortical barrel columns is whisker-specific. *Proc Natl Acad Sci U S A* 110, 19113-19118.
- Meyer, H.S., Schwarz, D., Wimmer, V.C., Schmitt, A.C., Kerr, J.N., Sakmann, B., and Helmstaedter, M. (2011). Inhibitory interneurons in a cortical column form hot zones of inhibition in layers 2 and 5A. *Proc Natl Acad Sci U S A* 108, 16807-16812.
- Meyer, H.S., Wimmer, V.C., Hemberger, M., Bruno, R.M., de Kock, C.P., Frick, A., Sakmann, B., and Helmstaedter, M. (2010a). Cell type-specific thalamic innervation in a column of rat vibrissal cortex. *Cereb Cortex* 20, 2287-2303.
- Meyer, H.S., Wimmer, V.C., Oberlaender, M., de Kock, C.P., Sakmann, B., and Helmstaedter, M. (2010b). Number and laminar distribution of neurons in a thalamocortical projection column of rat vibrissal cortex. *Cereb Cortex* 20, 2277-2286.
- Migliore, M., and Shepherd, G.M. (2002). Emerging rules for the distributions of active dendritic conductances. *Nat Rev Neurosci* 3, 362-370.
- Miyoshi, G., Hjerling-Leffler, J., Karayannis, T., Sousa, V.H., Butt, S.J., Battiste, J., Johnson, J.E., Machold, R.P., and Fishell, G. (2010). Genetic fate mapping reveals that the caudal ganglionic eminence produces a large and diverse population of superficial cortical interneurons. *J Neurosci* 30, 1582-1594.
- Moore, C.I., and Nelson, S.B. (1998). Spatio-temporal subthreshold receptive fields in the vibrissa representation of rat primary somatosensory cortex. *J Neurophysiol* 80, 2882-2892.
- Morrison, J.H., and Hof, P.R. (1997). Life and death of neurons in the aging brain. *Science* 278, 412-419.
- Mountcastle, V.B. (1957). Modality and topographic properties of single neurons of cat's somatic sensory cortex. *J Neurophysiol* 20, 408-434.
- Nagel, G., Szellas, T., Huhn, W., Kateriya, S., Adeishvili, N., Berthold, P., Ollig, D., Hegemann, P., and Bamberg, E. (2003). Channelrhodopsin-2, a directly light-gated cation-selective membrane channel. *Proc Natl Acad Sci U S A* 100, 13940-13945.
- Neher, E., and Sakaba, T. (2008). Multiple roles of calcium ions in the regulation of neurotransmitter release. *Neuron* 59, 861-872.

- Neumann, E., Schaefer-Ridder, M., Wang, Y., and Hofschneider, P.H. (1982). Gene transfer into mouse lymphoma cells by electroporation in high electric fields. *EMBO J* 1, 841-845.
- Niswender, C.M., and Conn, P.J. (2010). Metabotropic glutamate receptors: physiology, pharmacology, and disease. *Annu Rev Pharmacol Toxicol* 50, 295-322.
- Nyitrai, G., Kekesi, K.A., and Juhasz, G. (2006). Extracellular level of GABA and Glu: in vivo microdialysis-HPLC measurements. *Curr Top Med Chem* 6, 935-940.
- O'Connor, D.H., Clack, N.G., Huber, D., Komiyama, T., Myers, E.W., and Svoboda, K. (2010). Vibrissa-based object localization in head-fixed mice. *J Neurosci* 30, 1947-1967.
- Oberlaender, M., Boudewijns, Z.S., Kleele, T., Mansvelder, H.D., Sakmann, B., and de Kock, C.P. (2011). Three-dimensional axon morphologies of individual layer 5 neurons indicate cell type-specific intracortical pathways for whisker motion and touch. *Proc Natl Acad Sci U S A* 108, 4188-4193.
- Oertner, T.G., Sabatini, B.L., Nimchinsky, E.A., and Svoboda, K. (2002). Facilitation at single synapses probed with optical quantal analysis. *Nat Neurosci* 5, 657-664.
- Ohno-Shosaku, T., Maejima, T., and Kano, M. (2001). Endogenous cannabinoids mediate retrograde signals from depolarized postsynaptic neurons to presynaptic terminals. *Neuron* 29, 729-738.
- Oliva, A.A., Jr., Jiang, M., Lam, T., Smith, K.L., and Swann, J.W. (2000). Novel hippocampal interneuronal subtypes identified using transgenic mice that express green fluorescent protein in GABAergic interneurons. *J Neurosci* 20, 3354-3368.
- Oswald, A.M., and Reyes, A.D. (2008). Maturation of intrinsic and synaptic properties of layer 2/3 pyramidal neurons in mouse auditory cortex. *J Neurophysiol* 99, 2998-3008.
- Oswald, A.M., and Reyes, A.D. (2011). Development of inhibitory timescales in auditory cortex. *Cereb Cortex* 21, 1351-1361.
- Packer, A.M., Peterka, D.S., Hirtz, J.J., Prakash, R., Deisseroth, K., and Yuste, R. (2012). Two-photon optogenetics of dendritic spines and neural circuits. *Nat Methods* 9, 1202-1205.
- Packer, A.M., and Yuste, R. (2011). Dense, unspecific connectivity of neocortical parvalbumin-positive interneurons: a canonical microcircuit for inhibition? *J Neurosci* 31, 13260-13271.
- Papagiakoumou, E., Anselmi, F., Begue, A., de Sars, V., Gluckstad, J., Isacoff, E.Y., and Emiliani, V. (2010). Scanless two-photon excitation of channelrhodopsin-2. *Nat Methods* 7, 848-854.
- Penttonen, M.a.B., G. (2003). Natural logarithmic relationship between brain oscillators. *Thalamus Relat Syst* 2, 145-152.
- Perin, R., Berger, T.K., and Markram, H. (2011). A synaptic organizing principle for cortical neuronal groups. *Proc Natl Acad Sci U S A* 108, 5419-5424.
- Perkel, D.H., Gerstein, G.L., and Moore, G.P. (1967). Neuronal spike trains and stochastic point processes. II. Simultaneous spike trains. *Biophys J* 7, 419-440.
- Petersen, C.C., Grinvald, A., and Sakmann, B. (2003a). Spatiotemporal dynamics of sensory responses in layer 2/3 of rat barrel cortex measured in vivo by voltage-sensitive dye imaging combined with whole-cell voltage recordings and neuron reconstructions. *J Neurosci* 23, 1298-1309.

- Petersen, C.C., Hahn, T.T., Mehta, M., Grinvald, A., and Sakmann, B. (2003b). Interaction of sensory responses with spontaneous depolarization in layer 2/3 barrel cortex. *Proc Natl Acad Sci U S A* 100, 13638-13643.
- Petersen, C.C., and Sakmann, B. (2000). The excitatory neuronal network of rat layer 4 barrel cortex. *J Neurosci* 20, 7579-7586.
- Petersen, C.C., and Sakmann, B. (2001). Functionally independent columns of rat somatosensory barrel cortex revealed with voltage-sensitive dye imaging. *J Neurosci* 21, 8435-8446.
- Petilla Interneuron Nomenclature, G., Ascoli, G.A., Alonso-Nanclares, L., Anderson, S.A., Barrionuevo, G., Benavides-Piccione, R., Burkhalter, A., Buzsaki, G., Cauli, B., Defelipe, J., *et al.* (2008). Petilla terminology: nomenclature of features of GABAergic interneurons of the cerebral cortex. *Nat Rev Neurosci* 9, 557-568.
- Petreaunu, L., Huber, D., Sobczyk, A., and Svoboda, K. (2007). Channelrhodopsin-2-assisted circuit mapping of long-range callosal projections. *Nat Neurosci* 10, 663-668.
- Petreaunu, L., Mao, T., Sternson, S.M., and Svoboda, K. (2009). The subcellular organization of neocortical excitatory connections. *Nature* 457, 1142-1145.
- Pfeffer, C.K., Xue, M., He, M., Huang, Z.J., and Scanziani, M. (2013). Inhibition of inhibition in visual cortex: the logic of connections between molecularly distinct interneurons. *Nat Neurosci* 16, 1068-1076.
- Pierret, T., Lavallee, P., and Deschenes, M. (2000). Parallel streams for the relay of vibrissal information through thalamic barreloids. *J Neurosci* 20, 7455-7462.
- Pinault, D. (1996). A novel single-cell staining procedure performed *in vivo* under electrophysiological control: morpho-functional features of juxtacellularly labeled thalamic cells and other central neurons with biocytin or Neurobiotin. *J Neurosci Methods* 65, 113-136.
- Pinault, D. (2011). The Juxtacellular Recording-Labeling Technique. In *Electrophysiological Recording Techniques*, R.P. Vertes, Stackman, R. W. Jr., ed. (Springer), pp. 41-75.
- Pitler, T.A., and Alger, B.E. (1992). Postsynaptic spike firing reduces synaptic GABA_A responses in hippocampal pyramidal cells. *J Neurosci* 12, 4122-4132.
- Plenz, D., and Aertsen, A. (1996). Neural dynamics in cortex-striatum co-cultures--II. Spatiotemporal characteristics of neuronal activity. *Neuroscience* 70, 893-924.
- Polack, P.O., Friedman, J., and Golshani, P. (2013). Cellular mechanisms of brain state-dependent gain modulation in visual cortex. *Nat Neurosci* 16, 1331-1339.
- Porter, J.T., Cauli, B., Staiger, J.F., Lambolez, B., Rossier, J., and Audinat, E. (1998). Properties of bipolar VIPergic interneurons and their excitation by pyramidal neurons in the rat neocortex. *Eur J Neurosci* 10, 3617-3628.
- Poulet, J.F., Fernandez, L.M., Crochet, S., and Petersen, C.C. (2012). Thalamic control of cortical states. *Nat Neurosci* 15, 370-372.
- Poulet, J.F., and Petersen, C.C. (2008). Internal brain state regulates membrane potential synchrony in barrel cortex of behaving mice. *Nature* 454, 881-885.

- Pouratian, N., Toga, A. W. (2002). Optical Imaging Based on Intrinsic Signals. In *Brain Mapping : The Methods*, A.W. Toga, Mazziotta, J. C. , ed. (San Diego, USA: Elsevier Science), pp. 97-140.
- Prakash, R., Yizhar, O., Grewe, B., Ramakrishnan, C., Wang, N., Goshen, I., Packer, A.M., Peterka, D.S., Yuste, R., Schnitzer, M.J., and Deisseroth, K. (2012). Two-photon optogenetic toolbox for fast inhibition, excitation and bistable modulation. *Nat Methods* 9, 1171-1179.
- Purpura, D.P., Girado, M., and Grundfest, H. (1957). Selective blockade of excitatory synapses in the cat brain by gamma-aminobutyric acid. *Science* 125, 1200-1202.
- Rakic, P. (2009). Evolution of the neocortex: a perspective from developmental biology. *Nat Rev Neurosci* 10, 724-735.
- Rall, W. (1959). Branching dendritic trees and motoneuron membrane resistivity. *Exp Neurol* 1, 491-527.
- Rall, W. (1967). Distinguishing theoretical synaptic potentials computed for different soma-dendritic distributions of synaptic input. *J Neurophysiol* 30, 1138-1168.
- Ramoa, A.S., and Sur, M. (1996). Short-term synaptic plasticity in the visual cortex during development. *Cereb Cortex* 6, 640-646.
- Rathenberg, J., Nevian, T., and Witzemann, V. (2003). High-efficiency transfection of individual neurons using modified electrophysiology techniques. *J Neurosci Methods* 126, 91-98.
- Reig, R., Gallego, R., Nowak, L.G., and Sanchez-Vives, M.V. (2006). Impact of cortical network activity on short-term synaptic depression. *Cereb Cortex* 16, 688-695.
- Reig, R., and Sanchez-Vives, M.V. (2007). Synaptic transmission and plasticity in an active cortical network. *PLoS One* 2, e670.
- Ren, J.Q., Aika, Y., Heizmann, C.W., and Kosaka, T. (1992). Quantitative analysis of neurons and glial cells in the rat somatosensory cortex, with special reference to GABAergic neurons and parvalbumin-containing neurons. *Exp Brain Res* 92, 1-14.
- Reyes, A. (2001). Influence of dendritic conductances on the input-output properties of neurons. *Annu Rev Neurosci* 24, 653-675.
- Reyes, A., Lujan, R., Rozov, A., Burnashev, N., Somogyi, P., and Sakmann, B. (1998). Target-cell-specific facilitation and depression in neocortical circuits. *Nat Neurosci* 1, 279-285.
- Reyes, A., and Sakmann, B. (1999). Developmental switch in the short-term modification of unitary EPSPs evoked in layer 2/3 and layer 5 pyramidal neurons of rat neocortex. *J Neurosci* 19, 3827-3835.
- Rial Verde, E.M., Zayat, L., Etchenique, R., and Yuste, R. (2008). Photorelease of GABA with Visible Light Using an Inorganic Caging Group. *Front Neural Circuits* 2, 2.
- Ribrault, C., Sekimoto, K., and Triller, A. (2011). From the stochasticity of molecular processes to the variability of synaptic transmission. *Nat Rev Neurosci* 12, 375-387.
- Rickgauer, J.P., and Tank, D.W. (2009). Two-photon excitation of channelrhodopsin-2 at saturation. *Proc Natl Acad Sci U S A* 106, 15025-15030.
- Rizzoli, S.O., and Betz, W.J. (2005). Synaptic vesicle pools. *Nat Rev Neurosci* 6, 57-69.

- Rodriguez, M., Sabate, M., Rodriguez-Sabate, C., and Morales, I. (2013). The role of non-synaptic extracellular glutamate. *Brain Res Bull* 93, 17-26.
- Roth, A., and Hausser, M. (2001). Compartmental models of rat cerebellar Purkinje cells based on simultaneous somatic and dendritic patch-clamp recordings. *J Physiol* 535, 445-472.
- Rowlands, G.F., and Roberts, P.J. (1980). Activation of dopamine receptors inhibits calcium-dependent glutamate release from cortico-striatal terminals in vitro. *Eur J Pharmacol* 62, 241-242.
- Rozov, A., Burnashev, N., Sakmann, B., and Neher, E. (2001a). Transmitter release modulation by intracellular Ca²⁺ buffers in facilitating and depressing nerve terminals of pyramidal cells in layer 2/3 of the rat neocortex indicates a target cell-specific difference in presynaptic calcium dynamics. *J Physiol* 531, 807-826.
- Rozov, A., Jerecic, J., Sakmann, B., and Burnashev, N. (2001b). AMPA receptor channels with long-lasting desensitization in bipolar interneurons contribute to synaptic depression in a novel feedback circuit in layer 2/3 of rat neocortex. *J Neurosci* 21, 8062-8071.
- Rudolph, M., Pospischil, M., Timofeev, I., and Destexhe, A. (2007). Inhibition determines membrane potential dynamics and controls action potential generation in awake and sleeping cat cortex. *J Neurosci* 27, 5280-5290.
- Rudy, B., Fishell, G., Lee, S., and Hjerling-Leffler, J. (2011). Three groups of interneurons account for nearly 100% of neocortical GABAergic neurons. *Dev Neurobiol* 71, 45-61.
- Sachdev, R.N., Ebner, F.F., and Wilson, C.J. (2004). Effect of subthreshold up and down states on the whisker-evoked response in somatosensory cortex. *J Neurophysiol* 92, 3511-3521.
- Sakata, S., and Harris, K.D. (2009). Laminar structure of spontaneous and sensory-evoked population activity in auditory cortex. *Neuron* 64, 404-418.
- Sanchez-Vives, M.V., and McCormick, D.A. (2000). Cellular and network mechanisms of rhythmic recurrent activity in neocortex. *Nat Neurosci* 3, 1027-1034.
- Scanziani, M., Gahwiler, B.H., and Charpak, S. (1998). Target cell-specific modulation of transmitter release at terminals from a single axon. *Proc Natl Acad Sci U S A* 95, 12004-12009.
- Schubert, D., Kotter, R., Luhmann, H.J., and Staiger, J.F. (2006). Morphology, electrophysiology and functional input connectivity of pyramidal neurons characterizes a genuine layer va in the primary somatosensory cortex. *Cereb Cortex* 16, 223-236.
- Segev, I., and Rinzel, J. (1995). *The Theoretical Foundation of Dendritic Function* (MIT Press).
- Shepherd, G.M., Stepanyants, A., Bureau, I., Chklovskii, D., and Svoboda, K. (2005). Geometric and functional organization of cortical circuits. *Nat Neurosci* 8, 782-790.
- Shepherd, G.M., and Svoboda, K. (2005). Laminar and columnar organization of ascending excitatory projections to layer 2/3 pyramidal neurons in rat barrel cortex. *J Neurosci* 25, 5670-5679.
- Shu, Y., Hasenstaub, A., Duque, A., Yu, Y., and McCormick, D.A. (2006). Modulation of intracortical synaptic potentials by presynaptic somatic membrane potential. *Nature* 441, 761-765.
- Shu, Y., Hasenstaub, A., and McCormick, D.A. (2003). Turning on and off recurrent balanced cortical activity. *Nature* 423, 288-293.

- Silberberg, G., and Markram, H. (2007). Disynaptic inhibition between neocortical pyramidal cells mediated by Martinotti cells. *Neuron* 53, 735-746.
- Silver, R.A., Lubke, J., Sakmann, B., and Feldmeyer, D. (2003). High-probability unquantal transmission at excitatory synapses in barrel cortex. *Science* 302, 1981-1984.
- Somogyi, P., Freund, T.F., and Cowey, A. (1982). The axo-axonic interneuron in the cerebral cortex of the rat, cat and monkey. *Neuroscience* 7, 2577-2607.
- Spruston, N., Jaffe, D.B., and Johnston, D. (1994). Dendritic attenuation of synaptic potentials and currents: the role of passive membrane properties. *Trends Neurosci* 17, 161-166.
- Staiger, J.F., Flagmeyer, I., Schubert, D., Zilles, K., Kotter, R., and Luhmann, H.J. (2004). Functional diversity of layer IV spiny neurons in rat somatosensory cortex: quantitative morphology of electrophysiologically characterized and biocytin labeled cells. *Cereb Cortex* 14, 690-701.
- Steriade, M., Contreras, D., Curro Dossi, R., and Nunez, A. (1993a). The slow (< 1 Hz) oscillation in reticular thalamic and thalamocortical neurons: scenario of sleep rhythm generation in interacting thalamic and neocortical networks. *J Neurosci* 13, 3284-3299.
- Steriade, M., Gloor, P., Llinas, R.R., Lopes de Silva, F.H., and Mesulam, M.M. (1990). Report of IFCN Committee on Basic Mechanisms. Basic mechanisms of cerebral rhythmic activities. *Electroencephalogr Clin Neurophysiol* 76, 481-508.
- Steriade, M., Nunez, A., and Amzica, F. (1993b). Intracellular analysis of relations between the slow (< 1 Hz) neocortical oscillation and other sleep rhythms of the electroencephalogram. *J Neurosci* 13, 3266-3283.
- Steriade, M., Nunez, A., and Amzica, F. (1993c). A novel slow (< 1 Hz) oscillation of neocortical neurons in vivo: depolarizing and hyperpolarizing components. *J Neurosci* 13, 3252-3265.
- Steriade, M., Timofeev, I., and Grenier, F. (2001). Natural waking and sleep states: a view from inside neocortical neurons. *J Neurophysiol* 85, 1969-1985.
- Stuart, G., and Spruston, N. (1998). Determinants of voltage attenuation in neocortical pyramidal neuron dendrites. *J Neurosci* 18, 3501-3510.
- Stuart, G.J., and Sakmann, B. (1994). Active propagation of somatic action potentials into neocortical pyramidal cell dendrites. *Nature* 367, 69-72.
- Sudhof, T.C. (2000). The synaptic vesicle cycle revisited. *Neuron* 28, 317-320.
- Sudhof, T.C. (2004). The synaptic vesicle cycle. *Annu Rev Neurosci* 27, 509-547.
- Sugita, M., and Shiba, Y. (2005). Genetic tracing shows segregation of taste neuronal circuitries for bitter and sweet. *Science* 309, 781-785.
- Sun, Q.Q., Huguenard, J.R., and Prince, D.A. (2006). Barrel cortex microcircuits: thalamocortical feedforward inhibition in spiny stellate cells is mediated by a small number of fast-spiking interneurons. *J Neurosci* 26, 1219-1230.
- Szabadics, J., Varga, C., Molnar, G., Olah, S., Barzo, P., and Tamas, G. (2006). Excitatory effect of GABAergic axo-axonic cells in cortical microcircuits. *Science* 311, 233-235.

- Tahvildari, B., Wolfel, M., Duque, A., and McCormick, D.A. (2012). Selective functional interactions between excitatory and inhibitory cortical neurons and differential contribution to persistent activity of the slow oscillation. *J Neurosci* 32, 12165-12179.
- Tamas, G., Lorincz, A., Simon, A., and Szabadics, J. (2003). Identified sources and targets of slow inhibition in the neocortex. *Science* 299, 1902-1905.
- Tamas, G., Szabadics, J., and Somogyi, P. (2002). Cell type- and subcellular position-dependent summation of unitary postsynaptic potentials in neocortical neurons. *J Neurosci* 22, 740-747.
- Tang, Y., Schlumpberger, T., Kim, T., Lueker, M., and Zucker, R.S. (2000). Effects of mobile buffers on facilitation: experimental and computational studies. *Biophys J* 78, 2735-2751.
- Taniguchi, H., He, M., Wu, P., Kim, S., Paik, R., Sugino, K., Kvitsiani, D., Fu, Y., Lu, J., Lin, Y., *et al.* (2011). A resource of Cre driver lines for genetic targeting of GABAergic neurons in cerebral cortex. *Neuron* 71, 995-1013.
- Thomson, A.M., Deuchars, J., and West, D.C. (1996). Neocortical local synaptic circuitry revealed with dual intracellular recordings and biocytin-filling. *J Physiol Paris* 90, 211-215.
- Thomson, A.M., Girdlestone, D., and West, D.C. (1988). Voltage-dependent currents prolong single-axon postsynaptic potentials in layer III pyramidal neurons in rat neocortical slices. *J Neurophysiol* 60, 1896-1907.
- Thomson, A.M., and Lamy, C. (2007). Functional maps of neocortical local circuitry. *Front Neurosci* 1, 19-42.
- Thomson, A.M., West, D.C., Wang, Y., and Bannister, A.P. (2002). Synaptic connections and small circuits involving excitatory and inhibitory neurons in layers 2-5 of adult rat and cat neocortex: triple intracellular recordings and biocytin labelling in vitro. *Cereb Cortex* 12, 936-953.
- Timofeev, I., Grenier, F., Bazhenov, M., Sejnowski, T.J., and Steriade, M. (2000). Origin of slow cortical oscillations in deafferented cortical slabs. *Cereb Cortex* 10, 1185-1199.
- Timofeev, I., Grenier, F., and Steriade, M. (2001). Disfacilitation and active inhibition in the neocortex during the natural sleep-wake cycle: an intracellular study. *Proc Natl Acad Sci U S A* 98, 1924-1929.
- Traynelis, S.F., Wollmuth, L.P., McBain, C.J., Menniti, F.S., Vance, K.M., Ogden, K.K., Hansen, K.B., Yuan, H., Myers, S.J., and Dingledine, R. (2010). Glutamate receptor ion channels: structure, regulation, and function. *Pharmacol Rev* 62, 405-496.
- Uhlhaas, P.J., Pipa, G., Lima, B., Melloni, L., Neuenschwander, S., Nikolic, D., and Singer, W. (2009). Neural synchrony in cortical networks: history, concept and current status. *Front Integr Neurosci* 3, 17.
- Veinante, P., Lavallee, P., and Deschenes, M. (2000). Corticothalamic projections from layer 5 of the vibrissal barrel cortex in the rat. *J Comp Neurol* 424, 197-204.
- Volgushev, M., Chauvette, S., Mukovski, M., and Timofeev, I. (2006). Precise long-range synchronization of activity and silence in neocortical neurons during slow-wave oscillations [corrected]. *J Neurosci* 26, 5665-5672.
- Volgushev, M., Voronin, L.L., Chistiakova, M., Artola, A., and Singer, W. (1995). All-or-none excitatory postsynaptic potentials in the rat visual cortex. *Eur J Neurosci* 7, 1751-1760.

- Wang, Y., Gupta, A., Toledo-Rodriguez, M., Wu, C.Z., and Markram, H. (2002). Anatomical, physiological, molecular and circuit properties of nest basket cells in the developing somatosensory cortex. *Cereb Cortex* 12, 395-410.
- Watanabe, J., Rozov, A., and Wollmuth, L.P. (2005). Target-specific regulation of synaptic amplitudes in the neocortex. *J Neurosci* 25, 1024-1033.
- Waters, J., and Helmchen, F. (2004). Boosting of action potential backpropagation by neocortical network activity in vivo. *J Neurosci* 24, 11127-11136.
- Waters, J., and Helmchen, F. (2006). Background synaptic activity is sparse in neocortex. *J Neurosci* 26, 8267-8277.
- Welker, C. (1971). Microelectrode delineation of fine grain somatotopic organization of (SmI) cerebral neocortex in albino rat. *Brain Res* 26, 259-275.
- Welker, C., and Woolsey, T.A. (1974). Structure of layer IV in the somatosensory neocortex of the rat: description and comparison with the mouse. *J Comp Neurol* 158, 437-453.
- Welker, E., Hoogland, P.V., and Van der Loos, H. (1988). Organization of feedback and feedforward projections of the barrel cortex: a PHA-L study in the mouse. *Exp Brain Res* 73, 411-435.
- Wickersham, I.R., Lyon, D.C., Barnard, R.J., Mori, T., Finke, S., Conzelmann, K.K., Young, J.A., and Callaway, E.M. (2007). Monosynaptic restriction of transsynaptic tracing from single, genetically targeted neurons. *Neuron* 53, 639-647.
- Williams, S.R., and Stuart, G.J. (2000). Site independence of EPSP time course is mediated by dendritic I(h) in neocortical pyramidal neurons. *J Neurophysiol* 83, 3177-3182.
- Wilson, C.J., and Kawaguchi, Y. (1996). The origins of two-state spontaneous membrane potential fluctuations of neostriatal spiny neurons. *J Neurosci* 16, 2397-2410.
- Wilson, R.I., and Nicoll, R.A. (2001). Endogenous cannabinoids mediate retrograde signalling at hippocampal synapses. *Nature* 410, 588-592.
- Woodruff, A.R., McGarry, L.M., Vogels, T.P., Inan, M., Anderson, S.A., and Yuste, R. (2011). State-dependent function of neocortical chandelier cells. *J Neurosci* 31, 17872-17886.
- Woolsey, T.A. (1967). Somatosensory, auditory and visual cortical areas of the mouse. *Johns Hopkins Med J* 121, 91-112.
- Woolsey, T.A., and Van der Loos, H. (1970). The structural organization of layer IV in the somatosensory region (SI) of mouse cerebral cortex. The description of a cortical field composed of discrete cytoarchitectonic units. *Brain Res* 17, 205-242.
- Wright, A.K., Norrie, L., Ingham, C.A., Hutton, E.A., and Arbuthnott, G.W. (1999). Double anterograde tracing of outputs from adjacent "barrel columns" of rat somatosensory cortex. Neostriatal projection patterns and terminal ultrastructure. *Neuroscience* 88, 119-133.
- Wu, L.G., and Saggau, P. (1997). Presynaptic inhibition of elicited neurotransmitter release. *Trends Neurosci* 20, 204-212.
- Xu, X., and Callaway, E.M. (2009). Laminar specificity of functional input to distinct types of inhibitory cortical neurons. *J Neurosci* 29, 70-85.

- Xu, X., Roby, K.D., and Callaway, E.M. (2006). Mouse cortical inhibitory neuron type that coexpresses somatostatin and calretinin. *J Comp Neurol* 499, 144-160.
- Xu, X., Roby, K.D., and Callaway, E.M. (2010). Immunochemical characterization of inhibitory mouse cortical neurons: three chemically distinct classes of inhibitory cells. *J Comp Neurol* 518, 389-404.
- Yamamoto, C., and McIlwain, H. (1966). Potentials evoked in vitro in preparations from the mammalian brain. *Nature* 210, 1055-1056.
- Yamashita, T., Pala, A., Pedrido, L., Kremer, Y., Welker, E., and Petersen, C.C. (2013). Membrane potential dynamics of neocortical projection neurons driving target-specific signals. *Neuron* 80, 1477-1490.
- Yizhar, O., Fenno, L.E., Davidson, T.J., Mogri, M., and Deisseroth, K. (2011). Optogenetics in neural systems. *Neuron* 71, 9-34.
- Yu, J., and Ferster, D. (2013). Functional coupling from simple to complex cells in the visually driven cortical circuit. *J Neurosci* 33, 18855-18866.
- Zahid, M., Velez-Fort, M., Papagiakoumou, E., Ventalon, C., Angulo, M.C., and Emiliani, V. (2010). Holographic photolysis for multiple cell stimulation in mouse hippocampal slices. *PLoS One* 5, e9431.
- Zayat, L., Noval, M.G., Campi, J., Calero, C.I., Calvo, D.J., and Etchenique, R. (2007). A new inorganic photolabile protecting group for highly efficient visible light GABA uncaging. *Chembiochem* 8, 2035-2038.
- Zhang, F., Wang, L.P., Boyden, E.S., and Deisseroth, K. (2006). Channelrhodopsin-2 and optical control of excitable cells. *Nat Methods* 3, 785-792.
- Zhang, F., Wang, L.P., Brauner, M., Liewald, J.F., Kay, K., Watzke, N., Wood, P.G., Bamberg, E., Nagel, G., Gottschalk, A., and Deisseroth, K. (2007). Multimodal fast optical interrogation of neural circuitry. *Nature* 446, 633-639.
- Zhang, Y.P., and Oertner, T.G. (2007). Optical induction of synaptic plasticity using a light-sensitive channel. *Nat Methods* 4, 139-141.
- Zhang, Z.W. (2004). Maturation of layer V pyramidal neurons in the rat prefrontal cortex: intrinsic properties and synaptic function. *J Neurophysiol* 91, 1171-1182.
- Zhang, Z.W., and Deschenes, M. (1997). Intracortical axonal projections of lamina VI cells of the primary somatosensory cortex in the rat: a single-cell labeling study. *J Neurosci* 17, 6365-6379.
- Zhu, Y., Stornetta, R.L., and Zhu, J.J. (2004). Chandelier cells control excessive cortical excitation: characteristics of whisker-evoked synaptic responses of layer 2/3 nonpyramidal and pyramidal neurons. *J Neurosci* 24, 5101-5108.
- Zimmer, H.G. (2006). Otto Loewi and the chemical transmission of vagus stimulation in the heart. *Clin Cardiol* 29, 135-136.
- Zipfel, W.R., Williams, R.M., and Webb, W.W. (2003). Nonlinear magic: multiphoton microscopy in the biosciences. *Nat Biotechnol* 21, 1369-1377.

Zou, Q., Rudolph, M., Roy, N., Sanchez-Vives, M., Contreras, D., and Destexhe, A. (2005). Reconstructing synaptic background activity from conductance measurements in vivo. *Neurocomputing* 65, 673-678.

Zucker, E., and Welker, W.I. (1969). Coding of somatic sensory input by vibrissae neurons in the rat's trigeminal ganglion. *Brain Res* 12, 138-156.

Zucker, R.S., and Regehr, W.G. (2002). Short-term synaptic plasticity. *Annu Rev Physiol* 64, 355-405.

CURRICULUM VITAE

Aurélie PALA

EPFL-SV-BMI-LENS, Station 19, CH-1015 Lausanne

23.10.1984

Swiss

Phone: +41 21 693 16 59

E-mail: aurelie.pala@gmail.com

EDUCATION

Swiss Federal Institute of Technology of Lausanne (EPFL), Switzerland

- Ph. D., EPFL PhD Program in Neuroscience (EDNE) 2009-Present
- M. Sc., Life Sciences and Technology with specialization in Neuroscience 2006-2008
- B. Sc., Life Sciences and Technology 2003-2006

RESEARCH EXPERIENCE

Swiss Federal Institute of Technology of Lausanne (EPFL), Switzerland

- PhD Research 2009-Present
Laboratory of Sensory Processing (LENS), Prof. Carl Petersen
Project: *In vivo measurement of excitatory synaptic transmission between identified neurons in layer 2/3 mouse barrel cortex*
- Bachelor Thesis 2006
Laboratory of Functional Neurogenomic (LNGF), Prof. Ruth Lüthi-Carter
Project: *Effects of RGS2 overexpression in an in vitro model of Huntington's disease*
- Internship 2005
Laboratory of Neural Microcircuitry (LNMC), Prof. Henry Markram
Project: *In vitro whole-cell patch clamp recordings of L5 cortical pyramidal neurons*

Yale University, USA

- Master Thesis and postgraduate research 2007-2009
Laboratory of sensory information processing, Prof. Gordon Shepherd
Project: *In vivo trans-synaptic tracing of the rat olfactory bulb neuronal network and in vitro electrophysiological recordings of centrifugal projections from piriform cortex onto deep short axon neurons*

PUBLICATIONS

- **Pala A.** and Petersen C. C. H. In vivo measurement of cell-type-specific synaptic connectivity and synaptic transmission in layer 2/3 mouse barrel cortex (submitted)

- Yamashita T., **Pala A.**, Pedrido L., Kremer Y., Welker E., Petersen C. C. H. Membrane potential dynamics of neocortical projection neurons driving target-specific signals. *Neuron* 80, 1477-90 (2013)

Non-scientific

- **Pala A.** and Suter P. A chanter avec les doigts: Les « Lieder ohne Worte » et l'esthétique romantique. *Revue Musicale Suisse*. Nr. 2. pp. 19-20 (2009)

TALKS AND COURSES

- CSHL neuronal circuits meeting, USA 2014
- Cellular and molecular neurobiology of mental diseases meeting, Switzerland 2013
- National Competence Center for Biomedical Imaging (NCCBI) meeting, Switzerland 2013
- National Competence Center for Biomedical Imaging (NCCBI) meeting, Switzerland 2011
- National Competence Center for Biomedical Imaging (NCCBI) meeting, Switzerland 2010
- Lemanic neuroscience meeting (LNAM), Switzerland 2010
- FENS-IBRO-Sfn summer school "Causal Neuroscience: interacting with neural circuits", Italy 2011

CONFERENCE ABSTRACTS

- **Pala A.** and Petersen C. C. H. In vivo measurement of synaptic transmission between identified neurons in layer 2/3 mouse barrel cortex. Swiss society for neuroscience meeting, Switzerland (2014)
- **Pala A.** and Petersen C. C. H. In vivo measurement of synaptic transmission between identified neurons in layer 2/3 mouse barrel cortex. Sfn meeting, USA (2013)
- **Pala A.** and Petersen C. C. H. In vivo measurement of synaptic transmission between identified neurons in layer 2/3 mouse barrel cortex. Sfn meeting, USA (2012)
- Yamashita T., **Pala A.**, Petersen C. C. H. Projection-specific functional properties of excitatory neurons in layer 2/3 barrel cortex of awake mice. Sfn meeting, USA (2012)
- **Pala A.** and Petersen C. C. H. In vivo measurement of excitatory synaptic transmission from single pyramidal neurons onto GABAergic neurons in layer 2/3 of the mouse barrel cortex. FENS Meeting, Spain (2012)
- Yamashita T., **Pala A.**, Petersen C. C. H. Subnetwork specificity of cortical excitatory neurons with long-range intracortical projections in vivo. FENS Meeting, Spain (2012)
- **Pala A.** and Petersen C. C. H. In vivo measurement of excitatory synaptic transmission from single pyramidal neurons onto GABAergic neurons in layer 2/3 of the mouse barrel cortex. CSHL neuronal circuits meeting, USA (2012)

- Kim D. H., Patel H. K., Phillips M. E., **Pala A.**, Nawroth J. C., Chang A. Y., Shepherd G. M., Willhite D. C. Examination of olfactory network architecture by trans-synaptic viral tracing from defined neuron populations. SfN meeting, USA (2008)
- **Pala A.**, Nawroth J. C., Kim D. H., Patel H. K., Phillips M. E., Shepherd G. M., Willhite D. C. An extensive intrabulbar axon collateral network shown by modified trans-synaptic tracing viruses in the rat olfactory bulb. SfN meeting, USA (2008)
- Kim D. H., Chang A. Y., **Pala A.**, Patel H. K., Phillips M. E., Nawroth J. C., Migliore M., Shepherd G. M., Willhite D. C. Trans-synaptic viral tracing from defined neuron populations in the olfactory system. International Symposium on Olfaction and Taste/ACChemS Annual meeting, USA (2008)
- **Pala A.**, Nawroth J. C., Patel H. K., Phillips M. E., Kim D. H., Shepherd G. M., Willhite D. C. Modified Trans-synaptic Tracing Viruses Reveal the Axon Collateral Network in the Rat Olfactory Bulb Granule Cell Layer. International Symposium on Olfaction and Taste/ACChemS Annual meeting, USA (2008)
- Nawroth J. C., **Pala A.**, Phillips M. E., Kim D. H., Shepherd G. M., Willhite D. C. Modified Trans-synaptic Tracing Viruses Reveal Novel Connectivity in the Rat Olfactory Bulb. CSHL neuronal circuits meeting, USA (2008)

REFERENCES

Prof. Carl Petersen

EPFL

SV-BMI-LENS, station 19

CH-1015 Lausanne

Phone: +41 21 693 17 21

E-mail: carl.petersen@epfl.ch

Prof. Gordon Shepherd

Yale Medical School

Department of Neurobiology

333 Cedar Street, New Haven, CT 06511

Phone: +1 203 785 4336

E-mail: gordon.shepherd@yale.edu

Prof. Ruth Lüthi-Carter

University of Leicester

Department of Cell Physiology and Pharmacology

University Road, P.O. Box 138, Leicester LE1 9HN

Phone: + 44 0116 252 2925

E-mail: relc3@leicester.ac.uk